NEUTRON FLUX MEASUREMENTS FOR UNCERTAINTY QUANTIFICATION AT THE MCMASTER NUCLEAR REACTOR

NEUTRON FLUX MEASUREMENTS FOR UNCERTAINTY QUANTIFICATION AT THE MCMASTER NUCLEAR REACTOR

By ELIZABETH MACCONNACHIE, B.SC. (ENG)

A Thesis Submitted to the School of Graduate Studies in Partial Fulfillment of the Requirements for the Degree Doctor of Philosophy

DOCTOR OF PHILOSOPHY (2021)	McMaster University
(Department of Engineering Physics)	Hamilton, Ontario

TITLE:	Neutron Flux Measurements for Uncertainty Quantification at the McMaster Nuclear Reactor
AUTHOR:	Elizabeth MacConnachie, B.Sc. (Eng) (Queen's University)
SUPERVISOR:	Dr. David Novog
PAGES:	xiv, 172

Abstract

Nuclear research reactors offer a unique opportunity to the scientific community to investigate phenomena that are significant to both the renewable energy sector and the radiopharmaceutical industry. As the neutron flux dictates in-core processes that are crucial both to reactor operations and isotope production, highly precise measurements of this value are generally required to optimize and validate reactor physics analyses and day-to-day operations. Although neutron flux measurements in research reactors are well-documented, a detailed investigation of their uncertainties, and a methodology to quantify and combine them, has not yet been undertaken. These uncertainties are required to perform direct validation studies between experimental data and simulation models, to perform high-fidelity sensitivity and uncertainty quantification analyses, and to provide a basis for optimizing experimental activation processes in research reactor facilities.

Several experimental campaigns in the McMaster Nuclear Reactor (MNR) were designed to quantify the effects of various reactor parameters on neutron flux measurements. It was determined that the indicated reactor power and the sample positioning in the irradiation site are the most significant contributors to the final reported neutron flux uncertainty. By combining an experimental campaign with historical core data and Monte-Carlo models of MNR, it was determined that the effects of fuel management were generally insignificant and do not contribute significantly to the reported neutron flux uncertainty.

A Bayesian-based, Markov-Chain Monte-Carlo (MCMC) model was developed to accept fully covariant sets of nuclear data as inputs, such that their uncertainties could be included in a spectrum unfolding analysis. While nuclear data uncertainties are generally insignificant compared to other sources of uncertainty, the choice of flux spectrum parameterization may account for the trends in the final flux uncertainty across the energy spectrum.

Acknowledgements

First and foremost, I would like to express my deepest thanks to my supervisor, Dr. David Novog, for guiding me on this journey. His encouragement, support, advice, and knowledge were instrumental not only in pursuit of this thesis, but in building my own confidence as a researcher and young professional. I would also like to thank the other members of my committee, Dr. Simon Day and Dr. Adriaan Buijs, who offered their valuable input and expertise and helped mold this project into its final form.

This thesis would not have been possible without the support of several different individuals and groups at McMaster. Thanks to Ross Harper for the design and construction of some vital pieces of experimental equipment and to Alice Pidruczny for graciously allowing me access to her lab. Thanks also to Health Physics for their continued support in my endeavors to create, handle, and transport radioactive material, and to the MNR operations team for carrying out my irradiations.

I am very grateful to my friends and colleagues, who have helped me tremendously in getting to the end of my Ph.D. Garik and Mike – thank you for all our productive discussions about physics, and all the goofing around we managed to do. Chris, Kendall, Devan, Mitch, Phil, Kai, Simon, Nik, and Fred: thank you for making my time with the Novog research group such a positive experience. I am also blessed to be surrounded by an amazing group of friends who are always up for beers and a good time! The Fiends – Sam, Paige, Vic, Jon, Paul, Van, Dev, Evan, Matt, Simon, Whit, Bertha, Julia, and Jeremy – thank you for all the fun we've had, and cheers to more to come!

I'm a Queen's gal at heart – to my wonderful friends from undergrad: thank you for all the laughs, adventures, and beers we've shared over the years; I can't wait for so many more. Meara: thank you for always sharing in my highs and lows and laughing with me when things take a turn for the ridiculous. To "the boys", Eric and Stephen: for always catching me right before I pull some nonsense, and for our great chats about everything and nothing.

Last (and certainly not least!), I would like to thank my family for their never-ending support over the years; Margs – thank you for teaching me how to use a semicolon and for all the silliness. Mum – thank you for always listening as I talk myself in circles, only to arrive back exactly where I started. Look out world, Dr., Dr., and Dr. MacConnachie are coming!

To Dad, who always made sure we weren't taking things too seriously –

We miss you, we love you

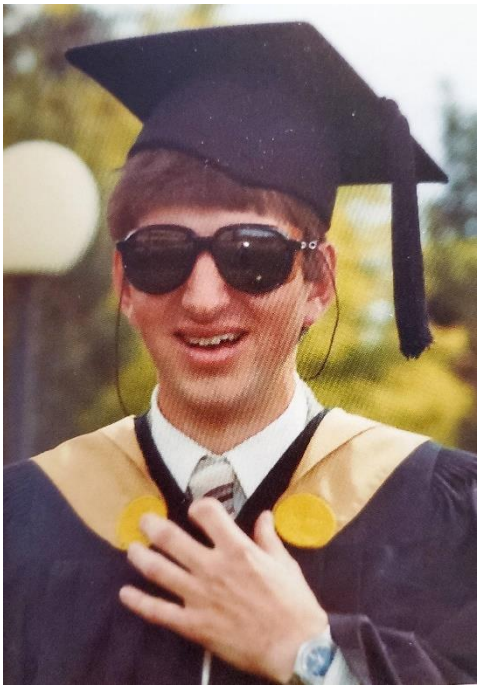

List of Figures

List of Tables

Acronyms

BOC	Beginning of Cycle
CNSC	Canadian Nuclear Safety Commission
ENDF	Evaluated Nuclear Data File
EOC	End of Cycle
GA	General Atomics
GE	General Electric
GHG	Greenhouse Gas
HEU	High-Enriched Uranium
HFIR	High Flux Isotope Reactor
HPGe	High-Purity Germanium
IAEA	International Atomic Energy Agency
JEFF	Joint Evaluated Fission and Fusion
LEU	Low-Enriched Uranium
LN2	Liquid Nitrogen
LWR	Light-Water Reactor
MACCNAA	McMaster Center for Neutron Activation Analysis
MCMC	Markov-Chain Monte-Carlo
MCNP	Monte-Carlo N-Particle
MGRAC	Multi-Group Reactor Analysis Code
MNR	McMaster Nuclear Reactor

MTR	Materials Testing Reactor
NAA	Neutron Activation Analysis
NDS	Nuclear Data Service
OSCAR	Overall System for CAlculation of Reactors
PPF	Power Peaking Factor
RIFLS	Reactor Irradiation Facilities for Large Samples
SAFARI	South African Fundamental Atomic Research Installation
SCALE	Standardized Computer Analyses for Licensing Evaluation
SMR	Small Modular Reactor
SOC	Start-of-Count
SOP	Standard Operating Procedure
TRIGA	Training, Research, Isotopes, General Atomics
UN	United Nations
UQ	Uncertainty Quantification
ZED-2	Zero Energy Deuterium Reactor

Symbols

Several branches of nuclear and reactor physics were applied in this work. Wherever possible, the conventions of these fields were followed when using any symbols; in the case that new symbols or Greek letters must be introduced to avoid confusion, the meaning and context of the symbol will be fully described.

Symbols

A	Activity [s^{-1}]
C	Normalization Constant [~]
CO_2	Carbon Dioxide
C_p	Specific Heat [J kg^{-1} $^oC^{-1}$]
dT	Temperature Difference [^{o} C]
E	Energy [eV]
$E_{fission}$	Energy Released per Fission Event [MeV]
E_0	Most Probable Energy for a Maxwellian Distribution at Room Temperature [E_0 = 0.0253 eV]
E[X]	Expectation Value Operator [~]
f(x)	Function with One Independent Variable [~]
$F_{control\ rod}$	Control Rod Correction Factor [~]
F_{Cd}	Cadmium Correction Factor [~]
F_{Xe}	Xenon Correction Factor [~]
G	Self-shielding Factor [~]
Gt	Gigatonne [kg]
I	Beam Intensity [cm^{-2} s^{-1}]

I_γ	Gamma-Ray Peak Yield [%]
j	Neutron Current Density [$cm^{-2}\ s^{-1}$]
k	Boltzmann Constant [$k = 8.617 \times 10^{-5}$ eV K^{-1}]
k_{eff}	Effective Multiplication Constant [~]
m	Mass [g]
M	Molar Mass [g mol^{-1}]
n	Neutron density [cm^{-3}]
$\hat{n}$	Vector Normal to a Surface [~]
N_A	Avogadro's Number [$N_A = 6.022 \times 10^{23}$ atoms mol^{-1}]
N	Number of Atoms [~]
N_ρ	Number of Atoms per Target Area [cm^{-2}]
p(E)	Resonance Escape Probability [~]
P	Reactor Power [kW or MW]
$P_i(x)$	i^{th} Legendre Polynomial
P(a → b)	Transition Probability from State a to State b [~]
q	Mass Flow Rate [$m^3\ s^{-1}$]
Q	Energy Conversion Factor, [$Q = 1.6022 \times 10^{-13}$ J MeV^{-1}]
$Q_{x,g}$	Cross Section Perturbation Factor [~]
r	Position Vector (e.g. (x, y, z)) [~]
$r_{x,g}$	Neutron-Induced Reaction Rate in Isotope x in Energy Group g [s^{-1}]
R	Activation Rate [atoms s^{-1}]
$\underline{R}(E)$	General Energy-Dependent Response Function [~]
S	Fission Source Term [$cm^2\ s^{-1}\ eV^{-1}$]

t	Time [s]
t_{decay}	Decay Time [s]
t_{irr}	Irradiation Time [s]
T	Time Constant [~]
T'	Temperature [K]
T_0	Room Temperature [T_0 = 293 K]
$UZrH_x$	Uranium-zirconium hydride
v	Speed [cm s^{-1}]
v_0	Most Probable Velocity for a Maxwellian Distribution at T_0 [v_0 = 2200 m/s]
V	Volume [cm^3]
w	Parameter Weight [~]

Greek Letters

α	Epithermal Neutron Flux Modification Parameter [~]
α'	Scattering Parameter [~]
∇	Differential Operator
η	Efficiency [~]
λ	Nuclear Decay Constant [s^{-1}]
ν	Average Number of Neutrons Released per Fission Event [~]
θ	Isotopic abundance [~]
σ	Cross Section [cm^2]
$\sigma_{n,x}(E)$	Energy Dependent Microscopic Cross Section for Reaction (n,x) [cm^2]
σ_{eff}	Effective Microscopic Cross Section [cm^2]

$\Sigma_{n,x}(E)$	Macroscopic Cross Section [cm^{-1}]
Σ_a	Macroscopic Absorption Cross Section [cm^{-1}]
Σ_s	Macroscopic Scattering Cross Section [cm^{-1}]
Σ_t	Macroscopic Total Cross Section [cm^{-1}]
$\phi(E)$	Flux per Unit Energy [$cm^{-2}\ s^{-1}\ eV^{-1}$]
Φ	Energy-Integrated Flux [$cm^{-2}\ s^{-1}$]
ψ	Angle [^{o} or rads]
Ω	Geometrical Correction Factor [~]
$\hat{\Omega}$	Solid Angle Directional Vector [~]

Declaration of Academic Achievement

This thesis was performed under the direct supervision of Dr. David Novog with support from the other members of the supervisor committee: Dr. Simon Day and Dr. Adriaan Buijs. The author performed all the work presented here, which includes: the background research, the design and execution of all experimental campaigns, the preparation of simulation models, the analysis of all data being generated (both experimental and computational), and the writing and editing of the three publications which make up the main body of this thesis.

The author designed and carried out a series of experimental campaigns to quantify significant sources of uncertainty in neutron flux measurements; these experimental endeavors were supplemented with Monte-Carlo simulation data whenever necessary. Additionally, the author created a Bayesian-based model to implement fully covariant sets of nuclear data in a spectrum unfolding analysis. For the first time, a generalized methodology to quantify, combine, and report neutron flux uncertainties has been developed; the methods presented in this thesis may be applied in other research reactor facilities where high-fidelity neutron flux measurements are required.

1 Introduction

1.1 Background

At the end of 2015, 195 countries entered in to the Paris Agreement – a historic, and ambitious global effort to combat the effects of climate change. The primary goal of this agreement is to limit the global temperature rise to 2 ºC, and actively pursue a scenario where this temperature increase is limited to 1.5 ºC [1]. Greenhouse gas (GHG) emissions owing to human activity have approximately doubled since 1970, with the production and usage of energy accounting for nearly two thirds of these emissions within the past 5 years [2]. To reduce these emissions, and reach the targets of the Paris Agreement, it is clear that a rapid decarbonization of energy is required. Nuclear energy has among the lowest GHG emissions per unit of electricity output, and it is estimated that the use of nuclear energy during the past decade has avoided approximately 2 gigatonnes (Gt) of carbon dioxide (CO_2) from being emitted, annually – which represents approximately 6% of the total emissions each year during the past decade [2], [3]. Although other low-carbon energy systems (such as solar-based or wind-based technologies) may offer some economic advantages, most pathways towards the achievement of the Paris Agreement rely on a significant degree of flexibility in the deployment of their low-carbon energy sources. Owing to the variable nature of most other low-carbon energy sources, it will be necessary to develop and deploy nuclear reactors to address the threats of climate change [2].

As of August 2020, nuclear energy provides approximately 10% of the world's electricity from over 400 power reactors around the world. The performance of nuclear reactors has steadily increased over time, and as of 2018, approximately two thirds of operational power reactors have reached a capacity factor of at least 80% [4]. In addition to the improvements being seen in the existing fleet of nuclear reactors, there is renewed interest in the deployment of small modular reactors (SMRs) to increase the nuclear capacity of any country that may adopt this technology, and to provide a low-carbon source of energy for remote communities.

In addition to the above discussed power-generating nuclear reactors, as of February 2020 there are currently 220 operational research reactors in 53 different countries [5]. The main purpose of these facilities is to provide a neutron source for a variety of different research projects – from non-destructive analysis and imaging applications to medical isotope development and production – and to serve as an educational facility for operational and regulatory personnel, and students [6]. These facilities are indispensable assets, and the research being done in these facilities can be

applied not only to external industries, but can provide key information about reactor physics and reactor operations. A renewed interest in increasing the nuclear capacity worldwide to meet the goals of the Paris Agreement provides a unique opportunity for novel research projects to be carried out in research reactors, such that their results may contribute to the advancement of a greener future for all.

There are several different types of research reactors – however, the two that are most significant in the development of this thesis are Training, Research, Isotopes, General Atomics (TRIGA) research reactors and materials testing reactors (MTRs). Many studies cited in the literature review used to motivate this thesis were carried out in TRIGA reactors and the facility where the experiments described in this thesis were conducted is a MTR.

The TRIGA reactor design was first conceived in the mid 1950s following the United Nations' (UN) conference on Peaceful Uses of Atomic Energy. This reactor was developed by General Atomics (GA), with the project lead being insistent that this reactor design "could be given to a bunch of high school children to play with, without any fear that they would get hurt" and that "engineered safety was not good enough" and that there should be a significant focus on the design having inherent safety characteristics [7].

The TRIGA design is an open-pool, light-water moderated reactor, using uranium-zirconium hydride ($UZrH_x$) fuel. The large negative fuel temperature coefficient of reactivity makes this a versatile design – the reactor can be operated under both steady-state conditions, and can be pulsed to high power for a short time [6]. TRIGA reactor cores consist of 90 assemblies (e.g. fuel, control rods, or dummy graphite elements) arranged in concentric circles surrounded by a graphite moderator. Although the number of fuel elements in a TRIGA core varies depending on the target operating power, there are typically between 60 and 87 fuel elements in the core configuration [7].

Figure 1 shows an overhead view of the TRIGA reactor located at the University of Pavia, in northern Italy, to demonstrate a typical core configuration for this reactor type.

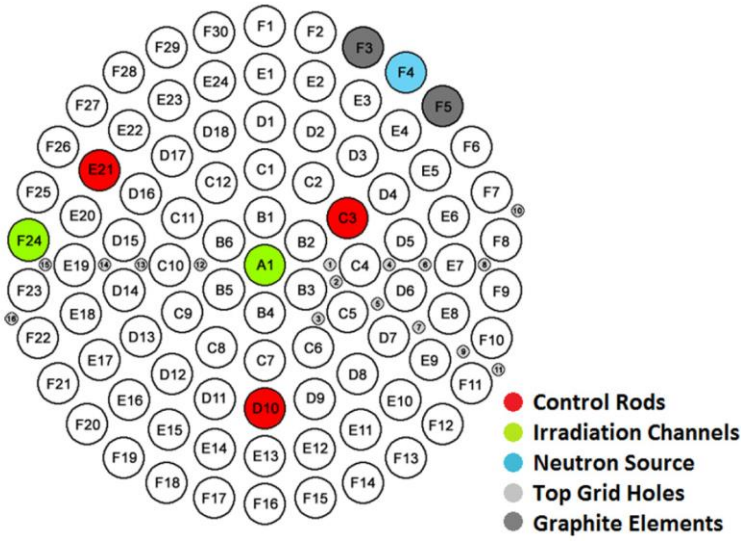

Figure 1: Overhead view of a typical TRIGA core configuration. The graphite reflector, which encircles the entire core configuration, is not shown in this figure [8].

While there have been several iterations of the TRIGA reactor design, some features of the TRIGA Mark-II are discussed here, to provide context for the motivation and literature review of this thesis. Designed to expand the experimental capabilities of the TRIGA Mark-I design, the Mark-II features four additional irradiation beam ports (providing a neutron flux of: $\Phi \sim 10^9$ neutrons cm^{-2} s^{-1}), as well as a thermal neutron column ($\Phi \sim 10^8$ neutrons cm^{-2} s^{-1}) flanking the core. To accommodate these new facilities, TRIGA Mark-II reactors are above-ground systems. As of 2015, there were 38 TRIGA reactors in operation, 16 of which are the Mark-II design [7].

Fuel assemblies in MTRs typically consist of several aluminium-clad fuel plates fixed in a parallel configuration. Early designs supported the use of high-enriched uranium (HEU) fuel (containing ~ 90% ^{235}U), however most MTRs have been converted to use low-enriched uranium (LEU) fuel (containing ~ 20% ^{235}U) within the past 20 years [6]. Though the exact dimensions of MTR cores vary between different facilities, the core is typically arranged in a cartesian grid pattern that allows for customizable fuel loading patterns. An example of an MTR core configuration – from the South African Fundamental Atomic Research Installation (SAFARI) research reactor located in South Africa – is shown in Figure 2.

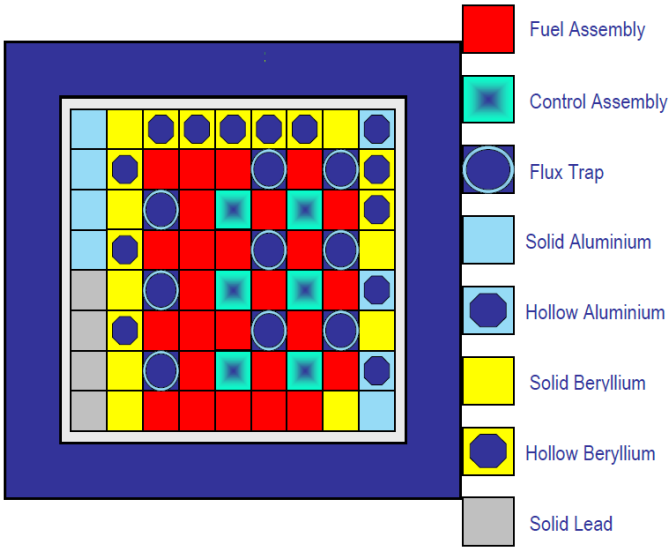

Figure 2: Overhead view of a typical MTR core configuration [9]. Although the core is reflected by beryllium in this case, other MTRs may be reflected by graphite assemblies.

The majority of the current fleet of MTRs have been in operation for over 40 years and are reaching the end of their planned lifetimes; they may face shutdown due to either obsolescence or limitations on experimental capabilities. Given that these reactors operate under low temperatures and at low pressures, their longevity is generally limited by external factors such as economics or licensing. However, the on-going need for the resources of research reactors has driven the construction of ten new research reactors within the past 10 years, with a further 9 that are currently under construction [10].

MTRs have been introduced here, however more detailed information about the McMaster Nuclear Reactor (MNR) (which is the experimental facility that is the focus of this work) can be found in Chapter 3 of this thesis.

1.2 Motivation

The neutron flux is an important parameter for analysis in nuclear reactors as its behavior dictates all neutron induced reaction rates in the core, and is therefore related to the fission power, the fuel burnup, and all other activation processes occurring in the reactor [11]. In addition to its operational significance, the neutron flux dictates the production yield of various medical isotopes that are often produced in research reactors [12], and may be used as an input for dose calculations and regulatory safety analysis in these facilities [13].

While local measurements of the neutron flux may be challenging in power reactors, they can be made more readily in research reactors, and such measurements are often used as the basis for code validation studies or operational decision making [14]. The uncertainties reported in these measurements include uncertainties in the measurement procedure (which are generally known), and are sometimes increased to reflect the effects of identified, but unquantified, uncertainties (e.g. by adding a simulation uncertainty in an attempt to bound the reported experimental uncertainty) or other systematic effects that have been identified during data processing [8]. While increasing the uncertainties in this way may generate a sufficiently broad or bounding estimate of the neutron flux for some analyses, a more precise quantification of the neutron flux uncertainty is required to perform high-fidelity validation studies, uncertainty quantification (UQ), sensitivity analyses, and to optimize both in-core activation procedures and operational decision making.

Indeed, several reactor parameters that may contribute a significant source of uncertainty during neutron flux measurements have been identified by previous studies carried out a several different TRIGA reactors, but have not been studied in detail. The following parameters have been identified in literature as being potentially significant sources of additional uncertainty in activation experiments (and hence flux measurements): the sample position [15], the accumulation of ^{135}Xe [8], the reactor power uncertainty [13], and the nuclear data uncertainties as they are applied during data processing [11]. In addition to the four parameters listed above, the position of the control rods in the core has also been identified as a potentially significant source of uncertainty in the neutron flux determination. A detailed study of these effects is presented in Chapter 4, in the first journal article that makes up this sandwich thesis.

Additionally, the effects of fuel burnup and fuel management operations (known to drive changes in the bulk k_{eff}) have not been studied in the context of their effects on activation procedures in general, or on measurements of the neutron flux in particular [15]–[17]. The impacts of fuel operations and management on neutron flux uncertainties are presented in Chapter 5.

To perform direct comparisons between computational and experimental results, and to lay the foundation for propagating neutron flux values through other high-fidelity analyses (e.g. dose calculations, sensitivity analyses, total Monte Carlo techniques or Bayesian analyses), it is necessary to study all significant sources of uncertainty present during neutron flux measurement procedures, and to quantify their contribution to the overall reported uncertainty.

1.2.1 Objectives

The main objectives of this work are to the quantify significant sources of uncertainty present in experimental determinations of the neutron flux and its spectrum, and to develop a generalized methodology for combining and reporting these uncertainty values. As the primary motivation of this work is to better understand experimental neutron flux measurements¸ this thesis will primarily focus on the development and implementation of several different experimental campaigns to achieve this goal. In some cases – where experimental efforts must remain limited to avoid significantly interrupting normal MNR operations – the experimental results will be supplemented with computational data.

The data and conclusions presented in this thesis are the result of several high-fidelity experimental campaigns and computational investigations in a graphite-reflector irradiation site, MNR Site 8C. As such, the results presented here cannot be applied indiscriminately to other irradiation sites in MNR, to other nuclear facilities, or to the study of reactor physics parameters in general (such as fuel isotopics or kinetics). Rather, the purpose of this thesis is to detail the methodologies that can be deployed to more thoroughly quantify the neutron flux and its uncertainty in other nuclear facilities.

Nevertheless, the novel contribution of this thesis will be to provide a more complete understanding of significant sources of uncertainty in these experiments, such that the procedures developed here can be applied to future research or reactor operations, where a precise knowledge of the uncertainties may be required.

1.3 Outline of the Thesis

This work is presented as a sandwich-style thesis that contains a total of seven chapters and one appendix of supplementary information. Chapter 2 introduces and develops the relevant theory applied in this work, including discussions of: the fundamentals of reactor physics (both theoretical and computational), the features of neutron flux spectra, and the principles of uncertainty analysis. Chapter 3 focuses on the specific methodologies and procedures (both experimental and computational) that were applied in generating, processing, and presenting the data discussed in this thesis. Chapters 2 and 3 are intended to provide the reader with additional theoretical knowledge and background information that may not be explicitly discussed in the three

publications that make up the main body of this thesis. These three articles are presented in full in Chapters 4, 5, and 6.

Chapter 4 presents the first publication of this sandwich thesis, an article published in the *Annals of Nuclear Energy* in 2019. This work develops a generalized methodology for quantifying and combining several significant sources of uncertainty that are present in experimental determinations of the neutron flux. As a direct continuation of the work presented in Chapter 4, the article presented in Chapter 5 investigates the contribution of fuel burnup, and fuel management operations to the overall experimental uncertainty. This work combines an experimental campaign over a period of 4 months of typical operations with several sets of historical core data. This article was published in the *Annals of Nuclear Energy* in 2021. Finally, chapter 6 presents the last article of this thesis, which was submitted for consideration to the *Annals of Nuclear Energy* in 2021. This publication presents a detailed investigation of a determination of the neutron flux spectra using a Bayesian methodology, which (to the authors knowledge), is the first such application to include nuclear data uncertainties and their covariances in the Bayesian methodology. Although this topic is briefly mentioned in the first two articles (Chapters 4 and 5), this last article quantifies these uncertainties without performing a cross-section collapsing procedure (described in Section 3.3), as has been applied in those previous works.

Chapter 7 of this thesis presents the major conclusions to be drawn from this work, and proposes some additional experimental and computational work that might be done in the future.

Appendix A contains a detailed standard operating procedure (SOP) of the experimental work presented in this thesis; the information contained in this appendix is intended to act as a supplement to the methodology discussed in Chapter 3.

2 Theoretical Background

2.1 Background

This chapter introduces the relevant theoretical background to accompany the work presented in this thesis. Reactor physics fundamentals (with an emphasis on the neutron flux and neutron interactions with matter) are presented, followed by a discussion of the application of computational methods to reactor physics problems and a derivation of the neutron flux spectrum in a light-water reactor (LWR). Finally, a detailed discussion of the principles of uncertainty analysis and propagation is presented.

2.2 Reactor Physics Calculations

In 1930, Walter Bothe and Herbert Becker observed that if high-energy α-particles impinged on certain light elements (such as lithium, beryllium, or boron), a highly-penetrating and electrically-neutral radiation was produced. Further studies by James Chadwick in 1932 concluded that this radiation was not high-energy γ-rays, but rather a hitherto unknown, neutral particle, with mass approximately equal to that of the proton [18]. These newly-discovered particles (*neutrons*) are not stable unless bound to a nucleus, and when in a free state, will undergo beta-negative decay with a half-life of approximately 12 minutes [19]. Neutron interactions with various types of matter are the cornerstone of reactor physics calculations. Here, the physics of general neutron interactions will be introduced, followed by a detailed discussion of the neutron lifecycle in reactors and the mathematical formalisms used to describe their behavior.

The discussion of neutron interactions with matter, and the relationship between neutron-induced reaction rates and the target cross section (in Section 2.2.1) form the basis for the methods used to recover the neutron flux from an activation measurement (which are presented in detail in Section 3.3). Additionally, the detailed discussion of the neutron lifecycle and the development of the neutron transport equation that is presented in this chapter, emphasizes the importance of understanding neutron behavior in a reactor core and presents a theoretical basis for studying the neutron flux spectrum.

2.2.1 Neutron Interactions with Matter

As a consequence of their charge neutrality, neutrons do not interact with the electron cloud surrounding an atom, but rather with the nucleus directly. The convention of representing a general

nuclear reaction $A + n \rightarrow A' + x$ as $A(n,x)A'$ (or more simply as $A(n,x)$) will be adopted throughout this thesis. Neutrons may interact with nuclei in the following ways [19]:

- Scattering: these reactions involve the production of one neutron in the exit channel i.e. an (n, n') reaction. If the target nucleus is not excited during the interaction, the process is called *elastic scattering*. Conversely, some scattering interactions result in a compound nucleus being formed (which may later decay) during an *inelastic scattering* reaction [20].
- Neutron capture: any reaction involving the absorption of a neutron by the target nucleus is defined as a *neutron capture* reaction. These reactions involve the production of an intermediate compound nucleus, which decays according to its own nuclear properties. In general, such reactions can be written in the form [20]:

$$^{A}X + n \rightarrow {}^{[A+1]}X^{*} \rightarrow Y + radiation \quad (1)$$

  Neutron capture reactions can be further sub-divided in to the following categories:

  - Radiative capture: the radiation in the exit channel is γ-rays, and these are therefore known as (n, γ) reactions [19].
  - Charged particle production: these reactions involve the production of a charged particle in the exit channel, i.e. (n, p) or (n, α) reactions accompanied by the release of energy in the form of γ-rays [19].
  - Fission: the defining feature of a fission reaction is the production of several neutrons in the exit channel, accompanied by the splitting of the target in to several lighter nuclei [20]. As the fission reaction is central to the operation of a nuclear reactor, it will be discussed in greater detail in the following paragraph.

The absorption of a neutron by a heavy target nucleus (i.e. uranium, polonium, or thorium) creates a highly unstable compound nucleus; this occurs with heavy target nuclei due to the fact that the binding energy per nucleon decreases with increasing target mass, and it is therefore more energetically favorable for several lighter fragments to exist [19]. As described by the liquid drop model of the nucleus, this highly excited target may then undergo severe physical deformation resulting in a dumbbell-shaped compound nucleus whose ends are Coulombically repelled from each other and will eventually scission [20]. The result is the release of energy and the production of two highly charged fission products being created, from which several neutrons are emitted

(and, in a reactor, may go on to initiate another fission event). Such fission products are generally unstable, and typically undergo a series of beta-negative decays [20].

The extent to which any neutron-induced reactions proceed is described by the quantity known as a *cross section* – a proportionality constant which can be interpreted as the probability of an (n, x) reaction occurring at a given incident neutron energy. Consider a mono-energetic beam of neutrons (of intensity I) incident on a target slab (of thickness x), as shown in Figure 3.

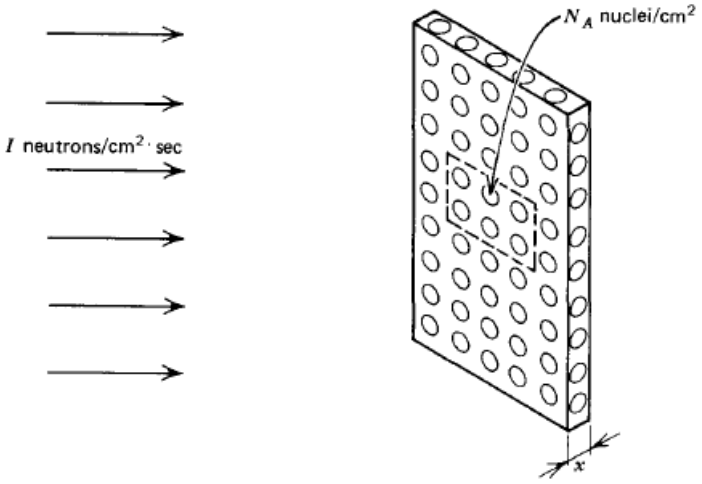

Figure 3: A mono-energetic beam of neutrons normally incident on a thin slab of target material [21].

Not every neutron that strikes the target will provoke an (n, x) reaction – many will pass through un-impeded. The number of neutrons that do initiate an (n, x) reaction is found to be proportional to the incident beam intensity and the microscopic cross section is therefore formally defined as the ratio of the number of reactions per target nucleus that do occur, to the number of neutrons incident on the target. This is typically expressed in terms of the reaction rate R, the beam intensity I, and the total number of target nuclei N [21]:

$$\boldsymbol{\sigma = \frac{R}{NI}} \qquad 2$$

The beam intensity can be further described in terms of the neutron density, and neutron speed:

$$\boldsymbol{I = nv} \qquad 3$$

In the context of reactor physics, this quantity is referred to as the *neutron flux*, Φ, such that:

$$\boldsymbol{R = N\sigma I = N\sigma\Phi} \quad (4)$$

This relationship between reaction rates, cross sections, and the neutron flux will be central to the development of a mathematical description of the neutron distribution in Section 2.2.3.

Cross sections vary according to the energy of the incident neutrons and the particular (n, x) reaction being studied. The following figure demonstrates both the behavior and magnitude of some typical cross sections that are useful to study in a reactor setting.

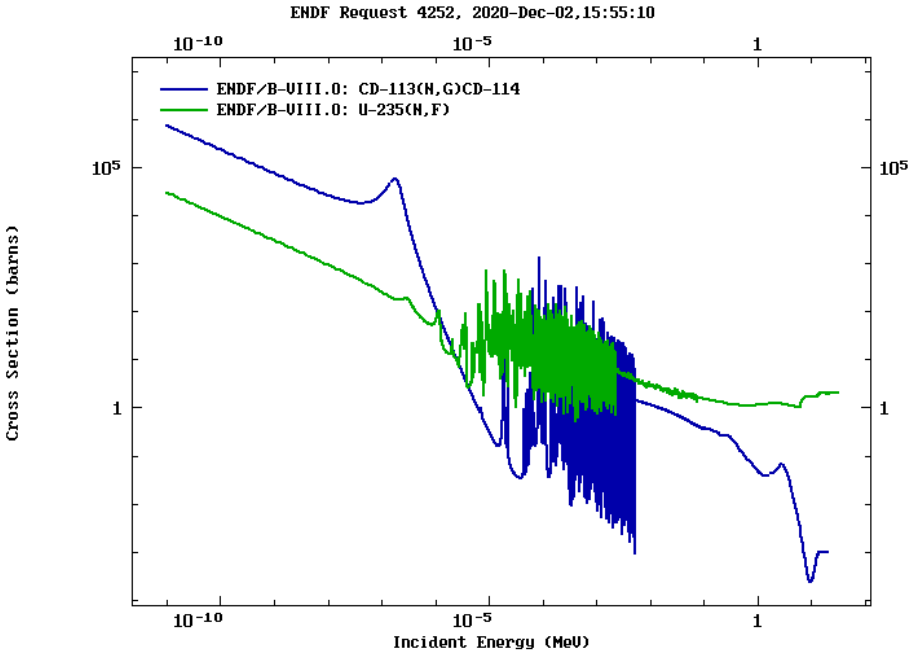

Figure 4: Cross sections of the ^{235}U(n, f) and ^{113}Cd(n, γ) reactions. This tabulated data is part of the Evaluated Nuclear Data File (ENDF) B-VIII.0 nuclear data libraries however, other versions of the data can be accessed through the International Atomic Energy Agency (IAEA) Nuclear Data Service (NDS) [22].

In general, different (n, x) reactions will dominate neutron interactions at certain energies and the cross section behavior varies significantly across the energy spectrum. Notably, the ^{235}U(n, f) cross section is several orders of magnitude higher at low energies than at high energies, indicating that low energy neutrons (i.e. those that have been thermalized) will initiate fission reactions more readily. This is a defining feature of thermal reactors, whose neutron lifecycle, and neutron flux spectrum, will be discussed in Sections 2.2.2 and 2.3.

2.2.2 Neutron Lifecycle

To sustain a fission chain-reaction, it is intuitive that *only one* of the neutrons produced during the initial fission event *must* go on to initiate another fission. Mathematically, the behavior of a fission chain reaction can be described by its effective reproduction number [19]:

$$\boldsymbol{k_{eff} = \frac{number\ of\ fissions\ in\ generation\ X}{number\ of\ fissions\ in\ generation\ (X-1)}} \quad 5$$

In general, the overall reactor system behavior can be described based on the value of k_{eff} [21]:

- $k_{eff} > 1$: an increasing number of fissions (and therefore an increasing release of energy) is occurring in the fuel. The reactor is *supercritical*.
- $k_{eff} < 1$: the number of fissions in the fuel decreases. The reactor is *subcritical*.
- $k_{eff} = 1$: fissions proceed at a constant rate in the fuel. The reactor is *critical*.

While there are many different control mechanisms to limit the fission rate and prevent super-criticality in a reactor, some neutron losses occur naturally as a result of their interactions with both fuel and non-fuel materials in the system. The following figure shows a schematic of the neutron lifecycle in a thermal reactor.

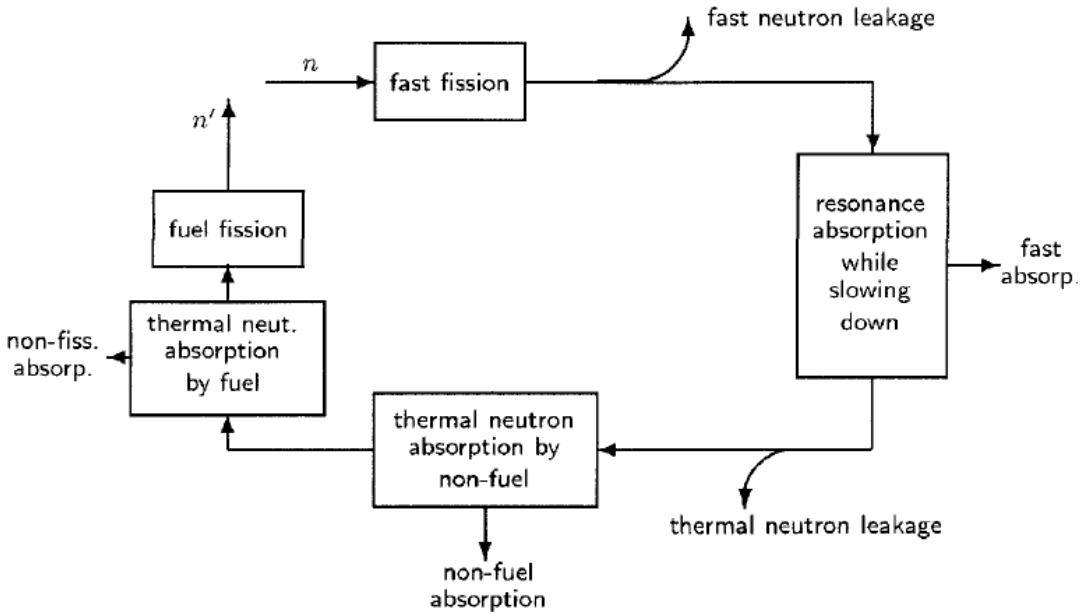

Figure 5: The neutron lifecycle in a thermal reactor showing losses due to their interactions with matter. There are n neutrons at the start of the lifecycle and n' neutrons – which will initiate the next generation of fissions – at the end [20].

As can be seen in this figure, only those neutrons that survive the thermalization process (i.e. are not lost to leakage or miscellaneous absorption), and undergo a successful fission reaction in the fuel, are useful in sustaining the chain reaction. Understanding the nature of the neutron lifecycle in a reactor in this way is a useful first step in mathematically describing the in-core neutron distribution. Section 2.2.3 is dedicated to the mathematical formulation of the behavior and distribution of neutrons in a reactor.

2.2.3 The Neutron Transport Equation

Having described neutron interactions with matter, and the progression of the neutron lifecycle in a thermal reactor, a full description of the neutron distribution in the core can now be developed. The Boltzmann Equation (or the Boltzmann Transport Equation; referred to hereafter as the *neutron transport equation*) adopts a neutron balance about a volume element d^3r to determine the behavior of the neutron field in the system, such that [21]:

$$\frac{\partial n}{\partial t} = \textbf{neutron gains} - \textbf{neutron losses} \qquad 6$$

A schematic of the volume element d^3r is shown in the following figure.

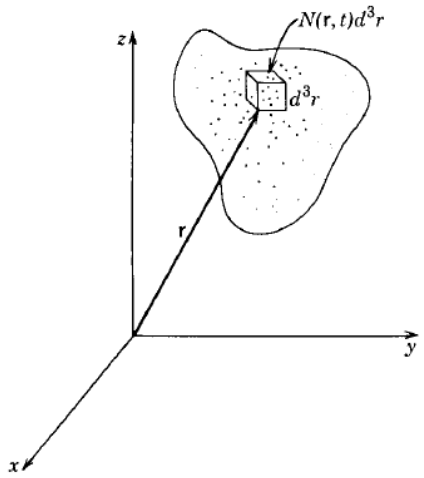

Figure 6: Elementary volume unit d^3r containing a neutron density n(r,t) (denoted in the figure as N(r,t)) [21]. In general, the neutron density will also have some angular and energy dependence i.e. n(r, E, $\hat{\Omega}$, t).

Before a complete description of the neutron balance within this volume element can be developed, some quantities relating to the neutron distribution must be defined.

The angular neutron density is defined such that $n(r, E, \hat{\Omega}, t)d^3rdEd\hat{\Omega}$ is the number of neutrons within the volume element d^3r, within the energy interval E + dE, travelling in direction $\hat{\Omega}$ about the solid angle $d\hat{\Omega}$ at time t. The angular neutron flux is defined as the product of the angular neutron density and the neutron speed [21]:

$$\boldsymbol{\phi}(\boldsymbol{r}, \boldsymbol{E}, \hat{\boldsymbol{\Omega}}, \boldsymbol{t}) = \boldsymbol{v}\boldsymbol{n}(\boldsymbol{r}, \boldsymbol{E}, \hat{\boldsymbol{\Omega}}, \boldsymbol{t}) \quad 7$$

A related quantity – the angular current density – is defined as [21]:

$$\boldsymbol{j}(\boldsymbol{r}, \boldsymbol{E}, \hat{\boldsymbol{\Omega}}, \boldsymbol{t}) = \boldsymbol{v}\hat{\boldsymbol{\Omega}}\boldsymbol{n}(\boldsymbol{r}, \boldsymbol{E}, \hat{\boldsymbol{\Omega}}, \boldsymbol{t}) = \hat{\boldsymbol{\Omega}}\boldsymbol{\phi}(\boldsymbol{r}, \boldsymbol{E}, \hat{\boldsymbol{\Omega}}, \boldsymbol{t}) \quad 8$$

These quantities – the angular neutron flux, and the angular current density – will be used extensively in mathematically describing the balance of neutrons within a volume element d^3r.

Neutrons are gained by internal source terms, by scattering events within d^3r that generate neutrons within the desired intervals, and by neutrons that physically enter d^3r from external sources. Neutrons can be lost by leaving the volume element (i.e. leakage), and by interactions within d^3r (i.e. absorption, scattering, etc.) that remove neutrons from the interval of interest [18]. These terms representing neutron gains and losses will now be presented and combined to form the neutron transport equation.

It follows from the definition of angular neutron density that source terms (i.e. fission sources, denoted by S) within d^3r generate $S(r, E, \hat{\Omega}, t)d^3rdEd\hat{\Omega}$ neutrons within the energy and directional intervals, per unit time. The complete source term in the neutron transport equation is therefore:

$$\left[\int_0^V \boldsymbol{S}(\boldsymbol{r}, \boldsymbol{E}, \hat{\boldsymbol{\Omega}}, \boldsymbol{t})\boldsymbol{d^3r}\right]\boldsymbol{dEd\hat{\Omega}} \quad 9$$

By extending the relationship between an (n, x) reaction rate, the neutron flux, and the cross section (presented in Section 2.2.1) to include an energy and directional dependence, the reaction rate of neutrons undergoing reactions that introduces them to the intervals of interest is:

$$\left[\int_0^{4\pi}\int_0^{\infty}\int_0^V \boldsymbol{\Sigma_s}(\boldsymbol{r}, \boldsymbol{E'} \rightarrow \boldsymbol{E}, \hat{\boldsymbol{\Omega}'} \rightarrow \hat{\boldsymbol{\Omega}}, \boldsymbol{t})\boldsymbol{\phi}(\boldsymbol{r}, \boldsymbol{E}, \hat{\boldsymbol{\Omega}}, \boldsymbol{t})\boldsymbol{d^3rdE'd\hat{\Omega}'}\right]\boldsymbol{dEd\hat{\Omega}} \quad 10$$

Here, the quantity Σ_s is known as the *macroscopic scattering cross section*, and is defined as the product of the number of target atoms and the associated microscopic cross section.

The terms involving neutrons either entering or leaving the volume element will be combined to determine the net leakage through the surface of d^3r. By definition, this quantity is [21]:

$$\int_{surface} \boldsymbol{j}(\boldsymbol{r},\boldsymbol{E},\hat{\boldsymbol{\Omega}},\boldsymbol{t})\cdot d\hat{\boldsymbol{n}} = \int_{surface} \hat{\boldsymbol{\Omega}}\boldsymbol{\phi}(\boldsymbol{r},\boldsymbol{E},\hat{\boldsymbol{\Omega}},\boldsymbol{t})\cdot d\hat{\boldsymbol{n}} \qquad 11$$

The divergence theorem can be applied to ensure that all terms in the neutron transport equation contain a volume integral, and have no surface integral terms [18]. The net leakage is therefore:

$$\left[\int_0^V \hat{\boldsymbol{\Omega}}\boldsymbol{\nabla}\cdot\boldsymbol{\phi}(\boldsymbol{r},\boldsymbol{E},\hat{\boldsymbol{\Omega}},\boldsymbol{t})\,\boldsymbol{d^3r}\right]\boldsymbol{dEd\hat{\Omega}} \qquad 12$$

Finally, the neutron losses by interactions within d^3r that remove them from the energy and direction intervals of interest are quantified by:

$$\left[\int_0^V \boldsymbol{\Sigma_t}(\boldsymbol{r},\boldsymbol{E},\hat{\boldsymbol{\Omega}},\boldsymbol{t})\boldsymbol{\phi}(\boldsymbol{r},\boldsymbol{E},\hat{\boldsymbol{\Omega}},\boldsymbol{t})\boldsymbol{d^3r}\right]\boldsymbol{dEd\hat{\Omega}} \qquad 13$$

By combining the equations above, the balance of neutrons can be written as [21]:

$$\boldsymbol{0} = \int_0^V \left[\begin{array}{c}\boldsymbol{\frac{\partial n}{\partial t}} + \boldsymbol{\Sigma_t}(\boldsymbol{r},\boldsymbol{E},\hat{\boldsymbol{\Omega}},\boldsymbol{t})\boldsymbol{\phi}(\boldsymbol{r},\boldsymbol{E},\hat{\boldsymbol{\Omega}},\boldsymbol{t}) + \hat{\boldsymbol{\Omega}}\boldsymbol{\nabla}\cdot\boldsymbol{\phi}(\boldsymbol{r},\boldsymbol{E},\hat{\boldsymbol{\Omega}},\boldsymbol{t}) - \\ \left(\int_0^{4\pi}\int_0^{\infty} \boldsymbol{\Sigma_s}(\boldsymbol{r},\boldsymbol{E'}\rightarrow\boldsymbol{E},\widehat{\boldsymbol{\Omega'}}\rightarrow\hat{\boldsymbol{\Omega}},\boldsymbol{t})\boldsymbol{\phi}(\boldsymbol{r},\boldsymbol{E},\hat{\boldsymbol{\Omega}},\boldsymbol{t})\boldsymbol{dE'd\hat{\Omega}'}\right) \\ -\boldsymbol{S}(\boldsymbol{r},\boldsymbol{E},\hat{\boldsymbol{\Omega}},\boldsymbol{t})\end{array}\right]\boldsymbol{d^3rdEd\hat{\Omega}} \qquad 14$$

As this equation can only be satisfied if the integrand is zero, the neutron transport equation is [21]:

$$\begin{array}{c}\boldsymbol{\frac{\partial n}{\partial t}} + \boldsymbol{\Sigma_t}(\boldsymbol{r},\boldsymbol{E},\hat{\boldsymbol{\Omega}},\boldsymbol{t})\boldsymbol{\phi}(\boldsymbol{r},\boldsymbol{E},\hat{\boldsymbol{\Omega}},\boldsymbol{t}) + \hat{\boldsymbol{\Omega}}\boldsymbol{\nabla}\cdot\boldsymbol{\phi}(\boldsymbol{r},\boldsymbol{E},\hat{\boldsymbol{\Omega}},\boldsymbol{t}) = \\ \int_0^{4\pi}\int_0^{\infty} \boldsymbol{\Sigma_s}(\boldsymbol{r},\boldsymbol{E'}\rightarrow\boldsymbol{E},\widehat{\boldsymbol{\Omega'}}\rightarrow\hat{\boldsymbol{\Omega}},\boldsymbol{t})\boldsymbol{\phi}(\boldsymbol{r},\boldsymbol{E},\hat{\boldsymbol{\Omega}},\boldsymbol{t})\boldsymbol{dE'd\hat{\Omega}'} + \boldsymbol{S}(\boldsymbol{r},\boldsymbol{E},\hat{\boldsymbol{\Omega}},\boldsymbol{t})\end{array} \qquad 15$$

When appropriate boundary conditions are specified, this integro-differential equation can be used to determine the neutron flux arising from a particular source distribution [18]. By simplifying the neutron transport equation to the case of a stationary neutron flux, it may be possible to solve this

equation analytically for certain basic reactor geometries and source types [19]. In general, however, computational methods must be applied to solve the neutron transport equation in reactor cores with complex geometries and material compositions. Section 2.2.4 introduces some computational methods as a means of recovering the solution to the neutron transport equation, with an emphasis on the Monte Carlo method.

2.2.4 Computational Reactor Physics

There are two families of methods that can be used to solve the neutron transport equation: deterministic methods, and Monte Carlo methods. As all computational data presented in this thesis is generated via Monte Carlo N-Particle (MCNP) simulations, Monte Carlo methods will be presented and developed in detail – with an emphasis on the particularities of the MCNP code package, though there are several other Monte Carlo codes that can be applied to reactor physics calculations. For completeness, deterministic methods with be briefly discussed below.

Although Monte Carlo methods may require more computational resources to generate high-fidelity results, they are typically better suited to produce local flux results as compared to deterministic methods, where the effects of mesh size or homogenization procedures may be detrimental.

2.2.4.1 Deterministic Methods

Deterministic methods solve the neutron transport equation by considering the average particle behavior within the system through the discretization of some, or all, of the six independent variables in the problem [21]. Here, the mathematical methods used to discretize the neutron transport equation with respect to $\widehat{\Omega}$, E, r, and t will be described.

In general, any function $f(x)$ can be expressed either as a series representation or as a set of discrete points [18].

In the method of discrete ordinates, the integrations over $\widehat{\Omega}$ are replaced by a summation over all required directions [23]:

$$\int_{0}^{4\pi} \boldsymbol{\phi}(\boldsymbol{r}, \boldsymbol{E}, \widehat{\boldsymbol{\Omega}}, \boldsymbol{t}) d\widehat{\boldsymbol{\Omega}} \cong \sum_{i=1}^{N} \boldsymbol{w_i} \boldsymbol{\phi_i}(\boldsymbol{r}, \boldsymbol{E}, \boldsymbol{t}) \quad 16$$

Alternatively, the angular distribution of the neutron flux can be represented as a finite series of Legendre Polynomials [23]:

$$\boldsymbol{\phi(r, E, \cos(\psi))} = \sum_{\boldsymbol{i=0}}^{\boldsymbol{N}} \left(\frac{\boldsymbol{2i+1}}{\boldsymbol{4\pi}}\right) \boldsymbol{\phi_i(r, E) P_i(\cos(\psi))} \quad 17$$

By making either of the above substitutions for the flux in the neutron transport equation, the problem in both cases is reduced to a system of linear differential equations – called the S_N and P_N equations for the application of discrete ordinates and series expansion, respectively [18].

The neutron flux energy spectrum is determined by distinct physical processes at different energies (i.e. fission above ~ 1 MeV, thermalization below ~ 1 eV, etc., discussed in detail in Section 2.3), and a series representation of the neutron flux with respect to the energy variable is therefore impractical. Additionally, the strong dependence of cross sections on energy (e.g. as in Figure 4) limits the application of the method of discrete ordinates, as the tabulation of cross sections at distinct energies is an inadequate description of their detailed structure [21]. The spectrum is instead divided into a set of energy groups and the cross sections within each group are defined as [21]:

$$\boldsymbol{\Sigma_g} = \frac{\int_{\boldsymbol{E_g}}^{\boldsymbol{E_{g+1}}} \boldsymbol{\Sigma(E)\phi(E)dE}}{\int_{\boldsymbol{E_g}}^{\boldsymbol{E_{g+1}}} \boldsymbol{\phi(E)dE}} \quad 18$$

Typically, an approximation of the neutron flux based on its idealized spectrum definition in a reactor will be used to generate the group cross sections defined in the equation above.

In addition to the treatment of $\widehat{\Omega}$ and E described above, deterministic transport solver codes also perform a discretization of the spatial and time variables (i.e. r = (x, y, z) and t) such that any derivatives and integrals can be replaced by the usual finite difference equations and numerical integrations. The following figure shows an example of a spatial mesh overlayed on a reactor.

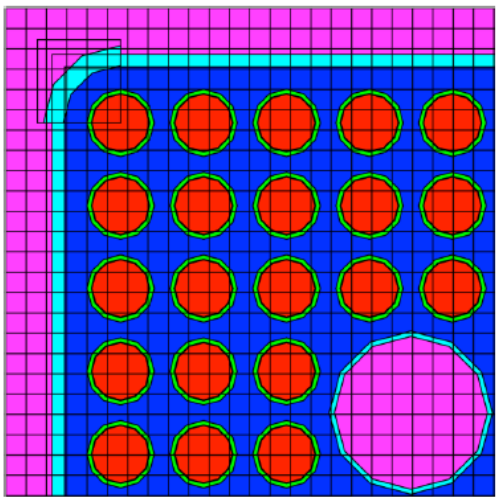

Figure 7: A mesh overlayed on a quarter-lattice of the General Electric (GE) 14 reactor, generated using the Standardized Computer Analyses for Licensing Evaluation (SCALE) software package [24].

This treatment of the neutron transport equation provides a basis for numerically recovering the neutron flux; further simplifications may be made to limit the computational resources required to generate an appropriate solution. For example, it is common to limit the problem to the case of static reactor behavior (i.e. all time-dependence is removed), and to only two energy groups [19].

While a deterministic approach may be appropriate for a single fuel pin or assembly in two dimensions, Monte Carlo methods are better suited to recovering local flux information where a precise definition of the geometry is required. [25]. The following section introduces the Monte Carlo method in general, and develops its application to reactor physics, with an emphasis on recovering either the in-core neutron flux, or particular (n, x) reaction rates.

2.2.4.2 Monte Carlo Methods

The use of random sampling as a means to solve a physical problem has existed since the late 18th century – the earliest documented example comes from the Comte de Buffon's now-famous game used to infer the value of π from the repeated toss of a needle on to a set of wooden slats. The more sophisticated Monte Carlo method emerged in the 1940s at Los Alamos alongside the development of nuclear weapons [25].

In their 1991 textbook, *Monte Carlo Particle Transport Methods: Neutron and Photon Calculations*, Drs. Lux and Koblinger defined the Monte Carlo method as follows [26]:

> "In all applications of the Monte Carlo Method a stochastic model is constructed in which the expected value of a certain random variable is equivalent to the value of a physical quantity to be determined. This expected value is then estimated by the average of several independent samples representing the random variable introduced above."

Consider a problem whose solution is characterized by the value Y; to use the Monte Carlo method to solve this problem, a stochastic model must be constructed such that the expectation value of the variable being recorded (i.e. tallied) is equal to Y [27]:

$$\boldsymbol{E}[\boldsymbol{X}] = \boldsymbol{Y} \tag{19}$$

The value of Y is determined by repeatedly simulating the problem, and evaluating the expectation value of X. According to the law of large numbers, if a sufficiently large number of simulations are carried out, E[X] will tend towards the true value of Y [27]. For example, rolling a fair, six-sided dice 10,000 times and tallying the result of each throw will yield a reasonably accurate estimate of the probability of any given throw producing a 2.

In the case of particle transport, interactions are *de facto* stochastic processes, and the Monte Carlo simulation is therefore a representation of real physical processes. Monte Carlo methods obtain a solution to the neutron transport equation by simulating a large number of individual neutrons and tallying user-requested aspects of their behavior (i.e. the (n, x) reaction rate at a particular location in the core). This method consists of following individual particles through their lifecycle, and using randomly sampled values from transport data to determine the outcome of the interactions they experiences [25]. This is shown schematically (for a neutron) in Figure 8.

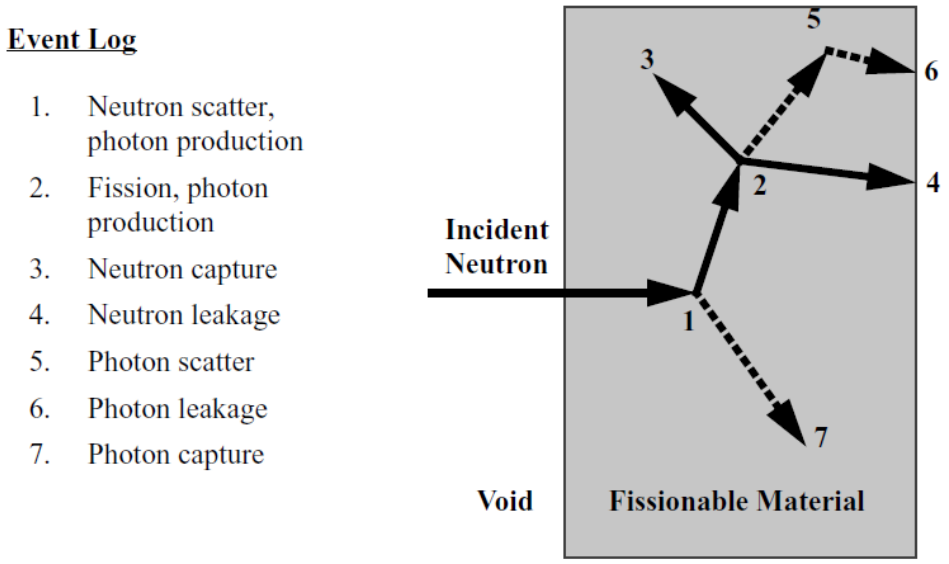

Figure 8: Representation of one incident neutron in a slab of material. Random draws are used to determine which interactions will take place, based on the transport data (i.e. cross section information) and the problem physics [25].

By tracking a large number of particles within the problem geometry, accurate estimates of various reactor physics parameters can be recovered. MCNP provides seven basic tally options to the user, which can be modified to recover different quantities of interest. The neutron flux tally, and some common modifications that are applied to it, will be discussed in a general sense. A detailed description of the way these tallies are applied in this research to recover the neutron flux from MCNP simulations in MNR can be found in Section 3.4, and a discussion of statistical uncertainties can be found in Section 2.4.1.

MCNP uses a pathlength estimator as the basis for determining the neutron flux. Consider a finite, three-dimensional region of interest: within this volume element (called a cell), the distance travelled by all neutrons, per unit volume, ultimately provides an estimate of the number of neutrons per cm^2 [28]. This quantity (neutrons per cm^2) can be tallied directly by MCNP for a user-designated volume, and is known as an F4 tally, which is formally defined as follows [25]:

$$\boldsymbol{F4\ tally} = \left(\frac{\mathbf{1}}{\boldsymbol{V}}\right)\int_{0}^{t}\int_{E_{lower}}^{E_{upper}}\int_{0}^{V}\boldsymbol{\phi}(\boldsymbol{r},\boldsymbol{E},\boldsymbol{t})\,\boldsymbol{d^3rdEdt} \qquad 20$$

By default, tallies are normalized per source particle (i.e. per fission neutron), so that the neutron flux can be recovered as follows:

$$\boldsymbol{\phi = (F4\ tally) \cdot \frac{(number\ of\ fission\ neutrons)}{(k_{eff})}} \quad 21$$

$$\boldsymbol{\phi = (F4\ tally) \cdot \left(\frac{P\nu}{QE_{fission}}\right) \cdot \left(\frac{1}{k_{eff}}\right)} \quad 22$$

In the equation above:

P: Reactor power [W = J s^{-1}]

ν: Average number of neutrons released per fission event [ν ~ 2.4 for ^{235}U [21]]

Q: Conversion factor [Q = 1.6022x10^{-13} J MeV^{-1}]

$E_{fission}$: Average energy released per fission event [$E_{fission}$ ~ 200 MeV for ^{235}U [19]]

k_{eff}: Effective multiplication constant of the system [~]

By default, F4 tallies report particles across the entire energy spectrum and for all time. However, this phase space can be subdivided by the user to recover information about a particular subset of particles. Additionally, these tallies can be modified with multipliers, to take the form [29]:

$$\boldsymbol{modified\ F4\ tally = C \int_{E_{lower}}^{E_{upper}} (F4\ tally)\underline{R}(E)dE} \quad 23$$

Here, $\underline{R}(E)$ is the user-designated response function (i.e. a cross section for a particular reaction), and C is a normalization constant. By judiciously applying these tally multipliers, quantities derived from the neutron flux (reaction rates, radiation doses, nuclear heating etc.) can be recovered within the core. As will be discussed in Chapter 3, certain types of reactor physics experiments estimate the neutron flux from a measurement of an (n, x) reaction within the core. The ability to recover these reaction rates with MCNP directly is a valuable asset in performing code validation studies via a direct comparison between experimental and computational results.

2.3 The Neutron Flux Spectrum

Computational methods are generally required to solve the neutron transport equation in a complex reactor environment. However, a theoretical form of the neutron flux in a LWR can be described by combining well-established experimental results with a series of simplifying assumptions. In what follows, this theoretical spectrum will be derived, and the final result will represent a basis

for understanding neutron behavior within a LWR core. This formulation of the flux spectrum will be applied in the measurements and analyses presented in Chapter 5 and Chapter 6.

The neutron flux spectrum in a LWR is defined by the distribution of neutrons released during the fission process, and by their subsequent moderation to lower energies. Typically, this spectrum is sub-divided in to three broad energy groups for analysis: the thermal, the epithermal, and the fast energy groups; this is shown in Figure 9.

In what follows, the derivation of the theoretical form of the neutron fluxes in each of these energy groups will be shown. Some of their important features and deviations from theoretical behavior that occur in a reactor setting, will be discussed.

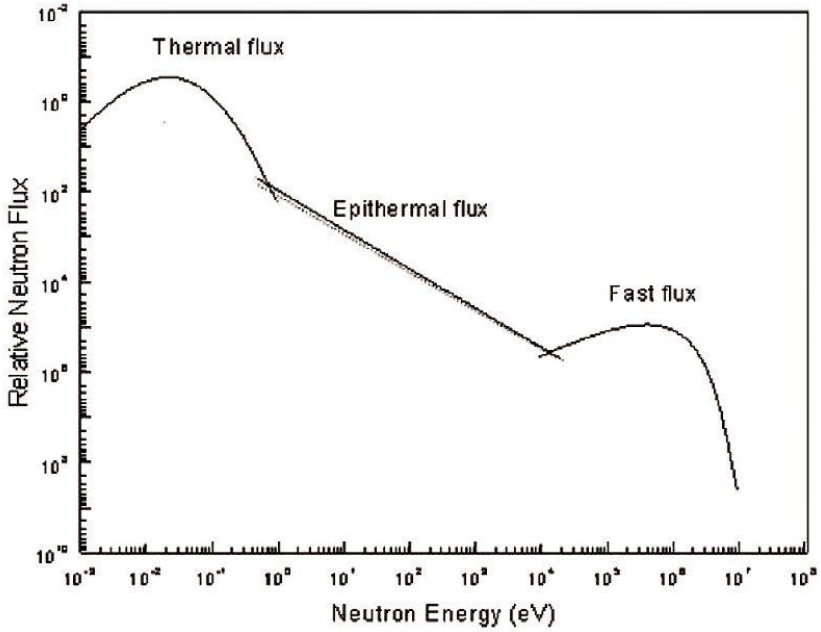

Figure 9: Neutron flux spectrum in a generic LWR system [30]. The three energy groups are shown here.

2.3.1 The Fission Spectrum

During the fission process, several neutrons ($\nu \sim 2.4$ for the fission of ^{235}U) are released with an energy above ~ 0.1 MeV [21]. The majority of the neutrons that are generated during fission are ostensibly released instantaneously (within ~ 10^{-14} s). However, a small fraction of these neutrons (less than 1%) are borne from the decay of fission products (i.e. > 1 ms after the fission event) [21]. These two groups of neutrons are referred to as the *prompt* and *delayed* neutrons, respectively. Delayed neutrons are typically described by six energy groups, each having an associated production time and representing a fraction of the total neutron yield. Such delayed

neutrons are generated at lower energies than the prompt neutrons and are insignificant above approximately 2 MeV [21]. While these delayed neutrons are instrumental in reactor control, for a ^{235}U system, they represent only 0.65 % of the total neutrons released during fission, and a set of MCNP simulations performed during the course of this research has determined that they are insignificant in the development of this research [19]. Unless explicitly described otherwise, further mentions of the fission spectrum or of the fast neutron flux refer solely to the prompt neutron spectrum.

This fission spectrum acts as the source of neutrons at all lower energies, and in the case of ^{235}U, is generally defined by the so-called Watt spectrum [31]:

$$\boldsymbol{\phi_{fission}(E) \propto \sqrt{E} e^{-bE} \sinh\left(c\sqrt{E}\right)} \quad 24$$

The fit parameters have been empirically determined to be b = 1.036 and c = 1.51 – and while these values may depend on the exact nature of the system being studied, this representation of the fission spectrum is generally appropriate for light-water reactor systems [32].

2.3.2 The Epithermal Spectrum

The nature of the epithermal neutron flux is determined by the slowing down of the neutrons released during fission, as they interact with the moderating material and lose energy through a series of either elastic or inelastic collisions. In what follows, a simplified case (i.e. moderation in an infinite, homogeneous medium with no up-scattering or loss due to absorption) will be derived, followed by a discussion of the deviations from this theoretical behavior that would be expected in a typical reactor system, with an emphasis on the role of neutron absorption. This case can be derived by starting with a simplified form of the neutron transport equation [18]:

$$\boldsymbol{\Sigma_s(E)\phi(E) = S(E) + \int \Sigma_s(E' \rightarrow E)\phi(E)dE} \quad 25$$

The above equation represents a neutron balance around the energy interval E: neutrons are lost by scattering on the left-hand side, and neutrons enter the interval either by scattering or other source terms on the right-hand side. Any moderation by inelastic scattering will be ignored in this analysis, as at all energies, $\Sigma_{elastic} >> \Sigma_{inelastic}$ for hydrogen, as shown in the figure below.

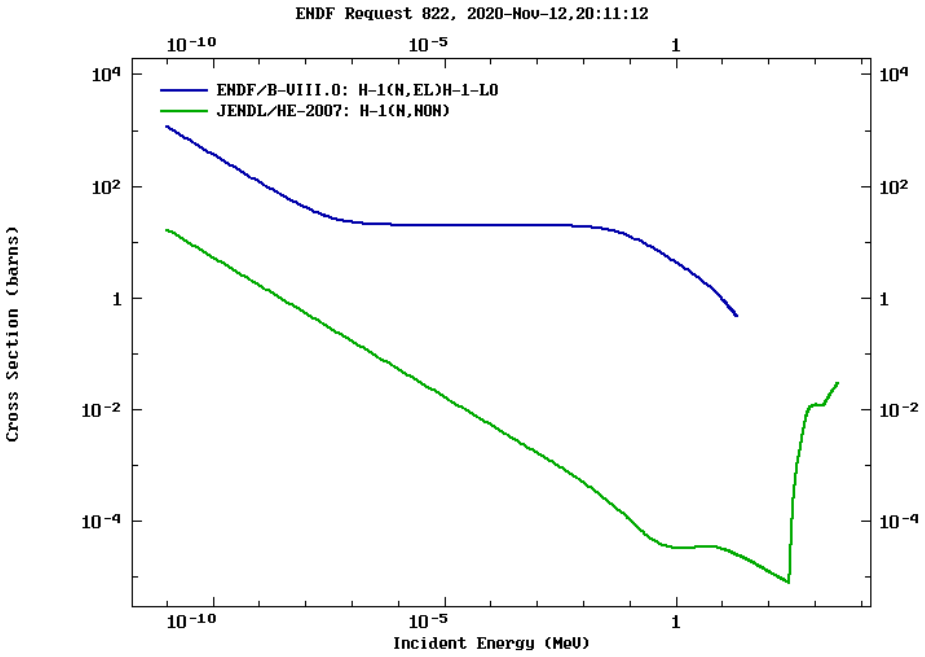

Figure 10: Elastic (blue) and inelastic (green) scattering cross sections of hydrogen [22].

The kinematics of elastic scattering must first be considered. The following figure shows an elastic scattering interaction between an incident neutron and a stationary moderator nucleus.

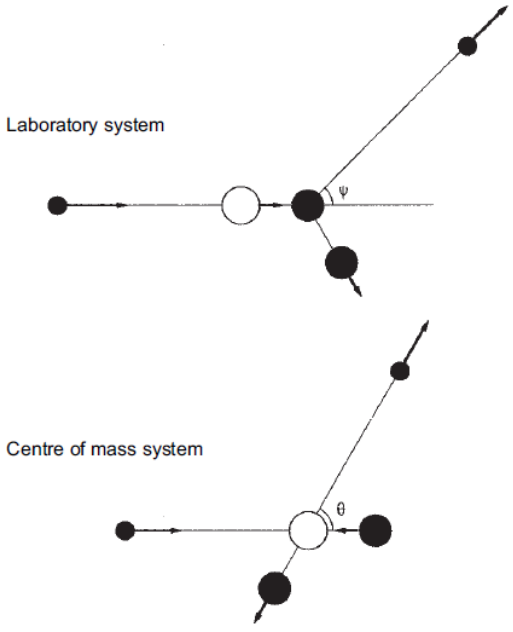

Figure 11: Schematic showing an elastic scattering event in both the laboratory and center-of-mass frames [27].

By applying a transformation to the center-of-mass frame, and using of the law of cosines, the relationship between the initial and final energy of the incident neutron can be determined [18]:

$$\frac{\boldsymbol{E}}{\boldsymbol{E'}} = \left(\frac{\mathbf{1}}{\mathbf{2}}\right)\left((\mathbf{1}+\boldsymbol{\alpha'}) + (\mathbf{1}-\boldsymbol{\alpha'})\mathbf{cos}\,(\boldsymbol{\psi})\right) \quad 26$$

Here, ψ is the scattering angle in the center-of-mass frame, and α' is the scattering parameter (α' = 0 for hydrogen). The maximum energy loss for a single elastic scattering event occurs in a head-on collision (i.e. ψ = 180º) so that E = α'E'. To simplify the in-scattering cross section term in Equation

$$\boldsymbol{\Sigma_s(E)\phi(E) = S(E) + \int \Sigma_s(E' \rightarrow E)\phi(E)dE} \quad 25$$

, consider the probability that a neutron having an initial energy E' is scattered in to an energy interval E + dE. Since the post-collision energy varies linearly with cos(ψ), and the scattering of neutrons by hydrogen is known to be isotropic, this probability can be expressed as [18], [27]:

$$\boldsymbol{P(E' \rightarrow E)dE} = \left(\frac{\mathbf{1}}{\boldsymbol{(1-\alpha')E'}}\right)\boldsymbol{dE} \quad 27$$

The in-scattering cross section in Equation

$$\boldsymbol{\Sigma_s(E)\phi(E) = S(E) + \int \Sigma_s(E' \rightarrow E)\phi(E)dE} \quad 25$$

can therefore be expressed as:

$$\boldsymbol{\Sigma_s(E' \rightarrow E)} = \begin{cases} \dfrac{\boldsymbol{\Sigma_s(E')}}{\boldsymbol{(1-\alpha')E'}} & \boldsymbol{\alpha E' < E < E'} \\ \mathbf{0} & \boldsymbol{otherwise} \end{cases} \quad 28$$

By making this substitution, the simplified version of the neutron transport equation becomes:

$$\boldsymbol{\Sigma_s(E)\phi(E) = S(E) + \int \frac{\Sigma_s(E')}{E'}\phi(E')dE'} \quad 29$$

The above equation can be solved by introducing the placeholder variable $F(E) = \Sigma_s(E)\phi(E)$ (noting that the scattering parameter α is equal to zero in the case of moderation by hydrogen), which gives [33]:

$$\boldsymbol{F(E) = S(E) + \int \frac{F(E')}{E'}dE'} \quad 30$$

By differentiating this equation with respect to E, this can be transformed in to an ordinary differential equation, and solved by introducing an integrating factor. At energies much lower than the source (i.e. E << E'), the result is:

$$\boldsymbol{F(E) = \left(\frac{1}{E}\right) \int S(E')dE'} \quad 31$$

The integrated source term in this equation is the total number of neutrons (across all energies) produced per $cm^2 \cdot s$ (in other words, this is the energy integrated fission spectrum). If this term is denoted by some constant C, then the epithermal neutron flux spectrum is defined by the following equation [33]:

$$\boldsymbol{\phi_{epithermal}(E) = \frac{C}{E\Sigma_s(E)}} \quad 32$$

In the case of hydrogen moderation, the scattering cross section is approximately constant in this energy range (see Figure 10), and the epithermal neutron flux spectrum is therefore proportional to E^{-1}.

This mathematical analysis can also be applied to determine the nature of the epithermal neutron flux spectrum when the neutrons are removed from the energy interval by both absorption and moderation processes; Equation 25 is modified so that the left-hand side contains the total interaction cross section (i.e. $\Sigma_t = \Sigma_s + \Sigma_a$). The solution to this updated equation reveals that the epithermal neutron flux is proportional to both E^{-1} and the resonance escape probability, p(E) [18]:

$$\boldsymbol{\phi_{epithermal}(E) \propto \left(\frac{1}{\Sigma_t(E)E}\right) p(E)} \quad 33$$

$$\boldsymbol{p(E) = e^{-\int \frac{\Sigma_a(E)}{\Sigma_t(E)}\left(\frac{dE}{E}\right)}} \quad 34$$

It may not be possible to determine the analytical form of either p(E) or $\Sigma_t(E)$ given the complex geometries and material compositions of real reactors however, in this case, it has been suggested that the epithermal neutron flux be represented by a modified E^{-1} spectrum [32]:

$$\boldsymbol{\phi_{epithermal}(E) \propto \frac{1}{E^{1+\alpha}}} \quad 35$$

The deviations from ideality are captured by the dimensionless constant α. If $\alpha > 0$, the spectrum is over-moderated, and if $\alpha < 0$, the spectrum is under-moderated.

2.3.3 The Thermal Spectrum

Neutrons in a reactor will not continue to be moderated indefinitely; if not lost to leakage, absorption, or thermal fission, they will reach a thermal equilibrium with their surroundings such that the thermal neutron flux spectrum can be described by a Maxwellian distribution [27], [32]:

$$\boldsymbol{\phi_{thermal}(E) \propto \left(\frac{E}{(kT')^2}\right) e^{-\frac{E}{kT'}}} \quad 36$$

The following values are associated with a room temperature Maxwellian distribution [27]: T_0 = 273 K, v_0 = 2200 m/s, E_0 = 0.0253 eV.

While there may be sufficient neutron losses in areas either near the fuel or at the periphery of the core that violate the equilibrium conditions, in regions with a large volume of moderator (i.e. in irradiation sites), the above form of the thermal neutron flux is generally valid [18]. In a reactor, the continuous source of neutrons from the epithermal energy range results in the thermal neutron flux being Maxwellian in nature, but having a higher average energy than the values noted above [32].

The neutron flux in a LWR can therefore generally be described by the following equation:

$$\boldsymbol{\phi(E) = \begin{cases} \phi_{thermal}(E) \propto \frac{E}{(kT')^2} e^{-\frac{E}{kT'}} \\ \phi_{epithermal}(E) \propto \frac{1}{E^{1+\alpha}} \\ \phi_{fast}(E) \propto \sqrt{E} e^{-bE} \sinh\left(c\sqrt{E}\right) \end{cases}} \quad 37$$

Having elucidated the fundamentals of reactor physics here, the following section discusses uncertainty analysis and error propagation to provide further context for the methods discussed in Chapter 3.

2.4 Uncertainty Analysis

Any quantity determined through experimental or computational methods must be accompanied by a reported uncertainty. Although it may be straightforward to recover this uncertainty from directly measured quantities, standard rules for propagating uncertainties must be applied when additional data processing is required. In what follows, these rules will be presented, followed by

a discussion of the source of these uncertainties, and some common variance reduction techniques for both experimental and computational methods. First, however, some common terminology in the context of uncertainty analysis and uncertainty propagation must be defined:

- Uncertainty: A quantification of the doubt associated with a quantity, and an expression of the fact that there are an infinite number of values dispersed around said quantity that are consistent with the physical definition of the problem [34]. When associated with a measured quantity, this uncertainty then represents "the dispersion of possible values that could reasonably be attributed to the measurand" [35].
- Error: The difference between the result of a measurement and the true value of the quantity. Errors may have both a random and systematic component [35].
- Random Error: A source of error whose effects are stochastic, and may be determined by repeated measurements of the same quantity [34].
- Systematic Error: This causes a uniform shift in the measured values, and is also known as a bias [36]. If this quantity is know, it can be accounted for with a correction factor [35].

In general, the true value of the quantity being studied is unknown, and the uncertainty (rather than the error) is therefore reported as the figure of merit [35].

The following equations are a summary of the standard rules of uncertainty propagation for common forms of numerical operations applied during data processing [35], [36].

For quantities that are added together:

$$\boldsymbol{y = \sum_{i=1}^{N} x_i}$$
$$\boldsymbol{\delta y = \sqrt{\sum_{i=1}^{N} (\delta x_i)^2}} \quad 38$$

For independent quantities that are multiplied together:

$$\boldsymbol{y = \prod_{i=1}^{N} x_i}$$
$$\boldsymbol{\delta y = y\sqrt{\sum_{i=1}^{N} \left(\frac{\delta x}{x}\right)^2}} \quad 39$$

For quantities that are processed by some general function, where some terms may be covariant:

$$y = f(x_1, x_2 \ldots, x_N)$$

$$\delta y = \sqrt{\sum_{i=1}^{N}\left(\frac{\partial y}{\partial x_i}\cdot \delta x_i\right)^2 + 2\sum_{i=1}^{N-1}\sum_{j=i+1}^{N}\left(\frac{\partial y}{\partial x_i}\right)\left(\frac{\partial y}{\partial x_j}\right)cov(x_i, x_j)} \quad (40)$$

These rules provide a framework for determining the uncertainty associated with a value recovered through some data processing steps – and can be readily applied to most procedures, where data processing may involve only the application of simple mathematical operations. The data processing undertaken for this thesis is developed at length in Chapter 3, where the uncertainties involved in the final determination of the neutron flux will also be discussed.

While these rules can be applied to either experimentally or computationally determined values, the source of uncertainties (and therefore the techniques that can be applied to minimize uncertainty) differ significantly. Some sources of experimental uncertainty, and variance reduction techniques that can be applied to both experimental and computational methods will be introduced, and generally discussed.

2.4.1 Statistical Uncertainty in Stochastic Neutron Transport Calculations

Uncertainties that arise from statistical sampling (i.e. as is the case of Monte Carlo methods) depend on several user-defined parameters, primarily among them: the sample size being considered, and the application of any variance reduction techniques [25]. The tally definition used to recover the quantity of interest may also impact the precision of the final result; a tally defined over a smaller volume element may produce less precise results than one defined over a larger volume element. In general, an efficient tally will consider as large a region as is practically possible [25]. As the size of the tally regions in this research are chosen to match the experimental conditions, this parameter cannot be modified as a means of variance reduction.

The precision of a statistically determined value is related to the sample size being considered [25]:

$$\delta y \propto \frac{1}{\sqrt{sample\ size}} \quad (41)$$

In general, the sample size is the number of events being considered (i.e. the number of rolls of a dice to determine the probability of rolling an even number); in the context of MCNP simulations, this refers to the number of particle histories set by the user. It is important to note that increasing

the number of histories (and by extension, the computation time) by a factor of four only improves the precision by a factor of two; it may therefore be impractical to achieve a desired precision simply by increasing the number of particle histories. Indeed, it is the computation time required to achieve a particular precision that should be minimized, rather than the precision itself [26].

To realize the desired precision, several different types of variance reduction techniques can be applied to the problem. Although no variance reduction techniques were applied in this thesis, they are briefly discussed here for completeness.

The simplest of these techniques involves truncating a portion of the phase space that does not contribute significantly to the final result. In MCNP, particles can be assigned cut-off values for both their time and energy, beyond which they are not tracked, thereby reducing the computation time required to generate a solution [25], [29]. Additionally, the problem can be modified so that sampling occurs not from the distributions that describe the physics of the problem, but from user-defined functions that favor the tallies of interest (i.e. selectively generating particles with a particular energy or direction) [28]. If necessary, deterministic-transport regions (the DXTRAN card in MCNP) can be inserted in the model to circumvent the usual random-walk methods and apply deterministic techniques in these regions instead [29]. Finally, techniques involving splitting the problem can be used to control the population of particles, such that there are more particles in regions deemed to be important by the user [26]. This is done by assigning each cell in the problem an importance, and based on the relationship between the importances of adjacent cells, either splitting, killing (by Russian Roulette), or allowing a particle to continue unimpeded as it passes from one cell to another [28].

2.4.2 Experimental Uncertainty

Although computational uncertainties are generally the result of the problem definition, and can be addressed by mathematical techniques to achieve a desired level of precision, it may not be possible to rigorously identify, quantify, and reduce experimental uncertainties in the same way. Uncertainties in experimental procedures may arise from repeatability issues (i.e. changing conditions during experimentation or instability in the measurand), the measurement procedure (i.e. instrumentation bias or calibration uncertainties), or from any imported quantities that are used during data processing [34]. Furthermore, uncertainties in high-level parameters such as the reactor power may manifest as additional uncertainties in the reported neutron flux. There is no

prescribed method for reducing uncertainties in a general experimental procedure; expert judgement must be relied upon to improve the results where possible. For example, when dealing with imported quantities, a judicious study of all available databases from whence these quantities came can be undertaken to determine appropriate uncertainty bounds. The main objectives of this thesis are: to identify, to quantify, and (if possible) to reduce significant sources of experimental uncertainty in flux measurements.

3 Methodology

3.1 Background

This chapter is dedicated to the experimental and computational methods that are applied in this research. MNR and its associated experimental facilities are first presented and discussed, followed by a detailed description of both the MCNP model of MNR and the specific data collection and data processing steps taken to recover in-core measurements of the neutron flux. The sources of experimental uncertainty (for which this thesis aims to develop a general procedure for their propagation and reporting through a detailed investigation of one site in MNR) are identified. A full SOP regarding the experimental methods can be found in Appendix A.

3.2 The McMaster Nuclear Reactor

MNR is a light-water cooled and moderated, open-pool MTR with a full negative pressure containment system, located on the campus of McMaster University in Hamilton, Ontario. Reactor operations began in 1959 and it has been continually used for academic, educational, commercial, and medical purposes in the time since. The reactor is currently licenced to operate at 5 MW_{th}, and is currently seeking to extend its operating license beyond its current 2024 mandate [37].

The MNR facility is currently a world-leader in the production of ^{125}I, which is typically used in brachytherapy treatments of prostate cancer. The development of other useful medical isotopes and various cross-disciplinary research projects are also actively being pursued in the facility [38]. The desire to supply isotope production planners with reliable neutron flux estimates that included fully realized uncertainty values was an additional motivator for this work.

In the following section, the reactor itself (and its associated experimental facilities) will be discussed, and will be accompanied by a description of the MCNP model of MNR that has been used to generate computational estimates of the in-core neutron flux.

3.2.1 Reactor Facilities

The core of MNR is defined by a (9 × 6) grid configuration that typically houses 34 fuel assemblies, and which is reflected along its southern side by graphite assemblies (see Figure 12); it is flanked by a lead block and six beam tubes on the remaining sides. Figure 12 illustrates some of these features in an overhead view of a reference core in MNR.

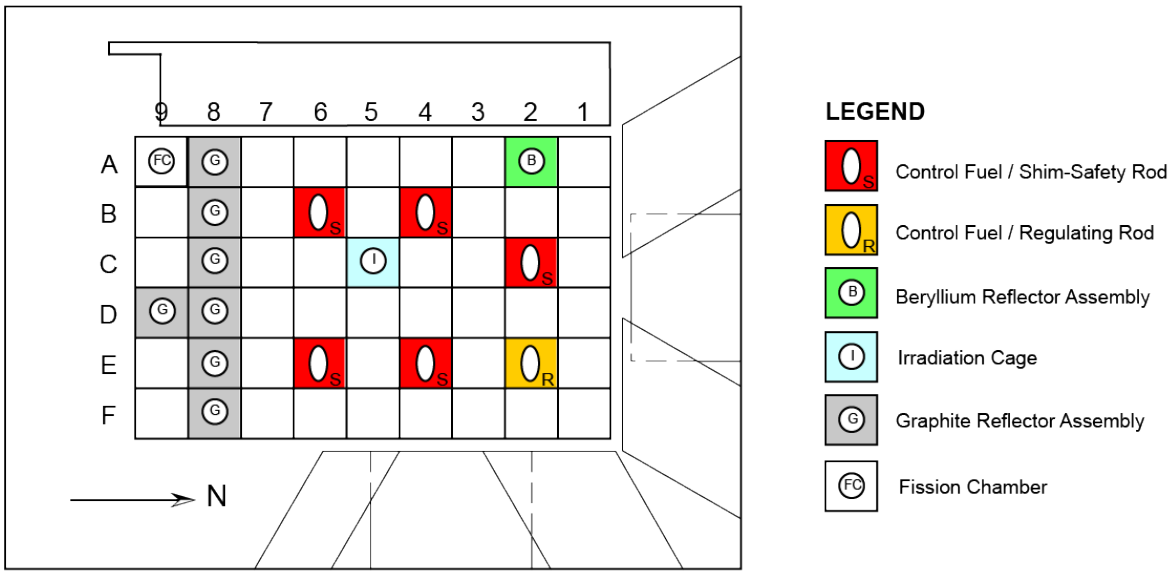

Figure 12: Overhead view of a reference core configuration of MNR. The fuel assemblies are housed in rows 1 to 7 and the graphite reflectors are located in rows 8 and 9. The lead block sits on the West side of the core, and the beam tubes flank the core on the North and East sides of the facility. Thanks to Dr. Simon Day for providing this figure.

At MNR, fuel management operations are performed as-needed, based on the inferred fuel depletion recovered from in-core neutron flux measurements and by tracking the integrated power produced in each assembly. The flux measurements utilize CuMn wires placed between the fuel plates of each assembly, and they provide an estimate of the power distribution in the core. When either these measurements, the integrated assembly power, or the control rod positions dictate, fuel management operations (i.e. refuelling or fuel shuffling) are performed. Under typical operating conditions (i.e. at 3 MW_{th}, on a 16 hours-per-day, 5 days-per-week schedule) the core is refuelled approximately twice per year (which constitutes the replacement of one or two assemblies), and fuel shuffling operations are performed approximately every two months [39].

Between 1959 and 1998, MNR fuel assemblies contained HEU (93% ^{235}U enrichment). However, following an 8-year core-conversion period, all fuel assemblies in the core are now loaded with LEU (19.75% ^{235}U enrichment) [40]. Standard MNR fuel assemblies consist of 18 curved plates stacked parallel to each other – of which the two outermost plates are solid aluminium, and are referred to as *dummy* plates. The active fuel region (which is 60 cm in length) is contained in the inner plates in the form of uranium silicide dispersed in an aluminium matrix. These plates are supported along their sides by thick aluminium plates, and are fitted with a snout on the bottom

such that they can be loaded into the underlying grid plate. Control assemblies are structurally similar to these standard assemblies; however, they contain only 9 plates (all of which contain fuel) and include a central guide tube to accommodate the control rod itself [39]. The following figure shows an overhead view of both a standard and control assembly in MNR.

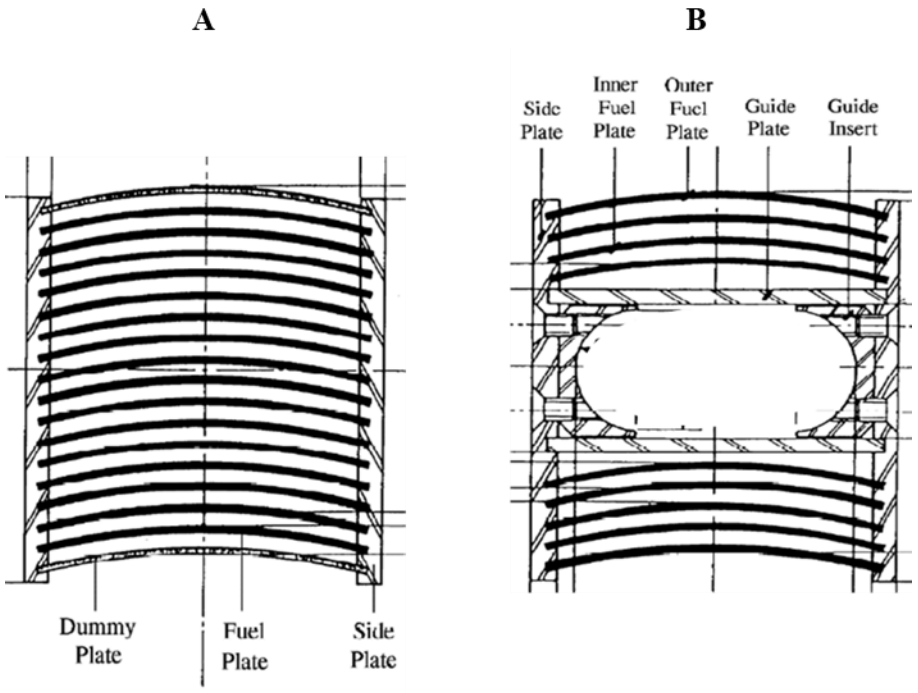

Figure 13: Overhead view of a standard assembly (A) and a control assembly (B) showing the fuel, dummy, and side plates, and the structural components that house the control rods [40]. Dimensions have been removed from this figure.

Of the six control assemblies housed in the core, five are gang-operated Ag-In-Cd shim safety rods (for coarse reactivity control and shutdown procedures), and one is a stainless-steel regulating rod that provides automatic fine reactivity control. Under normal operating conditions the control rods are driven downwards into the core using motors and an electromagnetic clutch. In the event of a loss of electrical power, or during shutdown procedures, the electromagnetic clutch will release and the control rods will fall under the action of gravity [39].

The features of MNR described above are central to its successful operation. However, there are also several sites within the core that can host a variety of irradiation procedures without interrupting normal operations. These sites – and the equipment necessary to conduct such procedures – will now be presented. A full description of the experimental methods applied, and how this equipment was used in this research can be found in Section 3.3.3.

Rows 8 and 9, as well as sites 5C and 2A of MNR (see Figure 12) are designed to accommodate irradiation procedures wherein samples may be placed in the core and exposed to its neutron flux. Such samples (which may take a variety of physical forms) cannot be placed directly in the core – they must be housed in either capsules or wire holders to preserve their structural integrity and to facilitate their placement in a precise location within the core.

When a capsule is used, it is possible to line the inside of the container with cadmium such that low energy neutrons are preferentially absorbed by this material and do not interact with the sample (Section 3.3.2 contains a detailed description of this method). If necessary, the capsules may also be loaded with discs of lead ballast to ensure the sample sits as desired in the core [39].

After the samples have been loaded in either of the pieces of equipment shown above (and confirmed to be water-tight in the case of capsule use), MNR operations staff can load it in to either a sample holder (for sites 2A, 5C and graphite assemblies in row 8) or a Reactor Irradiation Facilities for Large Samples (RIFLS) tube (for row 9). In the case of capsule irradiations, aluminium spacers measuring between 5.175” and 17” may also be loaded in the sample holder or RIFLS tube to ensure the sample sits at the desired elevation in the core [39].

Figure 14 shows an image of a sample holder next to a wire holder before they are inserted in to the core.

Figure 14: Image of a wire holder (top) and a sample holder (bottom) used during irradiation procedures [41]. A meter stick is shown between these two pieces of equipment, for scale.

This entire assembly (e.g. a sample holder containing a wire holder, which is itself housing the sample) is then placed in the core under the desired operating conditions.

The equipment used during irradiation procedures was designed to facilitate flexible experimental campaigns; wire holders and capsules can be used in any of the sites mentioned above, and their insertion and removal from the core can be readily performed by MNR operators as needed. The

modular nature of this equipment is also fully realized in the full-core MCNP model of MNR, allowing researchers to match in-core conditions for a direct comparison of computational and experimental results. A description of this model, and a discussion of some of its features and limitations, is given in the following section.

3.2.2 Computational Model

The MCNP model of MNR was originally developed in 2001 and has been regularly updated to reflect various changes in the material compositions and core layouts of MNR, and to include new equipment that may be used during experimental campaigns. In addition to its application to experimental work (as in this thesis), this model can also be used to support safety analyses and multidisciplinary research and design projects. At the time of writing, MCNP simulations of MNR are done using version 6 of the software, and make use of the ENDF-B/VI nuclear data libraries. The MCNP model of MNR is not limited to the core itself; both the beam ports flanking the pool, and the lead shielding along the western side of the core are included in its geometrical definition.

To prevent the full-core MCNP simulations from being prohibitively time-consuming and to make use of its built-in lattice geometry capabilities, several simplifications are made in the geometrical definition of the core. Primarily among them are the modelling of the fuel plates as straight (rather than curved, as seen in Figure 13), and – for burnup purposes – the subdivision of the fuel into 7 distinct regions along the vertical direction of the core. These features of the model are shown in Figure 15.

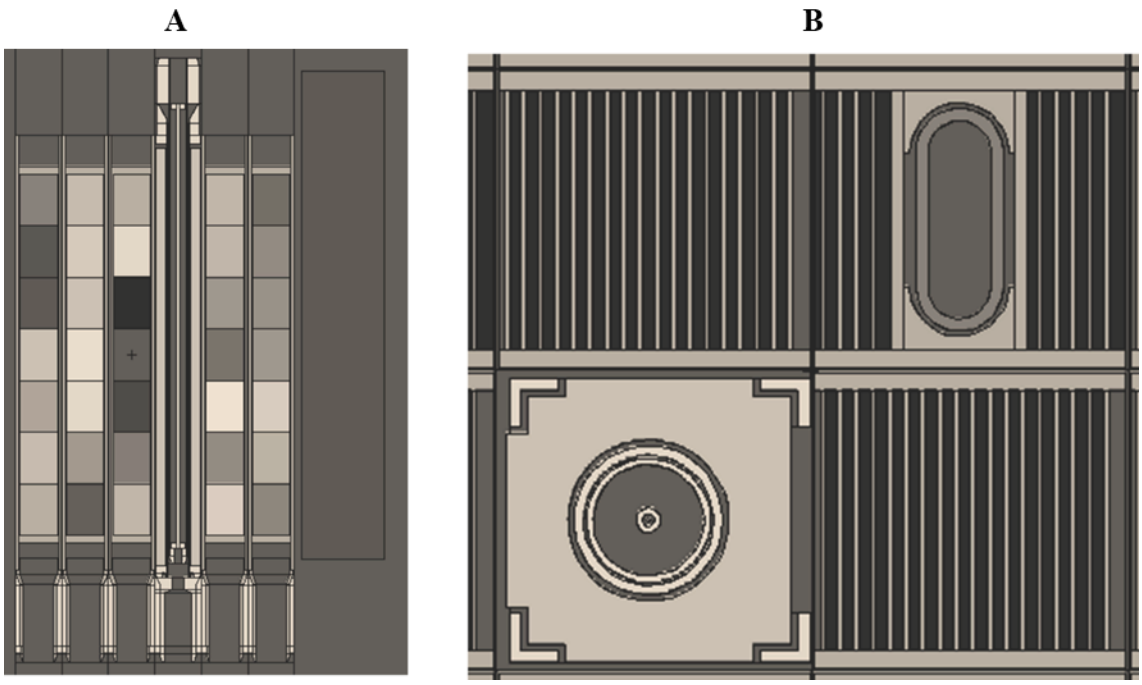

Figure 15: Some important features of the MCNP model of MNR. The 7 axial regions of the fuel are shown (A) in an east/west plane view of the core. The straight fuel plates can be seen (B), along with a control assembly and a graphite assembly containing a sampler holder + wire holder configuration. Colour has been removed from this image for clarity.

Although a coarse definition of burnup in the fuel has been observed in other research reactors to cause significant discrepancies between experimental and computational results [16], a sensitivity analysis performed on the TRIGA reactor at the Jožef Stefan institute has indicated that, with 5 axially-defined fuel regions, further refinement of the burnup definition does not significantly change the neutron flux results [15]. The use of 7 burnup-based fuel regions in the MCNP model of MNR is therefore appropriate for generating high-fidelity neutron flux results under any core configuration. Additionally, while both the fuel and dummy plates in all MNR assemblies are modelled as straight rather than curved, the volume of both the plates and the coolant channels are preserved, and this is therefore a purely geometrical simplification and does not represent a change to the underlying problem physics [41].

In order to describe the modular nature of MNR, the core is modelled in MCNP as a series of independent universes, where each can be filled with the different types of assemblies that are found in MNR (i.e. a standard fuel assembly, a graphite reflector, etc.). These universes are then used to fill the underlying grid configuration (i.e. lattice) of MNR. For example, a standard fuel assembly labelled as universe 1 can be used to fill site 2B in the core. This is extended to the model

definition at a sub-assembly level: a single standard assembly is fully defined, and the others are modelled based on this reference assembly using the *like but* syntax within MCNP. By structuring the model in this way (i.e. with fixed references to various cells and universes) changing the material definition of the fuel based on burnup data requires updating the material card *only*, rather than updating each fuel assembly individually. By exploiting the *universe*, *fill*, *lattice*, and *like but* MCNP commands in this way, any core configuration (real or proposed) can be modeled without making significant adjustments to the problem definition.

As described above, the model has been written such that adjusting the core configuration or the fuel composition to reflect typical operations can be readily performed. It is therefore possible to couple MCNP simulations with core-follow results to generate up-to-date data for MNR. The core-follow results for MNR used in this thesis are performed using the Overall System for Calculation of Reactors (OSCAR) code system as part of an on-going reactor physics project within MNR; the output from these simulations can be used as inputs for the MCNP fuel composition in each assembly. Although the full development of an OSCAR model remains outside the scope of this thesis, as OSCAR results were applied as inputs to the MCNP model of MNR, an overview of the code system is presented in the following paragraphs for completeness. Further discussions about the role of OSCAR results in this work can be found in the second journal article of this thesis (in Chapter 5).

OSCAR is a nodal-diffusion-based deterministic code that can be used to recover the material composition of the fuel at various points during its lifecycle. A two-dimensional cell calculation (wherein the Joint Evaluated Fission and Fusion (JEFF) 2.2 nuclear data libraries are applied) is followed by a three-dimensional core calculation using the Multi-Group Reactor Analysis Code (MGRAC) [42]. The following 38 isotopes are tracked explicitly throughout the analysis:

- $^{[234\text{-}238]}U$
- ^{237}Np, ^{239}Np
- $^{[242\text{-}248]}Pu$
- ^{241}Am, ^{243}Am
- $^{[242\text{-}245]}Cm$
- ^{135}I
- ^{135}Xe
- ^{141}Ce, ^{142}Ce, ^{144}Ce
- ^{143}Pr
- $^{[143\text{-}148]}Nd$
- $^{[147\text{-}149]}Pm$
- $^{[147\text{-}149]}Sm$
- ^{10}B

The MCNP material cards generated through the OSCAR-based analysis will be applied in this research, as necessary.

As the MCNP model of MNR is intended to complement the neutron flux measurements presented in this thesis, the experimental methods will first be presented, followed by a discussion of the computational methods that are used to match the experimental conditions. A discussion of these experimental methods is presented in Sections 3.3.1 and 3.3.2, and a complete description of the procedure is given in Section 3.3.3. A full SOP can be found in Appendix A, which provides specific details about the equipment and its calibration, the health physics considerations, and the code used to process the raw data.

3.3 Experimental Methods

Because neutrons are non-ionizing particles, their detection often requires that an intermediate reaction be exploited such that an ionizing particle can be created and directly measured. Several methods making use of an intermediate reaction (i.e. Bonner Spheres or recoil spectroscopy [43]) can (in general) be applied to measure the properties of a neutron source; since this thesis aims to recover the in-core neutron flux, this discussion will focus on the principles of neutron activation analysis (NAA), which provides a high degree of flexibility in its application. NAA is widely applied for chemical analyses of unknown samples by irradiating a target in a well-defined neutron field; however, in the present application, a well-defined material will be used to infer various properties of the in-core neutron flux [43]. While NAA for neutron flux measurements is well-documented, a full description of the techniques applied in this work is presented here to emphasize the full consideration of uncertainty at every stage of data collection and analysis.

In what follows, the principles of NAA will be discussed, along with relevant equations that govern a typical NAA-type experimental procedure. Some special cases and techniques that are common in the application of NAA in research reactors will also be presented and discussed. The techniques presented here are applied in each of the three articles that make up this sandwich thesis – a detailed discussion of the theory of computational Bayesian methods can be found in the third journal article of this sandwich thesis (Chapter 6), as those methods are unique to that study.

3.3.1 Neutron Activation Analysis

Of the neutron interactions listed in Chapter 2, many neutron capture reactions (i.e. (n, γ), (n, α), (n, p) etc. or more generally, (n, x) reactions) are known to create unstable isotopes in certain target materials. When placed in a neutron field (i.e. irradiated), this transmutation of the target via an (n, x) reaction proceeds at a rate governed by the following equation [18]:

$$\boldsymbol{R = AT = N \int \phi(E)\sigma_{n,x}(E)dE} \quad 42$$

The terms in the equation above are defined as follow:

R	(n, x) activation rate in the target material [atoms s^{-1}]
A	Net activity of the now-radioactive target material [s^{-1}]
T	Time constant to account for the evolution of radioactivity in the sample [~]
N	Number of precursor atoms in the target material [atoms]
ϕ(E)	Neutron flux energy spectrum [cm^{-2} s^{-1} eV^{-1}]
$\sigma_{(n, x)}(E)$	(n, x) cross section [cm^2]

The net activity of the now-radioactive sample (A) includes corrections for detection efficiencies, γ-ray intensities, self-shielding, and background radioactivity, such that:

$$\boldsymbol{A = \frac{A_{net}\Omega}{GI_\gamma}\left(\frac{1}{\eta}\right)} \quad 43$$

The time constant (T) accounts for the evolution of radioactivity in the sample during irradiation and during any decay time between irradiation and data collection:

$$\boldsymbol{T = \frac{e^{\lambda t_{decay}}}{1 - e^{-\lambda t_{irr}}}} \quad 44$$

The number of precursor atoms in the target (N) is determined from its molecular properties, and its mass:

$$\boldsymbol{N = \frac{mN_A\theta}{M}} \quad 45$$

The terms in Equations 43 to 45 can be divided in to two categories: directly measured quantities, and material or system parameters that can be accessed from various databases or calibration results. The following table lists each of these terms according to their category.

Table 1: Summary of the measured quantities and required parameters involved in experimental NAA procedures.

	Measured Quantities	
$\mathbf{A_{net}}$	**[s^{-1}]**	Net γ-ray activity of the sample
$\mathbf{t_{decay}}$	**[s]**	Decay time
$\mathbf{t_{irr}}$	**[s]**	Irradiation time
m	**[g]**	Sample mass
	Material or System Parameters	
Ω	**[~]**	Geometric correction factor
G	**[~]**	Self-shielding factor for the target nuclei in the bulk sample [44]
$\mathbf{I_\gamma}$	**[~]**	γ-ray intensity [45]
η	**[~]**	Detection efficiency at the γ-ray energy of interest
λ	**[s^{-1}]**	Decay constant of the nuclei of interest [45].
$\mathbf{N_A}$	**[mol^{-1}]**	Avogadro's number, $N_A = 6.022x10^{23}$
θ	**[~]**	Isotopic abundance of the target nuclei in the bulk sample [46], [47]
M	**[g mol^{-1}]**	Molar mass of the sample [46], [47]

Careful materials selection ensures that sufficient radioactivity can be induced to generate high-fidelity measurements without compromising the health physics criteria that regulate the safe transportation and handling of the material.

3.3.2 Flux Measurements with Neutron Activation Analysis

To convert a measurement of the activation rate R to a flux value, some information about the target cross section (see Equation 42) must be included in the data processing. For flux measurements in research reactors, it is common to calculate an *effective* cross section [8], [11]:

$$\boldsymbol{\sigma_{effective}} = \frac{\int_{E_{low}}^{E_{high}} \boldsymbol{\phi(E)\sigma_{n,x}(E)dE}}{\int_{E_{low}}^{E_{high}} \boldsymbol{\phi(E)dE}} = \frac{\int_{E_{low}}^{E_{high}} \boldsymbol{\phi(E)\sigma_{n,x}(E)dE}}{\boldsymbol{\Phi}} \quad 46$$

By combining Equation 42 and Equation 46 the energy-integrated neutron flux is therefore:

$$\boldsymbol{\Phi} = \left(\frac{\boldsymbol{R}}{\boldsymbol{N}}\right)\left(\frac{\mathbf{1}}{\boldsymbol{\sigma_{effective}}}\right) \quad 47$$

In the absence of experimental information about the neutron flux spectrum, effective cross sections can be determined computationally for both the (n, x) reactions and the energy regions of interest. It is common to sub-divide the neutron flux spectrum in to three broad groups (discussed in Chapter 2): the thermal, the epithermal, and the fast.

Many materials useful for neutron flux determination via NAA have activation cross sections that span all energies, and therefore cannot be used to recover any one particular energy region of the neutron flux. However, by applying some special techniques in NAA, it is possible to determine the neutron flux in some of the three broad energy groups discussed in Chapter 2. The cadmium difference method and the application of threshold (n, x) reactions in NAA will each be discussed in the context of recovering different portions of the neutron flux energy spectrum, as they are used extensively in this thesis.

The (n, γ) cross section of ^{113}Cd is ~10^5 b at low energies and drops sharply in the epithermal region, and it can therefore act as a high-pass filter for neutrons during irradiation procedures [32]. This behavior of the cadmium cross section is shown in Figure 16, along with the (n, γ) cross sections of commonly used materials for flux measurements via the NAA method.

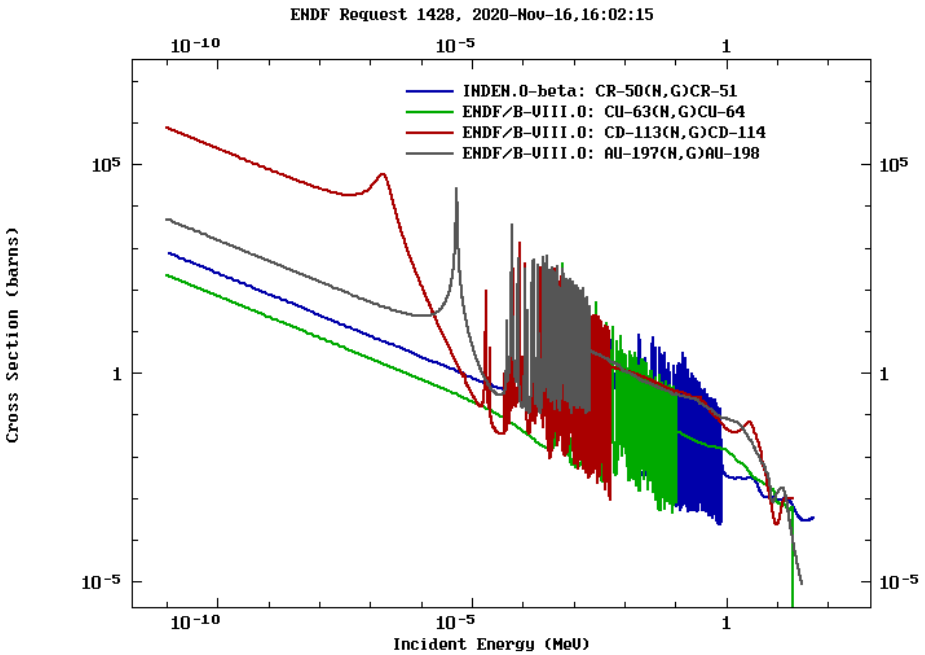

Figure 16: (n, γ) cross sections for ^{113}Cd (shown in red) and some other common materials used in NAA procedures [22].

For a neutron field with only a thermal and epithermal component, the thermal component can therefore be recovered by performing two irradiations: the first, with a bare sample, and the second with a thin layer of cadmium covering the sample, so that [18]:

$$\boldsymbol{R_{thermal} = R_{bare} - F_{Cd} R_{Cd}} \quad 48$$

In Equation 48, F_{Cd} is the *cadmium correction factor*, which accounts for epithermal neutrons that are absorbed by the cadmium layer. This value is defined as the ratio of epithermal to cadmium-covered activation rates and, though it has been tabulated for ideal neutron absorbers in an isotropic neutron flux [32]. This may also be determined computationally to capture the complex geometry and material composition of a real reactor. In general, the value of this parameter is on the order of $F_{Cd} \sim 2.5$.

Although the development of this method is based on a fictitious neutron flux without a fast component, this method can be applied in a reactor setting because the activation cross sections of most useful materials are sufficiently low for energies above ~ 0.1 MeV. This can be seen in Figure 16, where the cross sections above 0.1 MeV are generally below 1 b, such that Equation 48 remains valid. A cadmium layer of 1 mm is sufficiently opaque (having a transmission of $\sim 10^{-6}$) to thermal neutrons and is therefore appropriate for general use in NAA for flux determinations [18].

When the cross section collapsing methods (discussed at the beginning of Section 3.3.2) are applied with the cadmium difference method, the thermal neutron flux is therefore:

$$\boldsymbol{\Phi_{thermal} = \left(\frac{R_{thermal}}{N}\right)\left(\frac{1}{\sigma_{effective,thermal}}\right)} \quad 49$$

While recovering the thermal neutron flux requires two measurements, the fast neutron flux can be determined from a single measurement of the activation rate of a threshold reaction. These reactions occur only when the incident neutron has an energy that exceeds a particular threshold (typically above E ~ 0.1 MeV [18], [32]). The cross sections of some commonly used materials in the application of this method are shown in Figure 17. The fast neutron flux is therefore:

$$\boldsymbol{\Phi_{fast} = \left(\frac{R_{fast}}{N}\right)\left(\frac{1}{\sigma_{effective,fast}}\right)} \quad 50$$

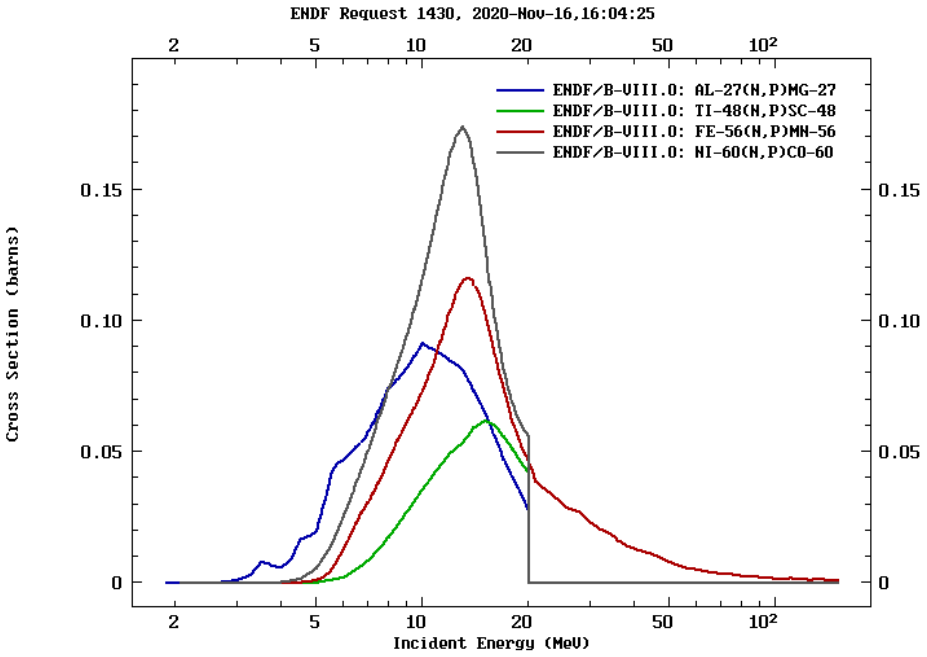

Figure 17: Threshold cross sections for some materials commonly used to recover the fast neutron flux [22]. Energies up to 100 MeV are shown here for demonstration purposes; the fast flux spectrum in a reactor does not extend beyond approximately 20 MeV [31].

The theory of measuring the neutron flux via NAA and some special techniques that can be applied to recover more precise information about the spectrum composition have been elucidated here; the following section is dedicated to a general description of the experimental procedure.

3.3.3 Experimental Procedure

To study both the magnitude and axial profile of the in-core neutron flux, the neutron activation technique (as described above) was applied with thin wire samples housed in the wire holders. The general procedure will be presented here as a five-step process that may span several days or weeks. Table 2 presents a typical schedule for such an experiment; the parentheses indicate flexibility in the schedule – i.e. step 4 may take place on either Friday or Monday, depending on lab availability and the researcher's other commitments. A full SOP can be found in Appendix A.

Table 2: Example of a schedule for an irradiation experiment. Weekends have been removed, as no experimental work was performed on either Saturdays or Sundays. This schedule was adopted for the duration of this research.

Monday	Tuesday	Wednesday	Thursday	Friday
				Step 1
Step 2				Step 3, (Step 4)
(Step 4), (Step 5)	(Step 5)	(Step 5)		

1. Sample preparation pre-irradiation

A wire (typically 1 mm in diameter and 70 cm in length) is marked at intervals of 3.5 cm with a marker, inserted in to a wire holder, and manually fastened at the top and bottom to prevent the loss of the sample during irradiation. Per MNR regulations, an irradiation request form is also filled out, indicating the date, time, in-core location and duration of irradiation, desired operating power, sample loading instructions, and the permit holder and their contact information.

2. Sample irradiation

The wire holder is loaded in to the sample holder, and finally in to the specified irradiation site in the core, by MNR operations staff after the reactor has reached stability at the desired operating power. During the irradiation, the following reactor parameters are manually recorded at intervals of 5 minutes: the reactor power, the shim and regulating rod positions, the temperature difference across the core, and the flow rate of coolant through the core. The sample is withdrawn from the irradiation site and placed in a holding position in the MNR pool to allow for any short-lived activation products to decay such that the sample is safe for handling.

3. Sample removal

Prior to sample collection, a material transfer form – which indicates all radioactive isotopes in the sample, and their approximate activity – is approved by the health physics team, and the sample may then be removed from the reactor. MNR operations staff remove the wire holder from the sample holder and transfer it to the researcher, who places the sample in a container suitable for

sample transport (in the case of low-activity wire samples, a plastic shipping tube is sufficient, though a lead shielded container may be necessary for higher-activity samples).

The sampled is surveyed with a portable dosimeter, and the surface dose and dose at a distance of 1 m are recorded on the irradiation request form; both MNR and the researcher keep a copy of this document. The sample is then removed from the reactor for further analysis.

> If Step 4 does not *immediately* follow Step 3, the health physics permit associated with this work requires that the sample is held in a locked container in a designated lab space with proper identification and researcher contact information.

4. Sample preparation post-irradiation

Samples are taken to the McMaster Center for Neutron Activation Analysis (MACCNAA) for preparation prior to data collection. The wire(s) are cut at the intervals marked in Step 1 (such that 21 data points are generated per wire, with each segment corresponding to an elevation in the core). Each wire segment is weighed using a high-precision scale (precise to 0.0001 g in this work), and this information is recorded on a counting record form (which will also be used to record various information during Step 5). The wire segments are inserted in to polyethylene vials numbered 1 through 21 (segment 1 indicates the bottom of the wire, segment 21 indicates the top) and are then sealed and transported to the lab space used for data collection.

> If Step 5 does not *immediately* follow Step 4, the health physics permit associated with this work requires that the sample is held in a locked container in a designated lab space with proper identification and researcher contact information.

5. Data collection

A high-purity germanium (HPGe) detector (cooled in advance with liquid nitrogen (LN2) and connected to a Windows 7 machine) is used to record the γ-ray activity of the prepared samples with the Genie 2000 software [48]. Both the energy and geometrical calibrations of the HPGe are known prior to data collection, and count times can be adjusted as necessary so that uncertainties due to counting statistics are approximately 1 %; in the limit of low-activity samples, up to 1000 s

count times may be required. A detailed discussion of the effects of measurement calibration on the final reported uncertainty is presented in Chapter 4.

To record the sample activity, the polyethylene vial (containing the active wire segment) is placed in front of the detector such that the wire is lying horizontally and parallel to the face of the detector, and is located at the midpoint of the detector face. This is accomplished by mounting the vial in a 3D-printed plastic component, as shown in Figure 18, and ensures that the measurements are repeatable and the geometric effects can be consistently accounted for during data processing.

Figure 18: Close-up of the detector configuration during data collection. The 3D-printed plastic component used to mount the sample-containing vials is seen in black, at the bottom. Also visible are the lead blocks used to shield the apparatus.

The start-of-count (SOC) time is recorded on the counting record form, such that the decay time between removal from the irradiation site and the beginning of data collection can be determined. The raw data is saved as an IEC 1455 (.IEC) file, and can be converted to a text file (.txt) that contains the count time, the SOC time, both the energy calibration and energy resolution parameters, and the counts recorded in each channel. The 21 wire segments are measured in sequence, followed by a collection of the background activity such that the net sample activity can be determined during Step 6.

As required by the health physics permit associated with this work, following data collection, all vials containing radioactive material are disposed in shielded, labeled waste containers.

When the in-core neutron flux is recovered according to the method described above, the uncertainties associated with the data collection and measurement procedures (i.e. Step 4 and Step 5 presented in Section 3.3.3) are generally well known, and can be readily combined according to the standard rules of uncertainty propagation (as presented in Chapter 2 of this thesis). However, the state of the reactor itself, and various reactor parameters that are recorded during Step 2 of the procedure described above, may also contribute a significant source of uncertainty to the final processed result.

The following variables/reactor parameters have been identified as potentially significant sources of additional uncertainty in neutron flux measurements: the sample position in the irradiation site, the uncertainty inherent in the indicated reactor power, the indicated control rod positions, the presence and accumulation of ^{135}Xe, and the nuclear data and its uncertainty which are applied during data processing. The articles presented as the body of this thesis study these uncertainties in detail – a complete description of the experimental campaigns undertaken to isolate and understand these uncertainties can be found in Chapters 4, 5, and 6.

3.4 Computational Methods

The nature of Monte Carlo simulations and their associated uncertainties, and some features of the MCNP system have been introduced in Chapter 2 however, these were presented in a general sense, and without the experimental context described above. In what follows, a description of the computational methods used to replicate experimental conditions in MNR will be presented. To generate the precise computational results required for this research, it was sufficient to increase the number of particle histories without applying additional variance reduction techniques. The tally convergence was confirmed by the convergence of k_{eff} and the source entropy convergence checks in the MCNP output file. In general, the computational procedure involves the adjustment of various model parameters, rather than the creation of new geometries or a new problem definition.

The following parameters are routinely adjusted in the MCNP model of MNR as dictated by experimental conditions: the control rod positions, the core loading pattern, and spatial and energy definitions of the tallies being used.

A set of planes perpendicular to the vertical axis in the core define the location of the control rods in the core; these planes bound the region of the absorbing material, and their z-intercept is related to the recorded rod position in the core by the following equations, for the shim rods and the regulating rod, respectively:

$$\boldsymbol{bottom\ of\ shim} = (\boldsymbol{shim\ position}) * \mathbf{0.6224} - \mathbf{31.12} \quad 51$$

$$\boldsymbol{bottom\ of\ reg} = (\boldsymbol{reg\ position}) * \mathbf{0.6151} - \mathbf{29.308} \quad 52$$

In the equations above, the *shim position* and the *reg position* refer to the recorded locations of the control rods in MNR operating room, and are reported as a percentage of the rod that is withdrawn (i.e. a control rod that is 100 % withdrawn is fully removed from the core). As lengths of both the shims and the regulating rod are known, the location of the top of the control rods can be determined by adding this length to the value calculated with the equations above. As described in Section 3.3.3, the control rod positions are recorded at regular intervals during experimental irradiation procedures, and these parameters can therefore be replicated in a simulation of MNR with high precision.

As described in Section 3.2.2, it is possible to update the MCNP model of MNR to reflect changes in either the core configuration or the material composition of the fuel, as necessary. The procedure for making these changes involves overwriting the material definition of the fuel with the OSCAR results, and updating the lattice structure to accurately reflect the contents (i.e. the universes) that fill each site in the core. These changes can be made readily and are easily reversible; it is therefore possible to study several different core configurations or burnup states in rapid succession.

To model the wire irradiation experiments described in Section 3.3.3, an F4 tally is imposed on the wire that is contained within its holder. By applying a tally segment modifier (FS command) the 21 wire segments generated during experimentation can be explicitly modeled. Additionally, a user-specified energy definition may be applied to the tally via an energy modifier (E command) if required. As discussed in Chapter 2, the F4 tally can be used to recover the neutron flux directly however, when it is necessary to require a (n, x) reaction rate from MCNP, tally multipliers (FM command) can be used.

When the appropriate adjustments are made to the model parameters described above, it is possible to reproduce the conditions of a wire irradiation experiment, and therefore recover computational

data that may be used for direct comparison to experimental results. The theory and methodologies described in Chapters 2 and 3, respectively, are intended to provide context for the journal articles that make up the main body of this thesis; these articles will be presented in full in Chapters 4, 5, and 6.

4 Paper I

4.1 Publication Details

E. MacConnachie, D. Novog, and S. Day, "Quantification of system uncertainties in activation experiments at nuclear research reactors," *Ann. Nucl. Energy*, vol. 134, pp. 432–440, 2019. doi: 10.1016/j.anucene.2019.07.037

The experiments described herein were all designed, planned, and carried out by the first author (E. MacConnachie) with support from both the MNR reactor manager (Rob Pasuta) and operations staff. The data collection, processing and analysis was carried out entirely by the first author. The MCNP model of the core had been developed by Dr. Simon Day in 2001, and was modified by the first author to perform the simulations required for this analysis. Dr. Simon Day was consulted on several occasions for guidance about the structure and specifics of this model, and Monte Carlo techniques in general. The computational results were processed and analysed by the first author. Dr. David Novog provided guidance on the development of this research. This paper was written entirely by the first author, with support in editing and revisions from both Dr. Simon Day and Dr. David Novog.

Additionally, special thanks must be given to the following people: Ross Harper of MNR, for designing and constructing the five-wire holder used in several experiments, Alice Pidruczny of MACCNAA for her help in training on data acquisition and for granting the first author on-going access to her lab space, and the entire McMaster Health Physics team for their support in these experimental endeavors.

4.2 Preface

Measurements of the neutron flux in research reactors are commonly used as the basis for validation studies, and to supplement both operational and experimental decision making. For example, if there is insufficient knowledge of the neutron flux at a given site, isotope production planning and batch yields may be negatively impacted. While the procedures for data collection and analysis are both well developed and well documented, a complete characterization of sources of uncertainties in these measurements remains limited – the reported uncertainties are typically limited to those associated with the measurement procedure (e.g. counting statistics in the case of the NAA technique).

The aim of this publication is to design and conduct a series of experiments and/or simulations such that the effects of various reactor parameters on the reported flux uncertainty can be isolated and quantified. In addition, this project seeks to develop a generalized procedure for combining and reporting these uncertainty values. The novel procedures described herein can be applied to detailed UQ analyses and validation studies, operational decision making, and the optimization of other activation procedures performed in reactor cores.

A custom piece of equipment was constructed to accommodate five flux-wires such that the uncertainty related to sample positioning could be investigated. By simultaneously irradiating five flux-wires, the range of measured values across an irradiation site could be determined, and a general uncertainty assigned to this parameter. It is important to note that this wire-holder could not "lock" in to a fixed orientation – i.e. during data collection, it was not possible to identify which wire was in the northmost position, etc. An extension of this work would involve cooperation between the first author and the MNR operations team to implement a system where the precise locations of each wire can be mapped.

The effects of both the ^{135}Xe and the changing control rod positions were investigated computationally. In each case, a series of correction factors was generated so that data collected under different reactor conditions could be compared to each other, directly. In the case of the presence of ^{135}Xe, operations immediately following reactor start-up on a Monday were taken as the reference case – e.g. before ^{135}Xe begins to accumulate in the core. The control rod correction factors account for the movement of both the shims and the regulating rod, and the reference case is taken when both the shims and the regulating rod are 50% withdrawn from the core. These correction factors were subject to their own statistical uncertainties, which is accounted for in the complete recommendation for data processing and uncertainty propagation.

Measurements of the reactor power are based on the flow rate of coolant through, and the temperature difference across, the core, and are recorded at regular intervals during reactor operations. Detailed uncertainty information about the instrumentation (e.g. flow meters or thermocouples) used to measure these quantities in MNR is not available, so the reactor power uncertainty must be estimated from historical readings of the flow of coolant through the core (q)

and the temperature difference across the core (dT)[1]. Given the importance of the reactor power uncertainty on all flux measurements, further examination of the flow meter and temperature sensors is recommended. This may involve a large-scale comparison between different flow meters, and thermocouples, or an outright replacement of these parts so that their specifications and biases are known.

Nuclear data is applied during data processing to convert activation rate measurements to neutron flux values. There are several different ways nuclear data can be included in these procedures – typically involving either the judicious selection of a single value, or by collapsing a multigroup library through some weighting procedure. While different researchers may apply different procedures to suit their aims, this publication provides one example of how to calculate, and propagate nuclear data uncertainties, based on the SCALE-6.2.2 252-group perturbation libraries. The nuclear data uncertainties are also addressed in the second and third publications that make up this thesis.

[1] Erratum: The reactor power is computed from the **mass flow** of coolant (not the volumetric flow defined in this article), its specific heat capacity (C_p), and the temperature difference across the core.

Quantification of System Uncertainties in Activation Experiments at Nuclear Research Reactors

Abstract

Neutron flux measurements in reactor cores are often used for code validation studies, however reported experimental flux uncertainties remain limited in scope. This work presents both a detailed assessment of several flux measurement uncertainties and a guideline for reporting these quantities. The effects of the sample position, the presence of ^{135}Xe, the control rod positions, reactor power, and nuclear data during activation procedures were individually quantified at the McMaster Nuclear Reactor. NiCr flux wires were used to study the ^{51}Cr (n,γ) activation reaction experimentally and through a series of MCNP6 simulations, and the SCALE-6.2.2 252-group library was used to study cross-section data uncertainty for use in translating activation measurements into neutron flux values. The placement of the sample and the reactor power measurements were found to be the most significant contributors to the overall measurement uncertainty. A procedure for reporting the results and uncertainties of an irradiation procedure is provided.

Key Words

McMaster Nuclear Reactor

Neutron activation analysis

MCNP

Uncertainty Quantification

Nomenclature

HPGe	High Purity Germanium
LEU	Low-enriched Uranium
MCNP	Monte-Carlo N-Particle
MNR	McMaster Nuclear Reactor

MTR	Materials Testing Reactor
TRIGA	Training, Research, Isotopes and General Atomics Reactors
UQ	Uncertainty Quantification

R	Activation rate [atoms/s]
A	Activity [1/s]
T	Time constant
dT	Temperature [ºC]
N	Number of atoms
m	Mass [g]
$\phi(E)$	Flux per unit energy [$cm^{-2}\ s^{-1}\ eV^{-1}$]
Φ	Energy-integrated flux [$cm^{-2}\ s^{-1}$]
σ	Cross-section [cm^2]
η	Efficiency
Ω	Geometrical correction factor
P	Reactor power
ν	Average number of neutrons released per fission event
$E_{fission}$	Energy released per fission event [MeV]
E_0	Most probable energy for a Maxwellian distribution
Q	Energy conversion factor, Q = 1.6022×10^{-13} J/MeV
$Q_{x,g}$	Cross-section perturbation factor
q	Mass flow rate [$m^3\ s^{-1}$]
k_{eff}	Effective multiplication factor
G	Self-shielding factor
I_γ	Gamma-ray peak yield [%]
λ	Decay constant [s^{-1}]
C_p	Specific heat [J/(kg · ºC)]
$F_{control\ rod}$	Control rod correction factor
F_{Xe}	Xenon correction factor

1 Introduction

The neutron flux is an important parameter for analysis in nuclear reactors, as its behavior dictates neutron induced reaction rates – notably, fission power, fuel burnup and activation rates. While detailed flux measurements may be difficult in power reactors, they can be performed more readily in research reactors. These measurements can be used for computer code validation and may also be used to derive inputs for Uncertainty Quantification (UQ). In such calculations, it is required to understand and quantify all components of measurement uncertainty. In addition to refining the UQ procedure, a complete characterization of the neutron spectra and its uncertainties may be used to optimize certain research and development projects that are carried out in research reactors. Many research reactors produce radioisotopes that can be used either directly in radiation therapy and imaging, or as radiopharmaceuticals. The efficiency of the production of these isotopes is influenced by the knowledge of the neutron flux and its uncertainty – specifically, this production is sensitive to both the spectra and the shape of the neutron flux in the reactor core. Additionally, materials irradiation studies can be carried out in a well-known neutron flux such that irradiation damage and nuclear heating can be investigated [49]. A complete characterization of the neutron spectra and the uncertainty associated with such measurements may be used to inform both operational and experimental procedures [15].

The axial distribution of the neutron flux has been studied at several Training, Research, Isotopes and General Atomics (TRIGA) Mark-II research reactors however, the reported uncertainty has been limited to the uncertainty associated with data collection. It has been noted that several reactor parameters – such as the presence of ^{135}Xe [8], control rods, and the uncertainties associated with nuclear data [11] and the reactor power [13] – may contribute to the overall uncertainty of flux measurements. Additionally, it has been stated in [15] that the "uncertainty is position of the irradiation channels … do affect the azimuthal neutron flux distribution…" While these effects have been identified, they have not been quantified, and the reported uncertainties remain limited to those associated with data collection. A complete quantification of these additional sources of uncertainty is required to optimize and understand the results of activation procedures being conducted at nuclear research reactors. The objective of this work is to quantify – through a series of experiments and Monte Carlo simulations – their contributions to the uncertainty of the activation rates and the derived neutron flux. In what follows, the McMaster Nuclear Reactor

(MNR) is being studied however, the methodology presented here may be applied to any research reactor – e.g. the High Flux Isotope Reactor (HFIR) or Zero Energy Deuterium (ZED-2) reactor[49], [50]. The results presented in this work may be used to develop a standard procedure for reporting neutron flux uncertainties for use in verification and validation studies.

1.1 The McMaster Nuclear Reactor

MNR is a light-water cooled and moderated, open-pool Materials Testing Reactor (MTR) located on the McMaster University campus in Hamilton, Ontario, Canada and currently operates using low-enriched Uranium (LEU) fuel. Currently, MNR is a world leader in the production of ^{125}I for use in the treatment of prostate cancer, and is actively pursuing the development of other radioisotopes and several cross-disciplinary research projects [38]. MNR typically operates on a 16-5 schedule – i.e. 16 hours per day, five days per week. The core is defined by a (9 x 6) grid plate which can support up to 54 fuel and reflector assemblies. A reference core configuration for MNR is shown below to illustrate the layout of the facility.

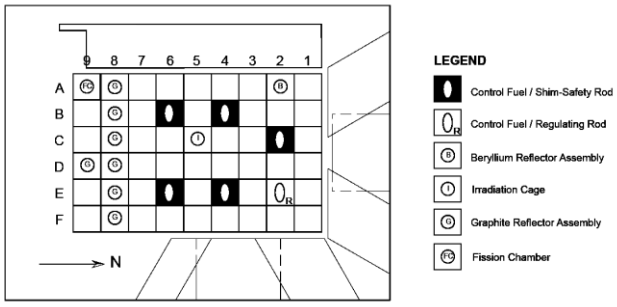

Figure 1: MNR reference core configuration showing the grid geometry of the core. Typically, there are 34 fuel sites housed in rows 1 to 7, 6 graphite reflector site, 12 vacant sites, a Beryllium reflector site, and a central irradiation facility.

MNR currently uses curved-plate LEU fuel (19.75 % ^{235}U). A standard fuel assembly contains 18 plates – the inner 16 plates contain fuel comprised of Uranium particles in an Aluminum matrix, and the outer two plates are pure Aluminium. Fuel shuffling events are typically performed every two months, and refuelling operations occur two to three times per year. Refuelling is performed on a burn-up basis, estimated using flux wire activation experiments.

Two different types of absorber rods are used in MNR – five gang-operated Ag-In-Cd shim-safety rods for coarse reactivity control and shutdown procedures, and a single stainless-steel regulating rod for automatic fine reactivity control. The rods are moved from the top of the core downwards using motors [39]. During a loss of electrical power, or by initiation from shutdown parameters,

the shim-safety rods will fall into the core under the action of gravity. The shim rods are located in sites 2C, 4E, 4B, 6B, and 6E and the regulating rod is housed in site 2E (see Figure) [41].

2 Quantification of Uncertainty

When experimental neutron flux data is used as the basis for code validation, the reported uncertainties are typically limited to those associated with the measured quantities – the effects of changing reactor conditions, positional uncertainty in the measurement location, and experimental repeatability are often omitted. This underestimation of the neutron flux uncertainty may result in inconsistent conclusions being drawn about the fidelity of reactor physics codes. These additional sources of uncertainty – along with the usual uncertainties in the measured quantities – must be quantified such that UQ is carried out with a full knowledge of all relevant uncertainties.

The sample position, the presence of ^{135}Xe, control rod positions, reactor power measurements and nuclear data have been identified as significant sources of uncertainty in activation experiments [8], [11], [13], [15]. To ensure a robust treatment of these sources of uncertainty, it is useful to group these effects into those associated with: power level, spatial location, Xenon effects, control rod position effects, and nuclear data uncertainties. The nuclear data uncertainties arise from the conversion of activation measurement data into local flux. The focus of this work is to quantify the effects of the parameters listed above, and to demonstrate their contribution to the overall UQ in a reactor physics experiment. Each of these parameters is described in detail below.

2.1 Power Level Uncertainty

The thermal power level is determined by measurements of the temperature difference across the core and the volumetric flow rate of coolant through the core and calculated using the first law of thermodynamics. Uncertainties in the measurement of both q and ΔT contribute to the uncertainty associated with the reactor power, which is directly related to the magnitude of the neutron flux. As such, the experimental uncertainty in flux is directly dependent on the uncertainty in the indicated reactor power during the experiment.

2.2 Spatial Uncertainty

In activation experiments the sample is often assumed to sit in the center of an irradiation site. However, in a reactor physics experiment there may be a deviation in the spatial positioning of the

wire from its intended location. For example, in MNR, due to the difference in the dimensions of the wire holder and sample holder used during irradiation procedures, a sample may be offset by as much as 1.58 mm from the center of the site [51]. In regions of high flux gradients (e.g. near fuel assemblies or at the edge of the core), the sample placement may have a significant impact on the magnitude of the neutron field to which it is exposed and reported flux measurements would not coincide with the specified center of the irradiation site. A series of irradiation experiments designed to isolate these effects, and the results, are presented in Section 4.4.

2.3 Xenon Accumulation

Given the importance of the isotopic inventory in the fuel in validation studies, it is important to quantify the core history prior to a measurement. For example, following reactor start-up after a weekend shutdown in a research reactor, the solution to the Bateman equations for ^{135}Xe indicate that, for steady power operation, the concentration of ^{135}Xe will increase over approximately 50 hours before reaching an equilibrium value [21]. Due to its large thermal neutron absorption cross section, the evolution of the ^{135}Xe load may cause a significant deviation in the flux distribution during Thursday and Friday operations as compared to Monday operations. For reactor physics models that apply steady-state ^{135}Xe loads, simulation results would deviate from measurements performed on a Monday, when ^{135}Xe has not reached equilibrium. Additionally, when comparing the results from irradiation procedures performed on different days at the same facility, it is necessary to have some standard method of reporting the data so that they may be compared in a meaningful way (i.e. when looking at experimental repeatability, one must be able to normalize the effect of ^{135}Xe changes). Both the effects of the ^{135}Xe accumulation, and a method for applying a correction factor to account for daily fluctuations, are presented in Section 4.3. During reactor operation, ^{135}Xe reactivity is compensated for by movement of the control rods. This work focuses on treating the effects of the control rods and ^{135}Xe separately and applying an appropriate correlation term during the final combination of all sources of uncertainty.

2.4 Control Rod Position

During activation experiments, the regulating rod position has been observed to vary in position by as much as 20%, while the shim rods typically remain fixed during an irradiation procedure. Over the course of a week, the day-to-day variation in the shim rod positions driven by changes in the ^{135}Xe load will also affect the spatial distribution of the neutron flux. Although the control rod

positions can be fixed in a simulation, it is again necessary to develop a standard procedure for reporting measured fluxes so that different sets of irradiations – corresponding to small changes in control rod positions – may be appropriately compared and accounted for in assessments of experimental repeatability. These results are discussed in Section 4.2.

2.5 Nuclear Data Uncertainty

To determine the absolute value of the neutron flux from the results of an irradiation experiment, knowledge of the activation cross section of the material used to measure the flux is required. As this cross-section information is used directly in the processing of experimental data, any uncertainties in the cross-section will propagate directly to a reported flux uncertainty. Nuclear data uncertainties may arise from differences in evaluated nuclear data files, or from uncertainties present in individual libraries. This work will focus on the latter, to isolate the effects of collapsing a multigroup library or selecting a reference cross section value. A complete discussion of the effects of nuclear data uncertainties can be found in Section 4.6.

3 Methodology

This work uses MNR to generate activation measurements and their uncertainties along the axial direction of the core, for a well-established core state where relevant operations variables are known. The techniques of neutron activation analysis are used, as described in Sections 3.1 and 3.2. In addition to these measurements, full-core MCNP simulations were performed to assess the data – this has been described in Section 3.3.

3.1 Irradiation

When exposed to a neutron field, certain materials may undergo nuclear transmutation via the (n,γ) reaction and become unstable, emitting γ-rays at characteristic energies as they decay. Other nuclear reactions may occur in the material (e.g. the (n,2n) or (n,n') reaction), however, the (n,γ) reaction is typically dominant and will result in a measurable activity. A measurement of this γ-ray activity can be used to determine the activation rate in the sample during an irradiation – that is, the number of radioisotopes created per second by the (n,γ) reaction. The activation rate is related to the neutron flux by the following equation:

$$\boldsymbol{R = AT = N \int_0^{\infty} \phi(E)\sigma_{n,\gamma}(E)\, dE} \quad \textbf{1}$$

The energy integrated neutron flux may be determined by collapsing the activation cross-section, or selecting a single representative value, so that Equation 1 becomes:

$$\boldsymbol{\Phi_{integrated} = \left(\frac{R}{N}\right)\left(\frac{1}{\sigma_{collapsed}}\right) = \left(\frac{AT}{N}\right)\left(\frac{1}{\sigma_{collapsed}}\right)} \quad \textbf{2}$$

In Equation 2 above, N is the number of precursor atoms in the sample, T is a time constant to account for the irradiation and decay times prior to measurement and A is the measured γ-ray activity. This measurement must be corrected for the energy and geometrical efficiency of the measurement system, decay parameters, and self shielding factor as described by Snoj et. al. [44]. The experimental results described herein involve the irradiation of NiCr (nominally 0.8:0.2 by weight on a 99% metals basis) to study the ^{50}Cr (n, γ) activation reaction and measure the subsequent decay of ^{51}Cr using the 320 keV γ-ray peak.

To determine the spatial profile of the neutron flux along the vertical direction of the core, full length wire irradiations are performed. A wire holder is used to house 70 cm of wire that is nominally 1 mm in diameter, which is then placed in a sample holder. After the reactor has been brought to the desired operating power, operations staff place the sample holder in the chosen irradiation site. Following irradiation and an appropriate decay time (typically 15 minutes and 5 days, respectively) to allow for safe handling, the wire is cut into segments each measuring 3.5 cm, generating 20 data points per wire.

3.2 Data Collection

The γ-ray activity is measured using a p-type, coaxial, high purity Germanium (HPGe) detector. The absolute detection efficiency of the system was determined by measuring the activity of several standard radiation sources. The results from this efficiency calibration can be seen in the figure below, where a standard fit type for HPGe detectors has been applied [52].

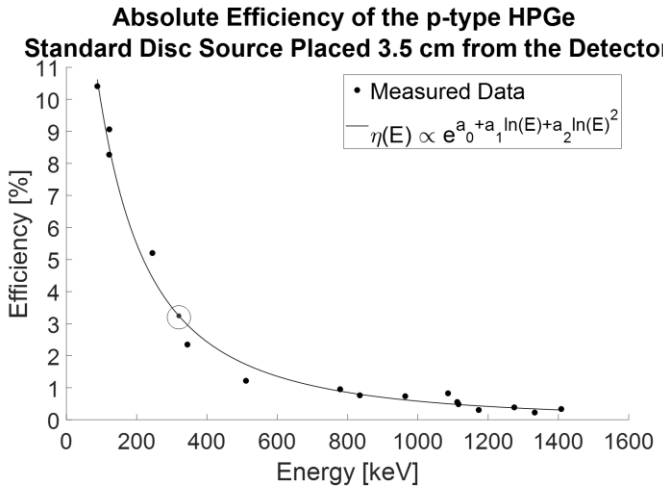

Figure 2: Absolute efficiency calibration of the HPGe. The fit parameters are: a0 = 0.1905, a1 = 1.575, a2 = -0.2434 and RMSE = 0.04482. Error bars have been omitted for clarity and are on the order of < 1 %. The efficiency of the γ-ray being studied is η(320 keV) = 3.2441 % and has been indicated on the figure by the circled point.

The root mean squared error (RMSE) parameter from a curve fit can be used to determine the standard error of the estimate (SEE) according to the following equation [36]:

$$SEE = \frac{RMSE}{\sqrt{N}} \qquad 3$$

The RMSE of the regression analysis performed for the absolute efficiency calibration of the HPGe is 0.04482, thus the SEE is 0.0112. The detection efficiency at E_{peak} = 320 keV is 3.2441 % and so the uncertainty associated with the detector efficiency is:

$$\frac{\delta\eta}{\eta} = \frac{SEE}{\eta(E)} * 100\% = 0.35\ \% \qquad 4$$

To determine the variability of this uncertainty, the curve fitting procedure was applied to several subsets of the data presented in Figure 2, and the detector efficiency uncertainty calculated from Equations 3 and 4. Each data point was removed in succession (so that the subset of data included 15 points), and it was determined that on average, the uncertainty was 6% smaller than the result presented above ($\frac{\delta\eta}{\eta} = 0.33\ \%$). This indicates that a detector efficiency uncertainty of 0.35% is an appropriate value to use throughout the uncertainty propagation process.

In addition to the detection efficiency of the HPGe, the geometrical efficiency of the measurement configuration must also be considered, as gammas emitted in directions away from the detector surface cannot be measured. The geometrical correction factor Ω is some fraction of the total solid

angle subtended by the sample (4π sr) and is used to multiplicatively adjust the measured sample activity. This correction factor was determined using the MCNP6 code for the configuration used during data collection. An overhead view of the measurement geometry is show in the figure below.

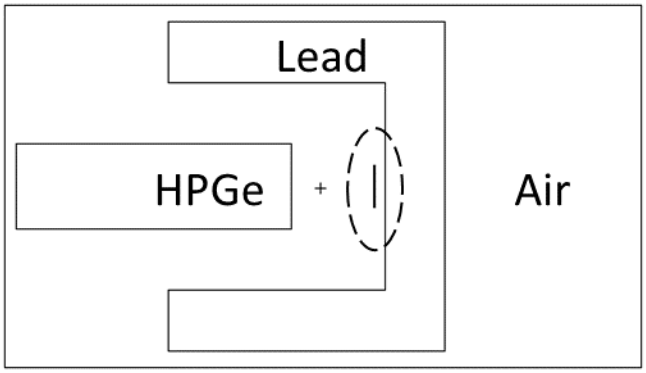

Figure 3: Overhead view of the simplified MCNP6 geometry of the measurement configuration, where the sample has been circled. Further refinement of the geometry did not have any effect on the results.

A series of simulations was run with an increasing number of particle histories until the output met a convergence criterion of less than 0.1 %. It was determined that 5.188 % of the emitted photons were incident on the detector, so that $\Omega = 0.6519 \pm 0.1$ %.

3.3 Monte Carlo Simulation

An MCNP6 model of MNR core was developed in 2001 and has been updated continually to reflect various changes in the geometry and material compositions. The simulation results presented here are based on core configuration 54A, which is the most recent core configuration to have been experimentally characterized, and was used to generate relative sensitivity estimates of the neutron flux to control rod and ^{135}Xe effects [41]. To simulate a flux wire irradiation, a segmented pure F4 tally on the wire material in the MCNP model is created. The criticality calculations are run so that the statistical uncertainty on the tallies are less than 1%. When a multiplier bin is used, the reaction rate in each segment can be extracted directly from the MCTAL file or the flux in each segment can be calculated according to the following equation, and is used to analyze the results presented in Sections 4.5 and 4.6:

$$\boldsymbol{\phi = \frac{P\nu(F4)}{QE_{fission}k_{eff}}} \qquad \mathbf{5}$$

4 Results

A series of experiments and simulations were conducted to isolate and evaluate each of the parameters described in Section 2. In what follows, the methodology and results from the work done to quantify the uncertainties present in a typical flux experiment at MNR are described. The nature of the covariant terms, and with a summary of the results, are described in Section 4.7.

4.1 Measurement Uncertainty

The activation rate R – the number of radioisotopes created by the (n,γ) per second – is determined from the measured sample activity by the following equation:

$$\boldsymbol{R = \left(\frac{A_{measured}\Omega}{I_\gamma} - A_{background}\right)\eta(E_{peak})\left(\frac{1}{GN}\right)\left(\frac{e^{\lambda t_{cool}}}{1 - e^{-\lambda t_{irr}}}\right)} \qquad \textbf{6}$$

In Equation 6, $A_{measured}$, $A_{background}$, N, t_{cool} and t_{irr} are measured during the experiment, the values and uncertainties for Ω and $\eta(E_{peak})$ have been reported in Section 3.2, and the values for λ and I_γ can be found in nuclear databases, having values of 2.89×10^{-7} s^{-1} and 9.91 %, respectively [45]. The calculation of the self-shielding factor G was performed according to [44] and found to have a value of G = 0.9270.

To calculate the measurement uncertainty, $\delta R_{measurement}$, two assumptions are made:

I. There is no significant uncertainty associated with t_{cool} and t_{irr}, as the irradiation and decay times are established with much higher certainty than the other terms. The values for t_{cool} and t_{irr} are determined from the time of sample insertion and removal from the irradiation site, which are performed by MNR operators. Both the time of removal and the start of count time are recorded to the second, thus the decay time is known exactly.
II. There is no available information about the uncertainty associated with G, and it is therefore treated as a known quantity [44].

The final calculation of $\delta R_{measurement}$ can be performed by combining all uncertainties from Equation 6 in quadrature, as the measured quantities are independent. Experiments are planned to ensure that samples are sufficiently active and Gaussian counting statistics may be applied to determine the uncertainty associated with $A_{measured}$ and $A_{background}$. In a typical experiment, the uncertainty associated with $A_{measured}$ and $A_{background}$ is between 1 % and 1.5%.

The geometrical efficiency Ω was determined by an MCNP calculation with an increasing number of particle histories until a convergence criterion of 0.1 % was met, as described in the preceding sections. The uncertainties associated with the parameters I_γ and λ are reported in nuclear databases and the value of N is calculated from a measurement of the sample mass using a scale precise to 0.0001 g and from information about the real composition of the sample [45]. The real composition of the samples being studied is reported in the product certificate of analysis, which indicates that the wires are 0.7789:0.2032 NiCr by weight, and has no reported uncertainty [53].

A summary of the uncertainties associated with these parameters are as follows:

- $\frac{\delta\Omega}{\Omega} = 0.1\ \%$
- $\frac{\delta\eta}{\eta} = 0.35\ \%$
- $\frac{\delta I_\gamma}{I_\gamma} = 0.01\ \%$
- $\frac{\delta\lambda}{\lambda} = 8.66x10^{-3}\ \%$
- $0.04\ \% < \frac{\delta N}{N} < 0.045\ \%$

The value of the measurement uncertainty is calculated by applying the usual rules of error propagation for multiplicative and additive terms to Equation 6. For a typical irradiation experiment, the relative uncertainty owing to measurement is between 1.1 % and 1.5 %, with counting statistics dominating the overall experimental uncertainty. These counting statistics may be improved with longer counting or irradiation times where possible.

4.2 Control Rod Positions

To quantify the effects of the control rod positions, a series of full-core MCNP simulations was carried out to study the effects of the shim rods and the regulating independently. The effects of the shim rods were studied by adjusting the rods between 0 % and 100 % withdrawn, in increments of 5 %. This was done for three different regulating rod positions: 0 %, 50 %, and 100 % withdrawn. Similarly, the response to the regulating rod was determined by varying the regulating rod position from 30 % to 70 % withdrawn in increments of 5 %, with the shim rods fixed at positions of 0 %, 50 %, and 100 % withdrawn. The limits of the control rod positions were determined based on observations of the control rods during irradiation experiments recorded in MNR operating logs.

The variation of the control rod positions systematically alters both the shape and amplitude of the axial neutron flux in the core. The effects of rod positions can therefore be accounted for by

applying a correction factor to measured data based on the simulation results from above. The case of both the regulating rod and the shim rods being 50 % withdrawn from the core is defined as the reference case and the total flux values are compared to this set of values. The correction factor for the regulating rod and shim rods at positions x and y, respectively, is:

$$F_{control\ rod} = \frac{\phi_{50,50}}{\phi_{x,y}} \qquad 7$$

Values for this correction factor range between 0.6 and 1.4, and a sample plot showing a subset of these correction factors corresponding to a regulating rod position of 50 % withdraw is shown below. Similar corrections for other regulating rod positions are also derived.

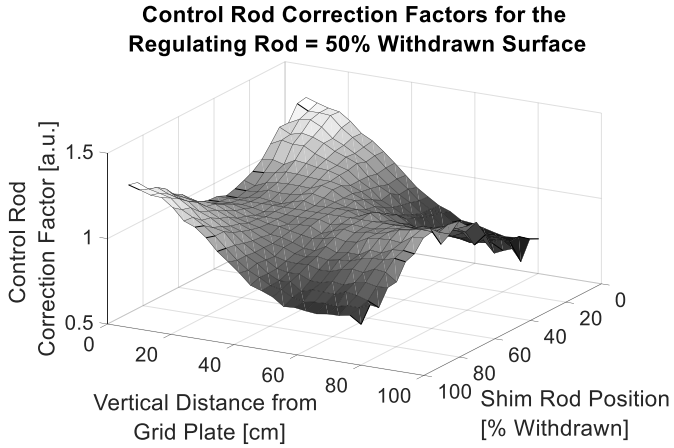

Figure 4: Sample of the control rod correction factors for the case of the regulating rod fixed at 50% withdrawn.

The burnup and depletion of the control rods was examined using the ORIGEN/ARP modules of SCALE-6.2.2 and found to be negligible – i.e. the efficiency of the control rods do not significantly change over time. The uncertainties associated with this correction factor are due only to the statistical errors determined during simulation. A statistical uncertainty of less than 1 % was achieved in all cases with 1,000 active histories x 100,000 particles per history.

A bilinear interpolation can be performed to determine the appropriate control rod correction factor for rod positions not explicitly investigated. In this case, the uncertainty associated with this control rod factor may be estimated by adding the statistical uncertainties of the starting points of the interpolation in quadrature – the resulting uncertainties are approximately 2%.

4.3 Xenon Accumulation

As many reactor physics experiments may take place over the course of several days, it is important to consider the impact of fuel composition over this period. For constant continuous power, the rate equations for ^{135}Xe predict that it will accumulate over approximately 50 hours before reaching an equilibrium value following a prolonged shutdown period [21]. However, MNR operating cycle is such that it is typically shutdown between approximately 2300 and 0800 during the work week. The concentration of ^{135}Xe was numerically calculated using MATLAB for a typical operation week and is shown in the figure below with recorded control rod positions.

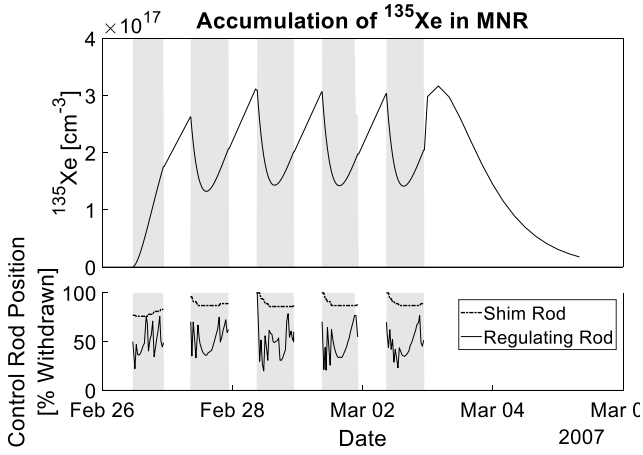

Figure 5: Behavior of ^{135}Xe (top) and control rod positions (bottom) during an operational week in MNR. The concentration of ^{135}Xe was calculated assuming start-up of a clean core to 3 MW following a weekend shutdown. The shaded area of the graph indicates the time during which the reactor is operating at 3 MW.

As the behavior of ^{135}Xe over time is known, the effects of this fission product on activation experiments can be systematically accounted for with a correction factor F_{Xe}. This correction factor was experimentally determined by performing a flux wire irradiation immediately following reactor start-up every day during an operational week (i.e. at different points in the ^{135}Xe loading). However, the accumulation of ^{135}Xe will also drive changes in the control rod positions as shown in Figure. Therefore, the control rod correction factor $F_{control\ rod}$ was first applied to the data to isolate the effects of ^{135}Xe on the measured data. The following figure shows both the axial profiles of the ^{51}Cr (n,γ) reaction rate and the maximum measured values.

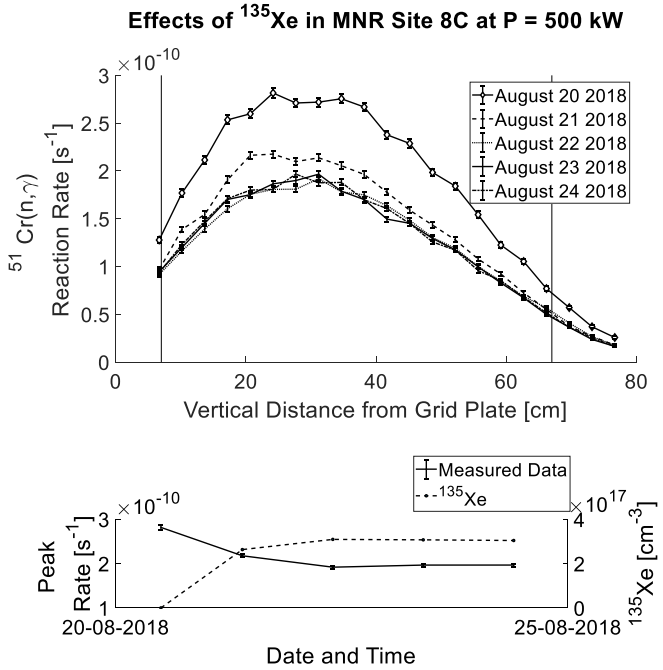

Figure 6: Axial reaction rate profiles in MNR Site 8C at 500 kW (top) and response of the peak rate over time (bottom). The ^{135}Xe atom density has been calculated assuming the Xenon is produced via fission and the decay of Iodine and is lost to neutron absorption and decay. The effects of changing control rod positions have been accounted for in the data presented here.

The data collected during Monday is defined as the reference value so that operations during the remainder of the week may be adjusted to account for Xenon accumulation, so for any day x:

$$\boldsymbol{F_{Xe} = \frac{\phi_{Monday}}{\phi_x}} \qquad \mathbf{8}$$

The correction factor in the equation above can be used to adjust measured data so that the results are representative of an irradiation taking place on a Monday, and values range between 0.6 and 1. The uncertainties associated with this correction factor are due to the combined uncertainties of the control rod correction factor $F_{control\ rod}$ and the measurement uncertainty described in Section 4.1 – typical values are on the order of 2%.

4.4 Spatial Uncertainty

To determine the uncertainty in the lateral sample placement, a wire holder was designed and constructed to accommodate five flux wires per irradiation site. The following figure shows an overhead view of this piece of irradiation equipment.

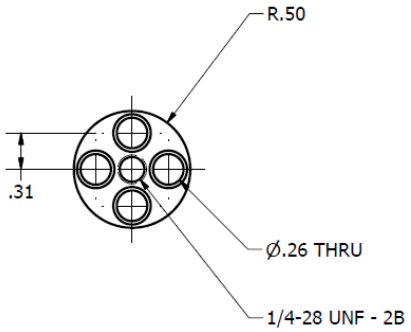

Figure 7: Overhead view of the multi-wire holder. Dimensions are indicated in inches and the part is constructed from Al6061. The length of this piece of irradiation equipment is the same as a standard single-wire holder, which is 73 cm.

Using this multi-wire holder, a series of irradiation experiments was performed to quantify the variation in the measurements of the ^{51}Cr (n,γ) reaction rate across a single irradiation site. These experiments were performed on three consecutive Mondays immediately following reactor start-up to minimize the impact of the ^{135}Xe load on the measurements. The following figure shows a sample data set taken on September 24, 2018 in MNR Site 8C at a reactor power of 500 kW.

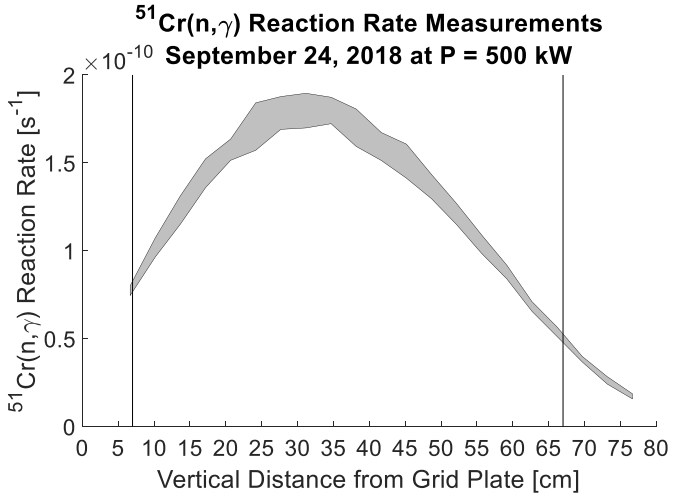

Figure 8: The spread of the measured reaction rates across an MNR irradiation site. The upper and lower bounds of the measured values at each axial point were used to generate the band in this figure. The active region of the core is between the vertical lines. Individual data points and uncertainties have been omitted for visual clarity.

The appropriate control rod correction factor discussed above was applied to each data set, and the relative standard deviation of the measurements was calculated at each axial point along the wires. No corrections for the presence of ^{135}Xe were applied, as all irradiations were performed on a Monday. The following figure shows the distribution of the standard deviation over all axial locations for each day an irradiation was performed.

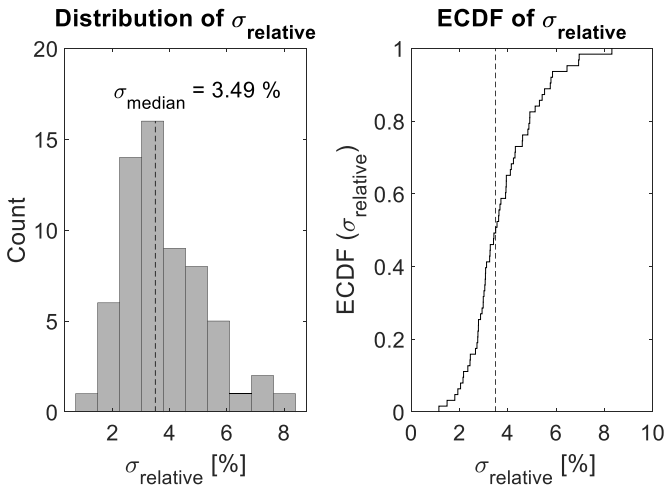

Figure 9: Distribution of $\sigma_{relative}$ (left) and the empirical cumulative distribution function of these values (right). The median value of the relative standard deviation is 3.49 % and is indicated by a dashed line on both figures.

From Figure, the distribution of the relative standard deviations follows an approximate Gaussian distribution with a median value of 3.49 %. Therefore, the distribution of measured reaction rates is also approximately Gaussian, and the uncertainty due to the sample placement is $\sigma_{relative}$ = 3.49 %.

4.5 Power Level Uncertainty

As the reactor power directly affects the magnitude of the neutron flux and is an important input parameter for many computer codes, uncertainties in reactor power can affect both measured and simulated fluxes. The reactor power measurement is based on the flow rate of coolant through, and the temperature difference across the core and are recorded approximately every 30 minutes during full-power operations and every 5 minutes during irradiation procedures. The available control room data from the full power (i.e. at 3 MW) operations of 2016 and 2017 was investigated to estimate the standard uncertainty of the power level in the reactor, which is calculated from the following equation:

$$\boldsymbol{P = qC_p dT} \quad \textbf{9}$$

The power in MNR is calculated using a fixed value for the specific heat of light water and does not account for variations that may exist due to temperature and pressure gradients in the core, or uncertainties that may arise from the methods used to calculate the value of C_P. However, for temperature and pressures between 77 ºF to 110 ºF and 1.0 atm to 1.7 atm – which are upper limits

for these gradients across the entire core – the value of C_P does not vary by more than 0.05 % [54]. This difference is negligible, and the value of C_P may be taken as exact in MNR.

The following figure shows the distribution of these measurements, and the distribution of the product $C_p q dT$ as a measure of the reactor power level.

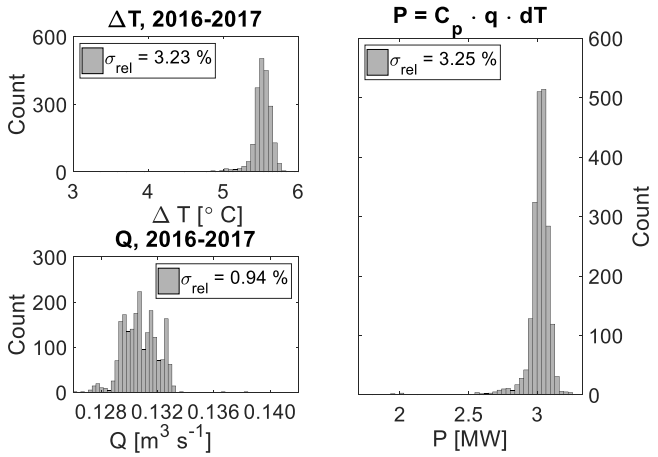

Figure 10: Distribution of the control room data recorded during full-power operations of 2016 and 2017.

The data shown in the figure above shows the effects of variability in the observed reactor power and does not include any information about biases that may exist in the instruments or systematic uncertainties in the calculation of the power level. Information about the instrumentation in MNR is not available, so the power level uncertainty cannot be determined for this facility. However, this can be estimated using product specifications from commercially available venturi flow meters and resistance temperature detectors (RTDs). Using the reported uncertainties for a Cole-Parmer RTD (δT = 0.05 ºC [55]) and a Badger Meter venturi flow meter ($\delta Q_{relative}$ = 0.75 % [56]), an estimate of the power level uncertainty is calculated as:

$$\frac{\delta P}{P} = \sqrt{\left(\frac{\delta P_{obs}}{P_{obs}}\right)^2 - \left(\frac{\delta P_{inst}}{P_{inst}}\right)^2} = 2.98\% \qquad 10$$

This is consistent with the variability in the observed power being a combination of the instrumentation and power uncertainties, and in the absence of further information about the power measurements in MNR, can be taken as an estimate of the reactor power error.

4.6 Nuclear Data Uncertainties

To quantify the nuclear data uncertainties, the SCALE-6.2.2 252-group cross section libraries (based on ENDF/B-VII.1 nuclear data) and perturbation factors were examined. One thousand perturbation factor libraries that were generated using the Medusa module of the XSUSA program are included in the SCALE code package. These perturbation factors can be applied to the reference multigroup cross-section data to obtain perturbed infinitely-dilute values. These perturbation factors can be expressed as [57]:

$$\boldsymbol{Q_{x,g} = 1 + \frac{\Delta\sigma_{x,g}}{\sigma_{x,g}}} \qquad \textbf{11}$$

In Equation 11, the subscripts x and g refer to a specific nuclide and reaction, and energy group number respectively. Using the PALEALE module, the data from each perturbation library for the ^{51}Cr (n,γ) reaction was examined [58]. For each energy group, the estimated standard uncertainty of the measurement (SEM) was calculated [35]. The following figure shows both the reference cross-section data and the estimated uncertainty owing to nuclear data variation in the 252-group cross section for the ^{51}Cr (n,γ) reaction.

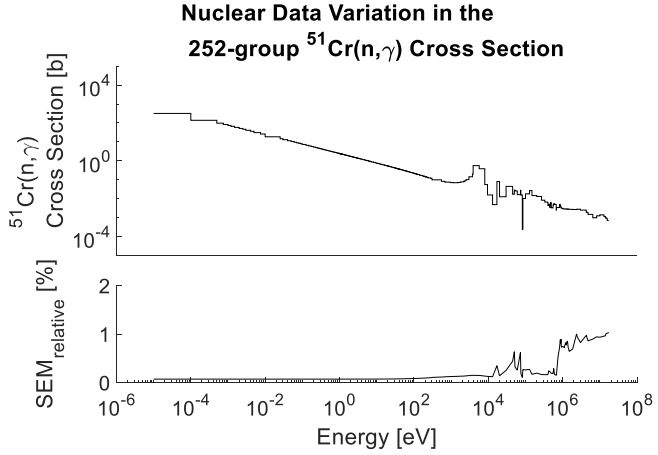

Figure 11: Reference cross section (top) and the relative SEM when 1000 perturbation libraries are sampled (bottom).

There are two different ways a cross-section value can be extracted from the multigroup library for use in a flux calculation: either a cross section value can be taken from one energy group or the multigroup library can be collapsed in an energy homogenization process. When a single cross-section value is used, the uncertainty can be taken directly from an investigation of the perturbed multigroup libraries.

A typical method of collapsing a multigroup library is by weighting the mean value of the cross section to the energy distribution of the neutron flux [11]:

$$\bar{\sigma} = \frac{\int \phi(E)\sigma(E)dE}{\int \phi(E)dE} = \frac{\sum \phi_g \sigma_g \Delta E_{g+1\to g}}{\sum \phi_g \Delta E_{g+1\to g}} \quad \textbf{12}$$

The cross-section uncertainty can be propagated through Equation 12 using the rules of uncertainty propagation for terms multiplied together. Typically, the spectrum information will be extracted from either a multi-group or continuous energy simulation of the reactor core. As an example, the energy distribution of the neutron flux at the axial midpoint of Site 8C in MNR was calculated using the SCALE 252-group energy structure in MCNP, as shown in the figure below.

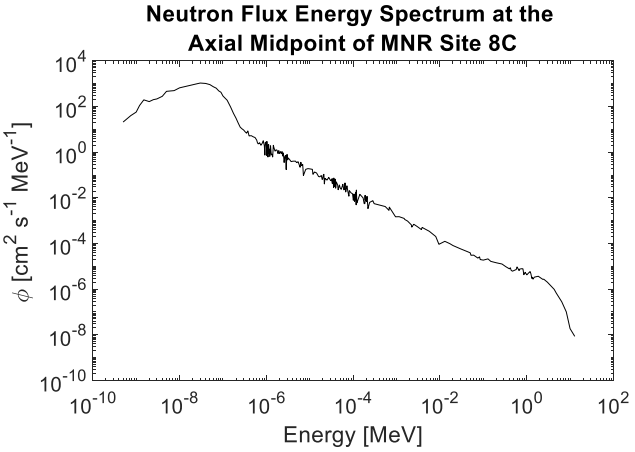

Figure 12: Neutron energy spectrum of the axial midpoint of MNR Site 8C using the SCALE 252-group energy structure.

The calculated spectrum is taken to be exact to determine only the effects of nuclear data uncertainties on a calculation of the collapsed cross-section. Using the calculated spectrum information shown in Figure above, and Equation 12, the collapsed ^{51}Cr (n,γ) cross-section and its relative uncertainty due only to the uncertainties in nuclear data is σ = 9.1123 b ± 0.0243 %. This value can be updated as more information about the energy spectrum becomes available and can be calculated for any nuclide and reaction that may be required.

4.7 Quantification of Uncertainty

As a first approximation, of the parameters discussed in the sections above, only the effects of the control rods and ^{135}Xe are clearly covariant, while the reactor power is selected for the experiment and is treated as an independent variable. The energy-integrated neutron flux and its complete uncertainty is [35]:

$$\boldsymbol{\Phi_{integrated} = \left(\frac{R}{N}\right)\left(\frac{1}{\sigma_{collapsed}}\right)F_{Xe}F_{rod}} \quad \textbf{13}$$

$$\boldsymbol{\sigma_{\phi}^2 \approx \sum_{i=1}^{n}\left|\frac{\partial \phi}{\partial x_i}\right|^2 \delta_{x_i}^2 + 2\sum_{i=1}^{n-1}\sum_{j=i+1}^{n}\frac{\partial \phi}{\partial x_i}\left(\frac{\partial \phi}{\partial x_j}\right)cov(\delta_i, \delta_j)} \quad \textbf{14}$$

From Equation 13, the partial derivative of the neutron flux with respect to the measurement, nuclear data, ^{135}Xe and the control rods can be determined directly. The reactor power level and the sample placement in the irradiation site contribute uncertainties to the flux measurements that are independent and random. The uncertainty from two terms can be added in quadrature.

The covariance between the positions of the control rods and ^{135}Xe was determined by investigating historical control room data and the calculated values for the concentration of ^{135}Xe (see Figure). The normalized covariance was calculated to be $cov(Xe, rod) = 0.924$.

The table below contains a summary of the uncertainty terms discussed in this work. If the uncertainties are combined according to Equation 14, the complete uncertainty on an activation measurement is approximately 7%. If the terms listed in Table 3 are not included in the UQ process, the resulting uncertainty on an activation measurement is on the order of 1.5%, which is dominated by counting statistics.

Table 3: Summary of the uncertainty terms and correction factors required to determine the uncertainty associated with a measurement of an activation rate or the neutron flux. Where applicable, a range of uncertainty values is presented.

Uncertainty Terms		**Notes**
$\boldsymbol{\delta R_{measurement}}$	[1.1%,1.5%]	Dominated by counting statistics
$\boldsymbol{\delta \hat{r}}$	3.49 %	Positional uncertainty
$\boldsymbol{\delta P}$	3.25 %	Reactor power uncertainty
$\boldsymbol{\delta(data)}$	0.0243 %	For conversion of activation rates to fluxes
Other Factors		**Notes**
$\boldsymbol{F_{control\ rod}}$	$\delta F_{control\ rod} = [1\%, 3\ \%]$	Referenced to all rods = 50 % withdrawn
$\boldsymbol{F_{Xenon}}$	$\delta F_{Xenon} = [2\ \%, 4\%]$	Referenced to Monday operations

The above breakdown of uncertainties is recommended as it provides a distinction between uncertainties that are directly related to the measurements and additional uncertainties that may be considered in the simulation or further UQ procedures – such as the ^{135}Xe load or the control rod positions.

5 Recommendations and Conclusions

Using the information discussed above, the uncertainty associated with a measured value of the integrated neutron flux or a measured reaction rate can be calculated directly. This uncertainty depends on the parameters in Table 3, and may take different values in different reactor systems and for different cross-section processing methods. The following is a guideline for reporting results and their uncertainties from an irradiation procedure, so that data taken over the course of multiple days may be meaningfully compared:

I. Determine measurement and detection uncertainties.
II. Determine the contribution of nuclear data uncertainties.
III. Determine the reactor power uncertainty.
IV. Determine the positional uncertainty for a sample in an irradiation site.
V. Calculate the neutron flux according to Equation 13 by applying the appropriate correction factors for both the control rod positions and the ^{135}Xe load.
VI. Calculate the complete neutron flux uncertainty according to Equation 14.

The reported flux and uncertainty will then explicitly include the effects of all variables which contribute to the reported results.

Ideally, validation studies would consider many of the sources of uncertainty explicitly within their simulations. This would allow for a direct comparison between the measured and simulated flux values and their uncertainties. In some cases, it may become intractable to include all the sources of uncertainty reported in Section 4.7 in a computational analysis. Additionally, other sources of uncertainty – such as detection efficiency and nuclear data parameters – may not be treated within the computational framework.

Given the discussion above, it is therefore recommended that activation experiments provide a clear distinction of each of the component uncertainties, as well as the total uncertainty on a flux or activation result. These component uncertainties should address as a minimum: the uncertainties in the measurement, sample position in the core, the recorded reactor power level, and environmental changes (e.g. control rod positions or Xenon accumulation) that may occur during the experimental procedure. The uncertainties in nuclear data must be considered when determining a neutron flux value. This can be done either by calculating the experimental

uncertainty according to Section 4.7, and comparing those results to the simulation outputs, or by using the uncertainties reported in Table 3 as inputs for the simulation. In the case of the latter, the control rod positions may be taken as fixed, and the most significant sources of environmental uncertainty – the sample position and the reactor power – may be sampled from an appropriate distribution so that the output neutron fluxes reflect these sources of variation. If the reactor physics code does not track the ^{135}Xe load, the correction factor described in Section 4.3 may be applied to the simulation results to reflect the experimental conditions.

6 Acknowledgements

Grateful acknowledgement is made towards all the operations staff and management team of MNR for their help during experimentation. Thanks also to Alice Pidruczny of the MACCNAA for her help in training on the data acquisition systems, and to the McMaster Health Physics team for their help in coordinating experimental efforts. Special thanks to Ross Harper for designing and constructing the five-wire holders, which are essential to the continued success of this project.

The authors thank Dr. Simon E. Day for providing the schematic of the MNR reference core configuration used in Figure 1, and Rob Pasuta for providing information about reactor power measurements in the MNR.

7 References

[1] "The Paris Agreement," *Governement of Canada*, 2016. [Online]. Available: https://www.canada.ca/en/environment-climate-change/services/climate-change/paris-agreement.html. [Accessed: 13-Oct-2020].

[2] International Atomic Energy Agency, "Climate Change and Nuclear Energy 2020," Vienna, 2020.

[3] IEA, "Global Energy Review: CO2 Emissions in 2020," *IEA*, 2021. [Online]. Available: https://www.iea.org/articles/global-energy-review-co2-emissions-in-2020. [Accessed: 12-Jul-2021].

[4] "Nuclear Power in the World Today," *World Nuclear Association*, 2020. [Online]. Available: https://www.world-nuclear.org/information-library/current-and-future-generation/nuclear-power-in-the-world-today.aspx. [Accessed: 13-Oct-2020].

[5] "Research Reactors," *World Nuclear Association*, 2020. [Online]. Available: https://www.world-nuclear.org/information-library/non-power-nuclear-applications/radioisotopes-research/research-reactors.aspx. [Accessed: 10-Oct-2020].

[6] International Atomic Energy Agency, "Research Reactors: Purpose and Future," Vienna, 2016.

[7] International Atomic Energy Agency, "History, development and future of TRIGA research reactors IAEA TRS 482," Vienna, 2016.

[8] D. Chiesa *et al.*, "Measurement and simulation of the neutron flux distribution in the TRIGA Mark II reactor core," *Ann. Nucl. Energy*, vol. 85, pp. 925–936, 2015.

[9] B. M. Makgopa, M. Belal, and W. J. Strydom, "Neutronic Characterization of the SAFARI-1 Material Testing Reactor," in *Proceedings of the 4th International Topical Meeting on High Temperature Reactor Technology*, 2008, pp. 1–7.

[10] N. Jawerth and E. Mattar, "Exploring Research Reactors and Their Use," *International Atomic Energy Agency*, 2020. [Online]. Available: https://www.iaea.org/newscenter/news/exploring-research-reactors-and-their-use.

[Accessed: 13-Oct-2020].

[11] A. Borio *et al.*, "TRIGA reactor absolute neutron flux measurement using activated isotopes," *Prog. Nucl. Energy*, vol. 70, pp. 249–255, 2014.

[12] M. Alqahtani and A. B. Alajo, "Characterization of prompt neutron spectrum of the Missouri University of Science and Technology Reactor," *Nucl. Eng. Des.*, vol. 320, pp. 57–64, 2017.

[13] V. Radulovic, Z. Stancar, L. Snoj, and A. Trkov, "Validation of absolute axial neutron fl ux distribution calculations with MCNP with 197 Au (n , γ) 198 Au reaction rate distribution measurements at the JSI TRIGA Mark II reactor," *Appl. Radiat. Isot.*, vol. 84, pp. 57–65, 2014.

[14] A. C. Fernandes, J. P. Santos, J. G. Marques, A. Kling, A. R. Ramos, and N. P. Barradas, "Validation of the Monte Carlo model supporting core conversion of the Portuguese Research Reactor (RPI) for neutron fluence rate determinations," *Ann. Nucl. Energy*, vol. 37, no. 9, pp. 1139–1145, 2010.

[15] L. Snoj, A. Trkov, R. Jacimovic, P. Rogan, G. Zerovnik, and M. Ravnik, "Analysis of neutron flux distribution for the validation of computational methods for the optimization of research reactor utilization," *Appl. Radiat. Isot.*, vol. 69, pp. 136–141, 2011.

[16] B. Richardson, C. H. Castano, J. King, A. Alajo, and S. Usman, "Modeling and validation of approach to criticality and axial flux profile experiments at the Missouri S & T Reactor (MSTR)," *Nucl. Eng. Des.*, vol. 245, pp. 55–61, 2012.

[17] D. Chiesa *et al.*, "Fuel burnup analysis of the TRIGA Mark II reactor at the University of Pavia," *Ann. Nucl. Energy*, vol. 96, pp. 270–276, 2016.

[18] K. H. Beckurts and K. Wirtz, *Neutron Physics*. Berlin: Springer-Verlag, 1964.

[19] J. Lamarsh and A. Baratta, *Introduction to Nuclear Engineering*, Third. Upper Saddle River: Prentice-Hall, 2001.

[20] J. K. Shultis and R. E. Faw, *FUNDAMENTALS OF NUCLEAR SCIENCE AND ENGINEERING*. Manhattan: Marcel Dekker, 2002.

[21] J. J. Duderstadt and L. J. Hamilton, *Nuclear Reactor Analysis*. Ann Arbor: John Wiley & Sons, Inc., 1976.

[22] "Evaluated Nuclear Data File (ENDF)." [Online]. Available: https://www-nds.iaea.org/exfor/endf.htm.

[23] F. Salaun, "Assessment and optimization of the Canadian SCWR reactivity control systems through reactor physics and thermal-hydraulics coupling," McMaster University, 2017.

[24] B. J. Ade, "SCALE / TRITON Primer : A Primer for Light Water Reactor Lattice Physics Calculations," 2011.

[25] X-5 Monte Carlo Team, "MCNP — A General Monte Carlo N-Particle Transport Code, Version 5 Volume I: Overview and Theory," Los Alamos, 2003.

[26] I. Lux and L. Koblinger, *Particle Transport Methods : Neutron and Photon Calculations Authors*. Boca Raton: CRC Press, 1991.

[27] P. Reuss, *Neutron Physics*. Paris: EDP Sciences, 2008.

[28] F. Brown, "Monte Carlo Techniques for Nuclear Systems – Theory Lectures." Los Alamos, 2016.

[29] D. B. Pelowitz *et al.*, "MCNP6 User's Manual," Los Alamos, 2013.

[30] L. Hamidatou, H. Slamene, T. Akhal, and B. Zouranen, "Concepts, Instrumentation and Techniques of Neutron Activation Analysis," in *Imaging and Radioanalytical Techniques in Interdisciplinary Research*, F. Kharfi, Ed. Rijeka: IntechOpen, 2013.

[31] B. E. Watt, "Energy spectrum of neutrons from thermal fission of U235," *Phys. Rev.*, vol. 87, no. 6, pp. 1037–1041, 1952.

[32] "Neutron Fluence Measurements," *Iaea*, vol. TRS-107, 1970.

[33] K. C. Hines, "Energy and Lethargy Distribution of Neutrons Slowing Down in Graphite," Sydney, 1959.

[34] S. Bell, "Beginner's Guide to Uncertainty of Measurement," Teddington, 1999.

[35] International Bureau of Weights and Measures, "Evaluation of measurement data — Guide

to the expression of uncertainty in measurement," Sèvres, 2008.

[36] J. R. Taylor, "An Introduction to Error Analysis: The Study of Uncertainties in Physical Measurements," 2nd ed., University Science Books, 1997, pp. 93–120.

[37] Canadian Nuclear Safety Commission, "Record of Proceedings - McMaster University - Application to Renew the McMaster Nuclear Reactor Operating Licence," 2014.

[38] McMaster Nuclear Reactor, "Nuclear Operations and Facilities 2017," Hamilton, 2017.

[39] S. E. Day, "McMaster Nuclear Reactor Specification - IAEA CRP 1496, Innovative Methods for Research Reactors: "Benchmarking against Experimental Data of the Neutronic and Thermalhydraulic Computational Methods and Tools for Operation and Safety Analysis for Research," Hamilton, 2011.

[40] S. E. Day, M. P. Butler, and W. J. Garland, "Calculations in Support of the Mnr Core Conversion," Hamilton, 2002.

[41] S. E. Day, "McMaster Nuclear Reactor Benchmark Specification - IAEA CRP 1496, Innovative Methods for Research Reactors: "Benchmarking against Experimental Data of the Neutronic and Thermalhydraulic Computational Methods and Tools for Operation and Safety Analysis for," Hamilton, 2013.

[42] M. Alqahtani, A. Buijs, and S. E. Day, "Serpent-2 and OSCAR-4 computational tools compared against McMaster nuclear reactor improved operational data history for U-235 fuel inventory tracking , local power tracking and validation of multiplication factor," *Ann. Nucl. Energy*, vol. 145, p. 107590, 2020.

[43] A. Klett, "Handbook of Particle Detection and Imaging," C. Grupen and I. Buvat, Eds. Berlin: Springer, 2012, pp. 759–790.

[44] L. Snoj, M. Ravnik, A. Trkov, and G. Zerovnik, "On the self-shielding factors in neutron activation analysis," *Nucl. Instruments Methods Phys. Res. Sect. A Accel. Spectrometers, Detect. Assoc. Equip.*, vol. 610, pp. 553–565, 2009.

[45] "NuDat 2.7." [Online]. Available: http://www.nndc.bnl.gov/nudat2/.

[46] M. Berglund and M. E. Wieser, "Isotopic compositions of the elements 2009 (IUPAC

Technical Report)*," *Pure Appl. Chem.*, vol. 83, no. 2, pp. 397–410, 2011.

[47] J. Meija *et al.*, "Atomic weights of the elements 2013 (IUPAC Technical Report)," *Pure Appl. Chem.*, vol. 88, no. 3, pp. 265–291, 2016.

[48] *Genie ™ 2000 Spectroscopy Software*. 2000.

[49] D. Chandler, G. I. Maldonado, L. D. Proctor, and R. T. Primm, "Nuclear Transmutations in HFIR's Beryllium Reflector and Their Impact on Reactor Operation and Reflector Disposal," *Nucl. Technol.*, vol. 177, no. 3, pp. 395–412, 2017.

[50] M. B. Zeller, A. Celli, R. T. Jones, and G. P. McPhee, "Photo-neutron experiment performed in ZED-2," in *21st Conference of the Canadian Nuclear Society*, 2000.

[51] E. Macconnachie, D. Novog, and S. Day, "ICONE26-82412 Axial Flux Wire Measurements atthe McMaster Nuclear Reactor," 2018, pp. 1–8.

[52] G. E. Knoll, *Radiation Detection and Measurement Third Edition*, 3rd ed. Ann Arbor: John Wiley & Sons, Inc., 2000.

[53] Alfa Aesar, "Certificate of analysis." Thermo Fisher Scientific, 2018.

[54] National Institute of Standards and Technology, "Thermophysical Properties of Fluid Systems," 2018. [Online]. Available: https://webbook.nist.gov/chemistry/fluid/. [Accessed: 03-May-2019].

[55] Cole-Parmer, "Digi-Sense Prec. Ind. PRT, 0.25" x 12" , -60~160C, Bare Wire." [Online]. Available: https://www.coleparmer.com/i/digi-sense-prec-ind-prt-0-25-x-12-60-160c-bare-wire/9045200. [Accessed: 06-May-2019].

[56] Badger Meter, "Model SSL Venturi Classic Flow Meter." [Online]. Available: https://www.badgermeter.com/business-lines/flow-instrumentation/venturi-ssl/. [Accessed: 06-May-2019].

[57] B. T. Rearden and M. A. Jessee, "SCALE Code System," Oak Ridge National Laboratory, Oak Ridge, 2017.

[58] "SCALE User's Group." [Online]. Available: https://groups.google.com/forum/#!forum/scale-users-group.

[59] E. MacConnachie, D. Novog, and S. Day, "Quantification of system uncertainties in activation experiments at nuclear research reactors," *Ann. Nucl. Energy*, vol. 134, pp. 432–440, 2019.

[60] D. R. Helsel and R. M. Hirsch, "Statistical Methods in Water Resources," 2002, pp. 337–340.

[61] V. Suman and P. K. Sarkar, "Nuclear Instruments and Methods in Physics Research A Neutron spectrum unfolding using genetic algorithm in a Monte Carlo simulation," *Nucl. Inst. Methods Phys. Res. A*, vol. 737, pp. 76–86, 2014.

[62] M. Matzke, "9 UNFOLDING PROCEDURES," *Radiat. Prot. Dosimetry*, vol. 107, pp. 155–174, 2003.

[63] S. R. Malkawi and N. Ahmad, "Solution of the neutron spectrum adjustment problem in a typical MTR type research reactor," *Ann. Nucl. Energy*, vol. 28, pp. 17–22, 2001.

[64] F. Molina, P. Aguilera, J. Romero-barrientos, H. F. Arellano, J. Agramunt, and J. Medel, "Energy distribution of the neutron fl ux measurements at the Chilean Reactor RECH-1 using multi-foil neutron activation and the Expectation Maximization unfolding algorithm," *Appl. Radiat. Isot.*, vol. 129, no. August, pp. 28–34, 2017.

[65] J. A. Kennedy, "A COMPARISON OF MNR IRRADIATION EXPERIMENTS WITH SIMULATION," McMaster Univeristy, 2000.

[66] D. Chiesa, E. Previtali, and M. Sisti, "Bayesian statistics applied to neutron activation data for reactor flux spectrum analysis," *Ann. Nucl. Energy*, vol. 70, pp. 157–168, 2014.

[67] A. Leder, "Unfolding neutron spectrum with Markov Chain Monte Carlo at MIT research Reactor with He-3 Neutral Current Detectors," *Jounal Instrum.*, vol. 13, 2018.

[68] D. Chiesa *et al.*, "Measurement of the neutron flux at spallation sources using multi-foil activation," *Nucl. Instruments Methods Phys. Res. Sect. A Accel. Spectrometers, Detect. Assoc. Equip.*, vol. 902, pp. 14–24, 2018.

[69] E. L. Macconnachie and D. R. Novog, "Measurement , simulation and uncertainty quantification of the neutron flux at the McMaster Nuclear Reactor," *Ann. Nucl. Energy*,

vol. 151, 2021.

[70] B. J. Smith, “boa : An R Package for MCMC Output Convergence,” *J. Stat. Softw.*, vol. 21, no. 11, 2007.

[71] R. J. B. Goudie, R. M. Turner, and D. De Angelis, “MultiBUGS : A Parallel Implementation of the BUGS Modelling Framework for Faster Bayesian Inference,” *arXiv*, 2018.

[72] D. J. Spiegelhalter, N. G. Best, and B. P. Carlin, “Bayesian measures of model complexity and fit,” *J. R. Stat. Soc. Ser. B*, pp. 583–639, 2002.

[73] J. Wang, Z. Guo, X. Chen, and Y. Zhou, “Neutron spectrum unfolding based on generalized regression neural networks for neutron fluence and neutron ambient dose equivalent estimations,” *Appl. Radiat. Isot.*, vol. 154, no. August, p. 108856, 2019.

[74] International Atomic Energy Agency, “Compendium of Neutron Spectra and Detector Responses for Radiation Protection Purposes IAEA TRS 403,” Vienna, 2001.

5 Paper II

5.1 Publication Details

E. L. Macconnachie and D. R. Novog, “Measurement , simulation and uncertainty quantification of the neutron flux at the McMaster Nuclear Reactor,” *Ann. Nucl. Energy*, vol. 151, 2021.

The experimental campaign undertaken here was designed, planned, and implemented by the first author (E. MacConnachie), with on-going support from the MNR reactor manager (Rob Pasuta), as well as the MNR operations staff. The experimental data was collected, processed, and analysed entirely by the first author. The MCNP model of MNR – used to generate the computational results that supplement the experimental data – was developed by Dr. Simon Day in 2001, and updated by the first author as needed for this analysis. The OSCAR-4 data used as inputs to these simulations was provided by Mohammed Alqahtani. The computational data was processed and analysed by the first author. Dr. David Novog provided guidance on the development of this research. This paper was written entirely by the first author, with support in editing and revisions from Dr. David Novog.

Special thanks to Alice Pidruczny of MACCNAA for granting the first author on-going access to her lab space, and the entire McMaster Health Physics team for their support during this experimental campaign.

5.2 Preface

The focus of this thesis is to completely characterize and quantify sources of uncertainty in neutron flux and flux spectra measurements. Such measurements in research reactors are typically used as the basis for code validation studies, and may be applied in planning both operational and experimental procedures. Additionally, a full understanding of these uncertainties would enable more detailed UQ and sensitivity analyses of the reactor system to be carried out. The work developed in the previous chapter developed a generalized procedure for measuring, combining and reporting the uncertainties due to changing reactor parameters (e.g. control rod positions, reactor power etc.)[59]. As an extension of that work, this publication is focused on understanding the effects of fuel management operations on measurements of the neutron flux, and performing a preliminary validation study of the MCNP model of MNR.

These effects have been identified as being potentially important in activation experiments, and are known to drive significant changes in the bulk k_{eff}, however the exact nature of any uncertainty

they might contribute remains unquantified [15]–[17]. An experimental campaign was carried out over a period of 4 months (which included one refuelling operation in MNR) - and by combining the cadmium-difference method with threshold-activation detectors, the neutron flux in the thermal, the epithermal, and the fast energy groups was repeatedly measured over time.

While a seasonal Mann-Kendall test applied to the experimental data indicates no presence of a trend over time, the magnitude of uncertainties on the neutron flux measurements may prevent meaningful conclusions from being drawn from this information alone. The uncertainties associated with these neutron flux measurements were determined according to the method of [59], and were on the order of 5 % in the total, the thermal, and the fast energy groups. Owing to the methods used to determine the epithermal neutron flux, these values had an uncertainty of approximately 35 %. As has been noted, these uncertainties are generally dominated by the sample placement in the irradiation site, and the reactor power uncertainty. If these uncertainties could be significantly reduced (i.e. to below approximately 2%), it may be possible to investigate fuel management effects via purely experimental means. Given the magnitude of the uncertainties however, the following journal article supplements the flux measurements with simulation results to isolate the effects of fuel management on flux uncertainty

A series of MCNP simulations were conducted based on historical MNR configurations – with an emphasis on investigating pairs of cores that existed approximately 4 months apart (i.e. similar in duration to the experimental campaign). In each case, the change in axial power peaking factors (PPFs) was an approximately normal distribution centered at zero. This indicates that for the historical cores examined with MCNP, there is no significant bias in the neutron flux over a period of 4 months.

Over the duration of a typical fuelling cycle, this article demonstrates that the impact of fuel management is negligible and flux measurements for the validation of either operational or activation procedures may only be required once per core configuration. Several additional MCNP simulations were performed to investigate these impacts over a period of several years and multiple core changes, and showed similarly insignificant effects on flux results in site 8C. Nevertheless, if high-fidelity flux results are required, it is recommended that activation measurements be repeated after significant core changes in order to experimentally capture any changes in the spectrum.

After the publication of the following article, an additional parametric study using MCNP simulations was carried out to investigate an atypical fuelling scenario in MNR such that the effects of fuel burnup and fuel management could be investigated in an extreme case. Here, core 54A at Beginning-of-Cycle (BOC) was modified to create a flux-tilt so that every site adjacent to 8C was filled with fresh fuel (i.e. the power distribution was tilted towards the south end of the core). The same computational analysis was carried out between this tilted core, the original core 54A BOC, and core 55B BOC.

These results are presented in the following figures, which present the percent change in PPFs with the energy groups displayed in the following order (from top to bottom): thermal, epithermal, fast, and total. The distribution of these values within the active core region, along with its mean and standard deviation, is also presented.

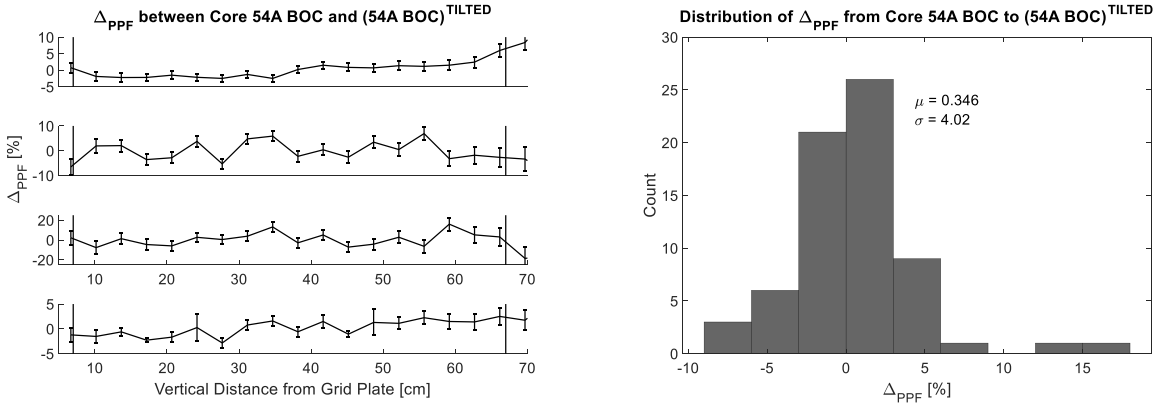

Figure 19: Change in PPFs between a typical core configuration, and a tilted version of that same configuration. The active region of the core is denoted by the vertical lines.

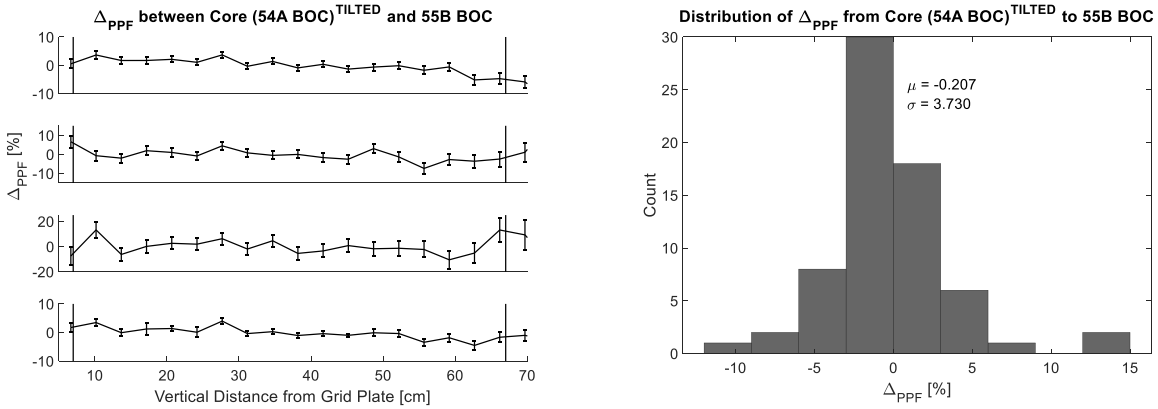

Figure 20: Change in PPFs between a tilted core configuration, and a subsequent typical core configuration. The active region of the core is denoted by the vertical lines.

The results from these additional simulations show that, even in an extreme case (i.e. where the power distribution of the core is significantly tilted towards the irradiation site), the effect of these

core modifications on the neutron flux results remains small, and in general accounts for less uncertainty than that resulting from either the indicated reactor power or the sample positioning.

Measurement, Simulation and Uncertainty Quantification of the Neutron Flux at the McMaster Nuclear Reactor

Abstract

Neutron flux measurements in research reactors can be used for code validation and optimizing in-core activation procedures. Since the fuel adjacent to an irradiation site undergoes burnup, and may be shuffled, local flux measurements may be subject to an additional source of burnup-dependent uncertainty. It is unfeasible to perform these measurements for all core conditions; therefore, reactor physics codes may provide supplemental flux information.

This work includes a validation study of the MCNP6 model of the McMaster Nuclear Reactor (MNR). Irradiations were performed over several months, with an emphasis on uncertainty quantification during data processing. No change in the local flux was measured over this period of operation, indicating that burnup effects may be insignificant compared to other sources of uncertainty. These results were validated by five sets of computational data from historical MNR cores. Burnup effects do not need to be accounted for in determining neutron flux uncertainties.

Key Words

McMaster Nuclear Reactor

Neutron activation analysis

Nuclear data uncertainty

MCNP

Uncertainty Quantification

Nomenclature

BOC	Beginning of Core
EOC	End of Core
HFIR	High Flux Isotope Reactor

HPGe	High Purity Germanium
LEU	Low-enriched Uranium
MCNP	Monte-Carlo N-Particle
MGRAC	Multi-Group Reactor Analysis Code
MNR	McMaster Nuclear Reactor
MTR	Materials Testing Reactor
OSCAR	Overall System for CAlculation of Reactors
PPF	Power Peaking Factor
TRIGA	Training, Research, Isotopes and General Atomics Reactors
UQ	Uncertainty Quantification
ZED-2	Zero Energy Deuterium Reactor

R	Activation rate [atoms/s]
A	Activity [1/s]
T	Time constant
N	Number of atoms
$\phi(E)$	Flux per unit energy [$cm^{-2}\,s^{-1}\,eV^{-1}$]
Φ	Energy-integrated flux [$cm^{-2}\,s^{-1}$]
$\sigma_{n,x}(E)$	Energy dependent cross section for reaction (n,x) [cm^2]
σ_{eff}	Effective cross section [cm^2]
$r_{x,g}$	Neutron induced reaction rate in isotope x in energy group g [1/s]
P	Reactor power
ν	Average number of neutrons released per fission event
$E_{fission}$	Energy released per fission event [MeV]
E_0	Most probable energy for a Maxwellian distribution
Q	Energy conversion factor, $Q = 1.6022 \times 10^{-13}$ J/MeV
k_{eff}	Effective multiplication factor
F_{Cd}	Cadmium correction factor

1 Introduction

The neutron flux is an important parameter in nuclear reactors, as its behavior dictates all neutron-induced reaction rates occurring in the core. Although local energy-dependent measurements of the neutron flux are difficult to perform in power reactors, they can be made more readily in research reactors, and thus may provide useful data for code validation studies, fuel management decisions, and medical isotope production. A complete knowledge of the uncertainties associated with these measurements is also critical, as they may limit the conclusions to be drawn from the data and motivate further work to reduce the significant contributors to the final combined uncertainty. For example, a measurement of the neutron flux spectrum at a given irradiation site may provide useful information for the optimization of isotope production, but may not provide sufficient fidelity to assist in fuel management operations. The aim of this work is to collect new measurements of the neutron flux in MNR to asses the performance of the MCNP6 model of the core and understand the measurement and simulation uncertainties over a prolonged period of operation.

While measurements of the fine energy structure of the neutron flux spectra can be challenging, there are well-established techniques to recover a few-group energy structure of the neutron flux. These methods combine the study of threshold activation reactions with the selective shielding of low energy neutrons by a cadmium filter, such that the total, the thermal, the epithermal, and the fast neutron fluxes can be recovered. Previous work has shown that, during the measurement procedure, uncertainties may arise due to the counting time, the geometry, and the sample mass and configuration [59]. In addition to these typical measurement uncertainties, several reactor parameters have been posited to contribute to the overall uncertainty associated with a flux measurement. These parameters – the uncertainty in the sample position in the core [15], the presence of ^{135}Xe [8], control rod movement and nuclear data [11], and the reactor power [13] – have been studied for irradiations performed at MNR. A procedure for quantifying and combining these uncertainties has been developed such that future flux measurements can be reported with their complete uncertainty value [59].

It is necessary to understand how these measurements and their associated uncertainty can be used to validate reactor physics codes used during the planning of fuel management activities, specimen irradiation and isotope production. Finally, the effects of fuel burnup must also be studied to

determine whether some time-dependent effects must be considered in irradiation experiments. It has been indicated that the effects of fuel burnup may be significant, but in general, these have not been quantified [16]. Computational results from Training, Research, Isotopes and General Atomics Reactors (TRIGA) have indicated that the effects of burnup can drive significant changes in the bulk k_{eff}, but their effects on the neutron flux have not been fully investigated either computationally or experimentally [15], [17]. At MNR, the neutron flux distribution is assumed to remain fixed over the lifetime of a single core configuration under steady-state operation [39]. The aim of this work is to perform few-group flux measurements over an extended period of operation and compare these measurements and their uncertainty to the predictions from the MCNP6 model of MNR.

If all the components of neutron flux measurement uncertainties are quantified, the acquired data can be used directly with a selected reactor physics code in uncertainty quantification (UQ) procedures, or as inputs to a Bayesian model for further studies of the fine structure of the neutron flux energy spectrum. Knowledge of the neutron flux energy spectrum and its uncertainty may also be used to optimize certain activation procedures (such as medical isotope production) and to inform research and development decisions that involve changes to the core configuration, or that reflect system upgrades. For example, the production of radioisotopes for radiation therapy and imaging in many research reactors is sensitive to both the energy spectra and spatial distribution of the neutron flux in the core, and the balance between activation and the generation of unwanted by-products must be considered. Additionally, in a well-defined neutron flux, high-fidelity materials irradiation studies can be carried out to investigate both irradiation damage and nuclear heating in various samples [49].

The objective of this work is to make repeated measurements of the few-group energy structure of the neutron flux in MNR over an extended period of operation and use the results for a direct comparison to the outputs of the MCNP6 model of the core. While the analysis presented here is specific to MNR, the methodology can be applied for all research reactors that may use activation procedures to estimate the neutron flux, such as in the Zero Energy Deuterium (ZED-2) reactor or in the High Flux Isotope Reactor (HFIR) [49], [50].

1.1 The McMaster Nuclear Reactor

MNR is a light-water cooled and moderated, open-pool Materials Testing Reactor (MTR) located on the McMaster University campus in Ontario, Canada. The reactor typically operates 16 hours per day, from Monday to Friday, and is shutdown on weekends. MNR is currently a world leader in ^{125}I production for use in the treatment of prostate cancer, and is actively pursuing the development of other radioisotopes and a variety of cross-disciplinary research projects, where an accurate knowledge of the neutron flux in the irradiation sites is a key input parameter [38].

The core consists of MTR-type low-enriched uranium (LEU) fuel assemblies, reflector sites, and absorber rods that are housed in a 9 x 6 grid plate. The fuel assemblies typically contain 18 curved plates – where the inner 16 plates are uranium particles (enriched to 19.75% ^{235}U) in an aluminium matrix, and the outer plates are pure aluminium [59]. There are two types of absorber rods present in the core: five gang-operated Ag-In-Cd shim-safety rods for coarse reactivity control and shutdown procedures, and a single stainless-steel regulating rod for automatic fine reactivity control. These rods are moved in to the core from the top using motors and an electromagnetic clutch, except during a loss of electrical power or by the initiation of shutdown procedures, in which case they fall in to the core under the action of gravity [39]. An overhead view of a reference core configuration is shown in Figure.

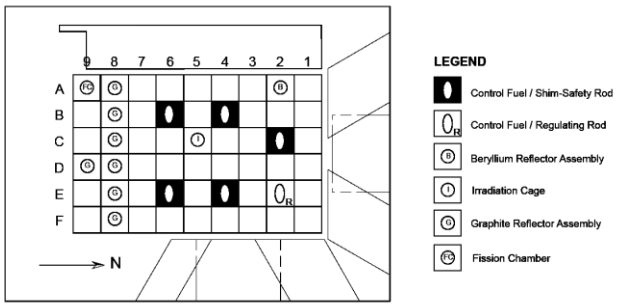

Figure 1: Overhead view of a reference core configuration for MNR. There are typically 34 fuel sites housed in rows 1 to 7, 6 graphite reflector sites, 12 vacant sites, a beryllium reflector site (site 2A), and a central irradiation facility (5C).

Refueling and fuel shuffling operations are performed on an as-needed basis, based on neutron flux estimates in the core and the inferred fuel depletion. These flux estimates are based on the activation of CuMn wires placed between fuel plates at the axial centerline of each assembly in the core. The results of these activation measurements provide an estimate of the power distribution in the core, which is assumed to remain fixed over the next operational interval (called

the lifetime of the core, i.e. between refueling or shuffling operations). When either the flux wire measurements or control rod positions dictate, new fuel is introduced to the core, or a fuel shuffling operation is performed. For typical full power operations (3 MW_{th}), refueling takes places approximately twice per year, and fuel shuffling occurs approximately once every two months [39].

1.2 Uncertainty Quantification for Reactor Physics

This work uses a combination of MCNP6 simulations and in-core activation data to perform a validation study of the core model, with a focus on understanding the effects of fuel depletion and incorporation nuclear data uncertainties. As there are a limited number of materials that can generate useful activation data, the neutron flux in a continuous energy spectrum cannot be determined directly. However, through a careful materials-selection process and through the selective shielding of certain neutron energy ranges, it is possible to isolate the neutron flux in a few-group formalism. The first stage of analysis is to generate estimates for the activation cross sections in each of these coarse energy bins for each reaction being studied (which is done via MCNP6 simulations as described in Section 2.2). The recovered few-group cross sections can then be used to convert measured activation rates to neutron flux values. The uncertainties associated with each stage of analysis are then propagated through to the final result according to the methodology of previous work conducted in MNR [59]. This work is focused on generating few-group neutron flux data over many core loading patterns and depletion stages in MNR. This data will be used to perform a validation study of the MCNP6 model of MNR, with an emphasis on understanding the effects of depletion on the neutron flux.

2 Methodology

The work presented here uses irradiations performed in MNR to generate flux measurements and their associated uncertainties along the vertical axis of the core. The neutron activation technique (discussed in Section 2.1) is used to generate these measurements, which are to be analyzed according to the formalism of the neutron energy spectrum described in Section 3. Additionally, full-core MCNP6 simulations were performed to form the basis of the code validation study. A full discussion of the MCNP6 predictions over several months and core loading patterns, and their comparison to the experimental data are presented in Section 4.

2.1 Irradiation and Data Collection

When certain materials are exposed to a neutron field, they will undergo nuclear transmutation via some general (n, x) reaction, and become unstable. A measurement of the activity of these decaying daughter isotopes can be used to determine the activation rate in the sample during its irradiation. The activation rate, R (the number of radioisotopes created per second by the (n, x) reaction) is governed by the following equation [59]:

$$\boldsymbol{R = AT = N \int_0^\infty \phi(E)\sigma_{n,x}(E)dE} \quad \mathbf{1}$$

Here, $\phi(E)$ is the neutron flux energy spectrum and $\sigma_{(n,x)}(E)$ is the energy dependent (n, x) cross section, both of which are considered over all positive energies E. The measured quantities are: A – the net γ-ray activity of the decaying daughter products, T – a time constant to account for irradiation and decay times, and N – the number of precursor atoms in the sample. The experimental work described herein involves the irradiation of thin wires (approximately 1 mm in diameter) housed in custom-built sample holders over the active length of the core (approximately 70 cm). After the reactor has been brought to the desired operating power, operations staff place the sample holder in the chosen irradiation site. Following irradiation (typically 15 minutes), and a decay period to allow for safe handling (typically 5 days), the wire is cut into 3.5 cm segments, and the activity of each segment is measured. The axial location of each wire segment is recorded so that the spatial distribution of the neutron flux can be reconstructed.

The γ-ray activity of the samples is measured using a p-type, coaxial, high purity germanium (HPGe) detector. Both the detection and geometrical efficiencies of the system have been fully characterized using several standard radiation sources, and an MCNP6 model of the measurement setup, respectively [59]. The detector system and counting setup were characterized prior to the irradiation experiments performed during this work. Count times and detector-sample distances are routinely adjusted so that Gaussian counting statistics can be applied to the measured data, and the associated uncertainty is less than 1%.

In addition to measurement uncertainties, several reactor parameters are known to contribute to the overall uncertainty associated with results from an irradiation experiment. These parameters are: the presence and uncertainty in the ^{135}Xe load in the core, uncertainty in sample positioning, the reactor power level uncertainty, changing control rod positions, and the effects of nuclear data.

Based on a previous investigation of MNR Site 8C, a methodology for quantifying and combining these uncertainties has been developed [59]. The effects of changing control rod positions and ^{135}Xe are included in the analysis via individual correction factors, and have been found to be highly covariant. These effects, and the uncertainties associated with the sample positioning, reactor power level, nuclear data homogenization procedures, and the measurement procedure are combined according to the classical rules of uncertainty propagation with both independent and covariant terms present in the analysis. When this methodology is applied to the experimental procedure described above, the final reported uncertainty is approximately 7%, and is dominated by the uncertainty in both the sample positioning and the reactor power level. The experimental results presented in Section 4 will report neutron flux uncertainties according to this methodology.

While the movement of the control rods and the concentration of ^{135}Xe in the core follow weekly trends, an investigation of control room logs and data (e.g. the control rod positions) from 2017 does not indicate any time dependence of these variables on a larger time scale (i.e. overall several months, and with fuel depletion). Hence, burnup information is not captured by the evolution of the operational parameters included in the logs, and an additional source of uncertainty in neutron flux measurements due to fuel burnup may be present. A comprehensive study of the effects of fuel burnup must be carried out for the complete characterization of uncertainties in neutron flux measurements, in particular for use in operational assessments of fueling requirements and isotope production procedures.

2.2 Monte Carlo Simulation

The MCNP model of MNR has been in use since 2001 and has been updated continually to reflect changes in components, layout, and materials. This multipurpose model has been used to support safety and licensing, experimental work, and several multi-disciplinary design project. The model currently uses the latest version of MCNP (MCNP6) and the ENDF/B-VI nuclear data libraries. MCNP6 simulations have been used in previous work, particularly to quantify the control rod corrections factors discussed above [59]. The same model is adopted here to determine few-group activation cross sections (a detailed description can be found in Section 3.1.1), and is used as the basis for the comparison of in-core measurements to simulation results.

The MCNP6 model of MNR includes the geometry of the reactor pool, the six beam ports radially flanking the pool, and the shielding material surrounding the western side of the core. The

geometry of the fuel has been modelled by adopting the following simplifications: the curvature of the fuel plates is not modelled, and each fuel plate is divided in to seven axial sections for burnup distribution purposes. These features of the fuel geometry and other notable assemblies in the model are shown in Figure.

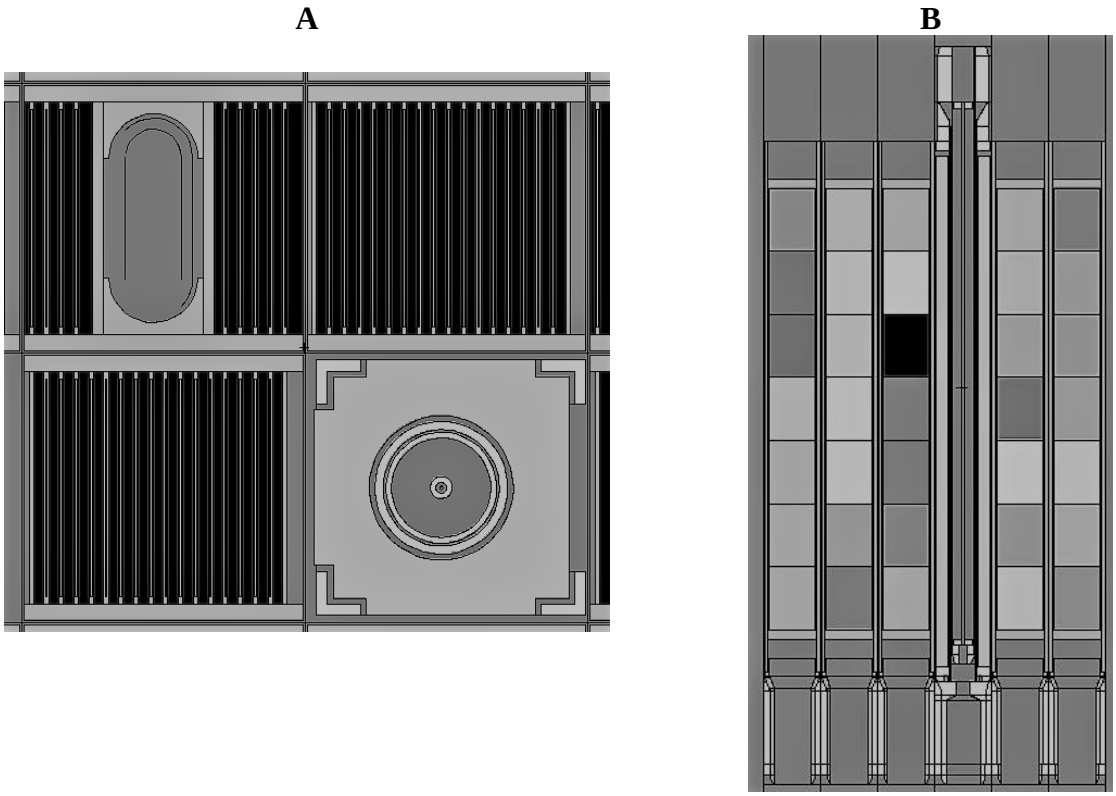

Figure 2: Features of the MCNP6 model showing the simplified geometry of the fuel material and other core assemblies. A: Overhead view of four assemblies. Clockwise from top-right: LEU fuel assembly, wire holder used for flux-wire experiments, LEU fuel assembly, and control rod assembly. The straight geometry of the fuel can be seen. B: A vertical slice through row 5 in MNR. The seven axial fuel regions can be seen, and the wire holder is also displayed.

The model has been written such that the material definitions for the fuel plates can be updated to reflect any core configuration and burnup state. To simulate several MNR cores, the output of the Overall System for CAlculation of Reactors (OSCAR-4) code was used to define the isotopic composition of the fuel in MCNP6 for each core configuration.

OSCAR-4 is a nodal-diffusion based deterministic code that can be used for the determination of the fuel inventory for different burnup states. A two-dimensional cell calculation which uses nuclear data based on the JEFF2.2 library is followed by a three-dimensional core calculation by Multi-Group Reactor Analysis Code (MGRAC), and the isotopic composition of the fuel in each plate can be extracted directly [42]. OSCAR-4 is being applied in MNR as part of an on-going project to perform core-follow calculations in the reactor, and daily burnup steps based on typical

operational schedules are the basis of these calculations. In these calculations, the following 38 isotopes are explicitly tracked:

- ^{234}U to ^{238}U
- ^{237}Np, ^{239}Np
- ^{248}Pu to ^{242}Pu
- ^{241}Am, ^{243}Am
- ^{242}Cm to ^{245}Cm
- ^{135}I
- ^{135}Xe
- ^{141}Ce, ^{142}Ce, ^{144}Ce
- ^{143}Pr
- ^{143}Nd to ^{148}Nd
- ^{147}Pm to ^{149}Pm (^{148m}Pm included)
- ^{147}Sm to ^{149}Sm
- ^{10}B

Minor fissions products are grouped together and set equal to the boron reaction rate.

The composition of each isotope being tracked is a function of the power history, and for fresh fuel has no uncertainty since fabrication processes are tightly controlled. The maximum isotopic uncertainty has been reported as 6.97%, which occurs at the end of cycle [42]. A previous study has shown generally good agreement between the outputs from Serpent-2, OSCAR-4, and flux-wire estimates of the burnup, in MNR. A full consideration of the isotopic uncertainties is therefore excluded from this work, and the material cards generated with OSCAR-4 will be applied to generate estimates of the local flux [42].

To simulate the wire irradiations described in Section 2.1, a pure F4 tally imposed on the wire within the wire holder (shown in Figure) can be used to determine the neutron flux directly, according to the following equation [29]:

$$\boldsymbol{\phi} = \frac{\boldsymbol{P\nu}}{\boldsymbol{QE_{fission}k_{eff}}} \cdot \boldsymbol{F4} \qquad \mathbf{2}$$

The criticality calculations are run so that the statistical uncertainty on the tallies is less than 1%, and this can generally be achieved with 1,000 active cycles s x 100,000 particles per cycle.

3 Neutron Flux Spectrum

The neutron flux spectrum in a well moderated system is often divided into three energy groups: thermal, epithermal, and fast [32]. Under this formalism, the total energy-integrated neutron flux can be expressed as the sum of the neutron fluxes integrated over these three energy groups:

$$\boldsymbol{\Phi_{total} = \Phi_{thermal} + \Phi_{epithermal} + \Phi_{fast}} \qquad \mathbf{3}$$

The thermal neutron flux is theoretically defined by a Maxwellian distribution whose most probable neutron energy is $E_T = kT$ (0.0253 eV for T = 293 K) and is defined by an upper energy limit between 0.1 eV and 0.68 eV [18], [32]. Section 3.1 provides a detailed investigation in to a suitable choice for the upper energy limit for the thermal region for the purposes of this research.

The epithermal energy region is characterized by the moderation of neutrons from the fast to the thermal energy groups and in an ideal system (i.e. one in which the moderator is infinite, homogeneous and non-absorbing) is defined by the following equation [18]:

$$\boldsymbol{\phi_{epithermal}(E) \propto \frac{1}{E}} \quad \textbf{4}$$

The fast flux spectrum is dominated by the release of fission neutrons in the fuel, and for the fission of ^{235}U, it takes the form of the Watt spectrum [31]. This region of the spectrum is defined by neutron energies greater than 1 MeV [32].

3.1.1 Cross Section Collapsing

To calculate the neutron flux from a reaction rate measurement, some information about the activation cross section must be known – either directly from a nuclear data library, through a homogenization procedure over a specified energy range, or through the judicious selection of a single value. Typically, the homogenization procedure involves the determination of an effective (or average) cross section over a given energy range – and is usually defined as the neutron spectrum weighted mean of the cross section. Using this definition of an effective (or average) cross section, the energy integrated neutron flux can be directly determined. These values can be calculated according to the following equation [8], [11]:

$$\boldsymbol{\sigma_{eff} = \frac{\int_{E_{low}}^{E_{high}} \phi(E)\sigma(E)dE}{\int_{E_{low}}^{E_{high}} \phi(E)dE} \quad \rightarrow \quad \Phi = \left(\frac{R}{N}\right)\left(\frac{1}{\sigma_{eff}}\right)} \quad \textbf{5}$$

In the absence of experimental information about the neutron energy spectrum, effective cross sections can be determined either computationally or by the adoption of a generic flux spectrum. Given that there is insufficient neutron flux data in MNR, and that using a generic light-water reactor spectrum may introduce some bias in the results due to the assumption of homogeneity in the system, this work will utilize MCNP6 simulations to estimate the collapsed cross sections. For a neutron induced reaction x in some energy group g, the effective cross section is:

$$\boldsymbol{\sigma_{eff(x,g)} = \frac{r_{x,g}}{\Phi_g}} \quad \textbf{6}$$

In Equation 6, $r_{x,g}$ is the neutron induced reaction rate, and Φ_g is the energy integrated neutron flux. Pure F4 tallies and F4 tallies modified with an FM card can be used to determine the fluxes and reaction rates, respectively [29]. This can then used to determine the effective cross section directly. Its uncertainty can be calculated by combining the uncertainties of the reaction rates and fluxes in quadrature, both of which are statistical in nature.

3.1.2 The Cadmium Difference Method

The neutron capture cross section of ^{113}Cd is sufficiently high at low energies (~ 10^5 b) that a layer of cadmium can act as a high-pass filter for neutrons during activation procedures [22]. For a neutron field with no fast component, a pair of irradiations can be carried out with one bare, and one cadmium covered sample, such that the activation owing to thermal neutrons is [18]:

$$\boldsymbol{R_{thermal} = R_{bare} - F_{Cd}R_{Cd}} \quad \textbf{7}$$

While reactors do have a significant fast flux component, most useful detector materials have insignificant (n,γ) cross sections above 1 MeV such that the activation owing to fast neutrons is negligible and Equation 7 is valid.

F_{Cd} is the cadmium correction factor and accounts for epithermal neutrons that are absorbed by the cadmium. This value is defined as the ratio of epithermal to cadmium-covered activation rates in the sample and can be determined from an MCNP6 simulation by using F4 tallies modified by FM multiplier cards. A cadmium cover having a thickness of 1 mm has a thermal transparency of ~ 10^{-6}, and is therefore sufficient for most experimental purposes [18]. Typically, ^{197}Au is used when applying this method, as it can generate measurable activities under cadmium with short irradiation times. However, other isotopes with suitable activation cross sections at lower energies (e.g. ^{50}Cr, ^{63}Cu or ^{55}Mn) can be used when longer irradiation times are possible.

When the cross section collapsing methods discussed in Section 2.2.1 are applied with the cadmium difference method, the thermal and the total neutron fluxes can be determined from the following equation (where R_{total} refers to the activation of the bare irradiated sample):

$$\boldsymbol{\Phi_{thermal\ or\ total} = \left(\frac{R_{thermal\ or\ total}}{N}\right)\left(\frac{1}{\sigma_{eff(thermal\ or\ total)}}\right)} \quad \textbf{8}$$

3.1.3 Threshold Activation

Certain neutron induced reactions will only occur above some threshold energy value, and can therefore be used to make measurements of the fast neutron flux directly. From the cross section collapsing methods outlined in Section 2.2.1, the fast neutron flux can be calculated from a measurement of a threshold activation reaction rate:

$$\boldsymbol{\Phi_{fast} = \left(\frac{R_{fast}}{N}\right)\left(\frac{1}{\sigma_{eff(threshold)}}\right)} \quad \textbf{9}$$

These threshold reactions will typically dominate the absorption of fast neutrons by ^{113}Cd, so judicious materials selection may allow for the determination of all components (i.e. total, thermal, epithermal, and fast) of the flux from the irradiation of a bare, and of a cadmium covered sample.

4 Results

Several few-group neutron flux measurements were generated in MNR Site 8C between the start of June 2019 and the end of September 2019. This new data set was used to perform a code validation study of the MCNP6 model of MNR, with an emphasis on the effects of fuel management operations and depletion. Sections 4.1 and 4.2 present the results from the cross section homogenization procedure, and the measured few-group neutron flux values, respectively, and the results from the simulations are discussed in Section 4.3.

To study each energy group defined in Equation 3, a NiCr alloy can be used. The ^{50}Cr (n,γ) cross section is sufficiently small and well-behaved for low neutron energies that the cadmium difference method can be used to recover the thermal and total neutron flux, and the ^{58}Ni (n,p) threshold reaction can be used to measure the fast neutron flux directly. The epithermal neutron flux can then be determined from Equation 3. These experimental procedures consist of the irradiation of bare NiCr wires, followed by the irradiation of an NiCr wire wrapped in a cadmium sheath. Irradiation times of 15 minutes at a reactor power of 500 kW, followed by a decay period of 7 days, were found to generate sufficient activity for measurement, while remaining within the safe handling limits prescribed by Health Physics. The results of the cross section collapsing procedure, followed by a complete investigation of the experimental results, are presented in the following sections.

Additionally, simulations of several historical MNR cores were carried out to investigate the effects of fuel burnup, fuel shuffling, and refuelling operations on local flux distributions. These simulations were carried with several core configurations that were deployed in MNR between 2007 and 2011. These represent the most current information available from core-follow calculations that have been completed for MNR. As these cores are not currently in use in MNR, the simulation results cannot be used to validate the absolute neutron flux, but may be used to understand any relative changes in the flux distribution over time. The typical operational schedule and fuel compositions (i.e. LEU fuel) have remained unchanged between 2007 and the present

day, and so this historical core information may be used to estimate the effects of fuel management and depletion.

Historical core maps were used to define the geometrical configuration of the MCNP6 model, and the isotopic composition of the fuel elements for each core configuration was provided by researchers developing an OSCAR-4 model for use with MNR. In all cases, statistical uncertainties of less than 1% were achieved by running the KCODE calculations with 100,000 particles per history and 4,000 active histories.

A detailed discussion concerning the results of these simulations is presented in Section 4.3.

4.1 Cross Section Collapsing

The effective cross sections required to determine neutron fluxes from activation measurements can only be determined following an appropriate division of the neutron energy spectrum. The energy groups in Equation 3 are defined by the upper limit of the thermal group, and the lower limit of the fast group. These bounds can be determined for the purposes of this research by an investigation of the behavior of the cross sections of interest within these energy groups.

The thermal energy group has previously been defined by a maximum energy between 0.1 eV and 0.65 eV [18], [32]. A series of MCNP6 simulations were carried out to determine an appropriate upper bound for the thermal energy group in MNR Site 8C. This was done by adjusting the upper limit of the thermal energy group from 0.1 eV to 0.65 eV in increments of 0.05 eV and investigating the trends in the collapsed ^{50}Cr (n,γ) cross section values. The appropriate lower energy bound was determined by iteratively excluding the lowest energy data point and fitting the remaining points to the ideal form of the effective cross section in the epithermal energy group. The subset of data which provided the best fit was found to be 0.2 eV, and this value is therefore taken as the upper limit of the thermal energy group.

The fast energy group is typically defined by a minimum energy of 0.1 MeV however, the ^{58}Ni (n,p) reaction has a cross section equal to zero below 0.8 MeV [22], [32]. In this case, information recovered about the fast flux is restricted to energies above this threshold, and 0.8 MeV is taken as the lower limit for the fast flux for the purposes of this investigation. In applying this lower limit to the fast energy group, both the prompt and delayed neutrons may contribute to the threshold activation of ^{58}Ni. Two MCNP6 simulations of a flux wire irradiation under this energy

discretization were carried out to determine the contribution of the delayed neutrons to the final activation result by applying the functionality of the TOTNU data card. It was determined that the contribution of the delayed neutrons to the ^{58}Ni (n,p) reaction was insignificant. The fast flux results presented here are therefore an indication of the prompt fission neutron spectrum.

Having determined the appropriate energy bounds for the thermal, the epithermal, and the fast groups, and the effective cross sections for each energy group and for each segment along the wires, were calculated according to Equation 6. The uncertainties associated with these effective cross sections were calculated by combining the uncertainties of $r_{(x,g)}$ and Φ_g – which are statistical in nature – in quadrature. In determining the thermal, the epithermal, the fast, and the total neutron fluxes, the effective cross section uncertainties were included according to the typical rules of error propagation. As has been noted in previous work conducted in MNR, nuclear data uncertainties are typically dominated by those associated with the reactor power level and the sample placement in the irradiation site [59].

A summary of these energy bounds and the calculated effective cross sections, is presented in Table 4. Average values (across the length of the wire) of the effective cross section are presented for demonstration purposes.

Table 4: Summary of the energy bounds and effective cross sections used to determine the neutron flux. An effective cross section is not required in the epithermal group, as this flux is determined directly from Equation $\boldsymbol{\Phi_{total} = \Phi_{thermal} + \Phi_{epithermal} + \Phi_{fast}}$3.

$0 < E_{total} < \infty$	$\sigma_{Cr} = 9.58 \pm 0.11$ b
$0 < E_{thermal} < 0.2$ eV	$\sigma_{Cr} = 13.73 \pm 0.05$ b
0.2 eV $< E_{epithermal} < 0.8$ MeV	
0.8 MeV $< E_{fast} < \infty$	$\sigma_{Ni} = 124.02 \pm 3.78$ mb

4.2 Neutron Flux Measurements

Several irradiations were carried out between the start of June, 2019 and the end of September, 2019. The initial irradiations were carried out in a core configuration that had been subject to approximately one month of steady-state operations. A refuelling operation was carried out on July 22, the date of an irradiation procedure reported in this work. During this fuel management operation, two fuel assemblies with high burnup were removed from the core, and replaced with new assemblies. Additionally, five fuel assemblies were moved to different positions in the core.

The core configuration established on July 22, 2019 remained in place for the remainder of the irradiation procedures described here.

All irradiations were carried out immediately following reactor start-up during Monday operations to minimize the corrections needed to account for the build-up of ^{135}Xe. The reported flux uncertainties were derived according to [59] and account for the effects of sample position, reactor power uncertainty, corrections for control rod movement, and nuclear data and measurement uncertainties.

Figure shows a sample of the measured neutron flux data in each energy group.

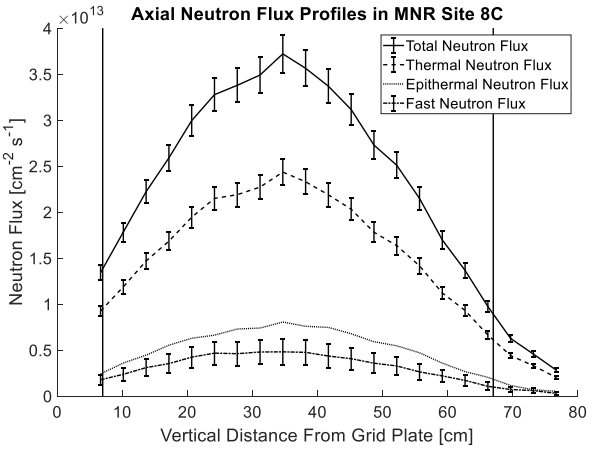

Figure 3: Representative axial neutron flux profiles, as measured on September 9 2019. The solid vertical lines indicate the active region of the core. The epithermal neutron flux uncertainties are on the order of 35% and are not shown here.

In general, the uncertainties associated with measurements of the total, thermal, epithermal, and fast fluxes are on the order of 5.5%, 5.7%, 35%, and 5.8%, respectively. In all cases, counting times and geometries were adjusted so that the measurement uncertainty was less than 1.5%. The uncertainties associated with sample position in the irradiation site and the reactor power level (both of which have magnitudes of approximately 3.5%) dominate the remaining portion of these reported uncertainties. The uncertainty associated with the epithermal flux is the largest, as this value is determined by subtraction of the fast and thermal fluxes from the total flux. In this case, the magnitude of the total, thermal, and fast uncertainties are added in quadrature. When combined with the presence of a threshold detector, the total, thermal, and fast fluxes can be recovered with high precision however, a large uncertainty associated with the epithermal neutron flux must be accepted.

As all measured flux data was corrected to account for variations in the control rod positions, any remaining trend in the data may indicate that fuel burnup and its associated spectral changes may cause additional uncertainty in the measurements. A seasonal Mann-Kendall test was carried out on the fluxes in each energy group to determine whether a trend in the data is present. The seasonality (i.e. the repetition of the axial distribution) of the data was accounted for by conducting the Mann-Kendall test on the flux data for segment separately, and investigating the combined result [60]. In all cases, at the 99% confidence level, the null hypothesis that there is no trend present in the data could not be rejected. The results from these tests has been summarized in Table 5.

Table 5: Results from the seasonal Mann-Kendall test applied to the measured fluxes in each energy group. H = 0 indicates the null hypothesis cannot be rejected at the 99% confidence level – i.e. there is no trend in the flux data.

	Total Flux	Thermal Flux	Epithermal Flux	Fast Flux
α	0.01	0.01	0.01	0.01
p	0.2979	0.2746	0.2129	0.2731
H	0	0	0	0

The results from these statistical tests are further confirmed by an investigation of the composition of the neutron flux spectrum between June and September of 2019. As shown in Figure, all the thermal and epithermal fractional values agree within uncertainty, and the majority of the fast flux fraction values agree within uncertainty.

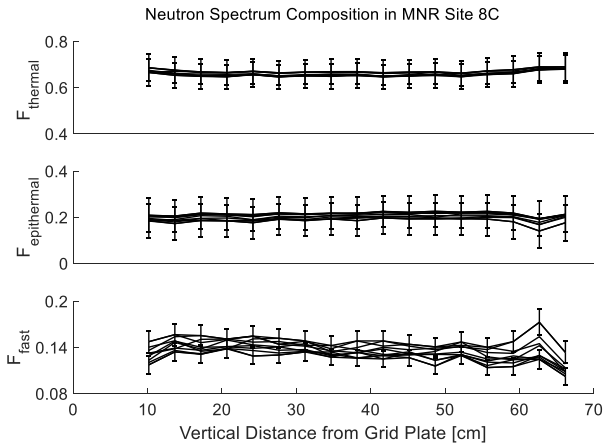

Figure 4: Neutron spectrum composition from June to September 2019 in MNR Site 8C. Each data set represents the results from a single irradiation. A legend including the date of irradiations is not shown here for clarity.

4.3 Computational Results

Several MCNP6 simulations of historical MNR core configurations were carried out to generate few-group neutron flux data for comparison the experimental results presented in Section 4.2. The experimental data that is supplemented with these computation results, will be investigated to understand the effects of burnup and fuel shuffling operations on estimates of the local neutron flux. In all simulations, the positions of both the regulating and shim rods were fixed, and the neutron fluxes were tallied in site 8C to match the current experimental setup. Several historical core changes representative of the duration of the experiments described in Section 4.2 were used to generate the MCNP6 neutron flux data. Table 6 summarizes the different pairs of cores being investigated, with a note indicating the elapsed time between the establishment of each core.

Table 6: Pairs of historical cores being used to examine the combined effects of fuel burnup and aging, and fuel shuffling operations. The cores are listed in chronological order. BOC indicates beginning of core, and EOC indicates end of core.

Core Pair		Notes
54A BOC	55B BOC	4 months, 0 days of typical operation
54B BOC	55C BOC	4 months, 6 days of typical operation
56DpI EOC	56G BOC	3 months, 25 days of typical operation
57C BOC	57E BOC	3 months, 23 days of typical operation
57E BOC	57G BOC	4 months, 3 days of typical operation

For each core reported in Table 6, the neutron flux was calculated in MNR Site 8C using a segmented, pure F4 tally. From these simulation results, the difference in the axial power peaking factors (PPFs) were calculated in the thermal, epithermal, fast, and total energy groups, where the PPFs are defined as:

$$PPF(y) = \frac{\phi(y)}{\bar{\phi}} \quad \textbf{10}$$

The distribution of these values within the active region of the core was investigated to determine whether a significant difference existed between the pairs of cores listed above.

The five pairs of cores listed in Table 6 were used for a direct comparison to the experimental data presented in Section 4.2, and a final set of core configurations (over 2 years, 17 days of typical operation) was used to draw conclusions about changes to the neutron flux over a larger operational time scale. The difference in the axial PPFs in the three energy groups, and a distribution of these values are shown in Figure 5 to Figure 10. Figure 5 to Figure 9 shows the information from the

core distributions listed in Table 6, and Figure 10 shows the change in PPFs over approximately 2 years of typical operation in MNR.

Figure 4 shows that the composition of the neutron flux along the length of the flux wires and across each day, agree within the reported experimental uncertainties for over 90% of the measured data points. The results presented in Table 5 indicating that there is no statistically significant trend in the measured few-group neutron flux over a period of approximately 4 months are corroborated by the MCNP6 results presented in Figure 5 to Figure 9. These results demonstrate that the combined effects of fuel management operations (refuelling and shuffling) do not contribute significant changes to the neutron flux, in any of the three energy groups. Having validated these MCNP6 results, the results presented in Figure 10 may be used to draw conclusions about the behavior of the neutron flux on a longer time scale. The information presented in this figure indicates that, even over the course of 2 years, the combined effects of fuel burnup and fuel management operations do not cause any significant changes in the few-group neutron flux.

Figure 5 through Figure 9 present the percent change in PPFs with the energy groups displayed in the following order in each figure (from top to bottom): thermal, epithermal, fast, and total. The uncertainties presented in these figures are the result of propagating the statistical uncertainties from MCNP6 through the calculations of the change in PPFs. The distribution of these values within the active core region, along its mean and standard deviation, is also presented.

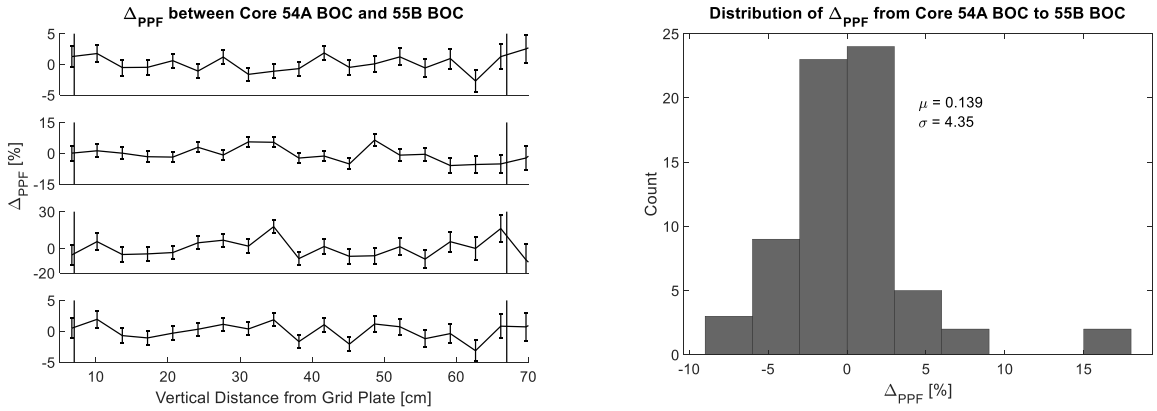

Figure 5: Change in PPFs following 4 months of typical reactor operations. The active region of the core is indicated by the vertical lines.

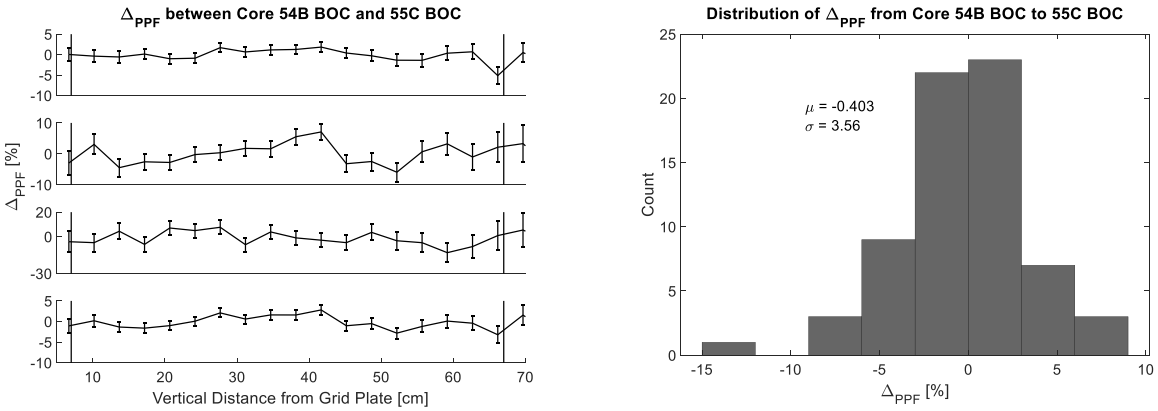

Figure 6: Change in PPFs following 4 months, 6 days of typical reactor operations. The active region of the core is indicated by the vertical lines.

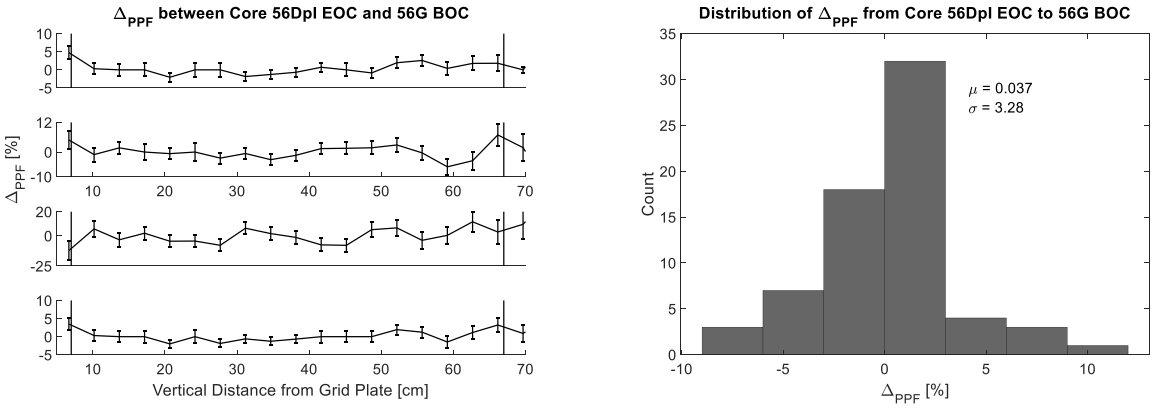

Figure 7: Change in PPFs following 3 months, 25 days of typical reactor operations. The active region of the core is indicated by the vertical lines.

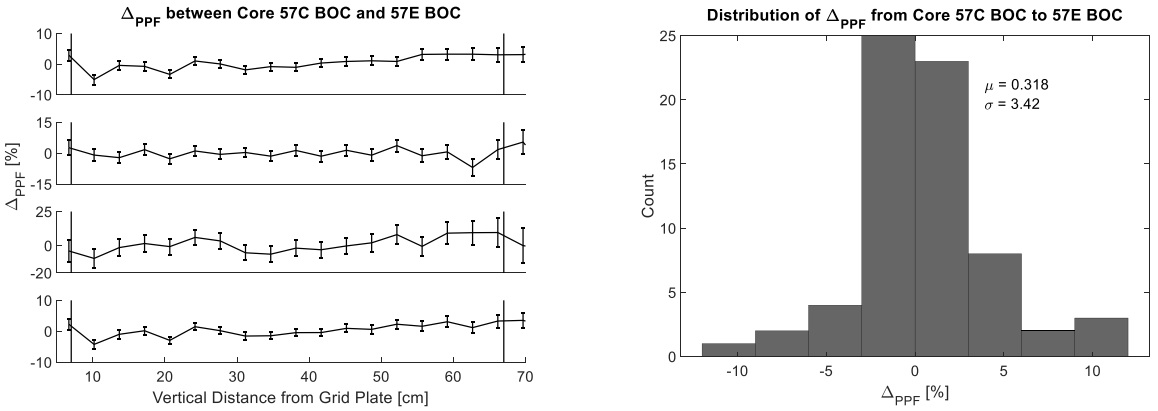

Figure 8: Change in PPFs following 3 months, 23 days of typical reactor operations. The active region of the core is indicated by the vertical lines.

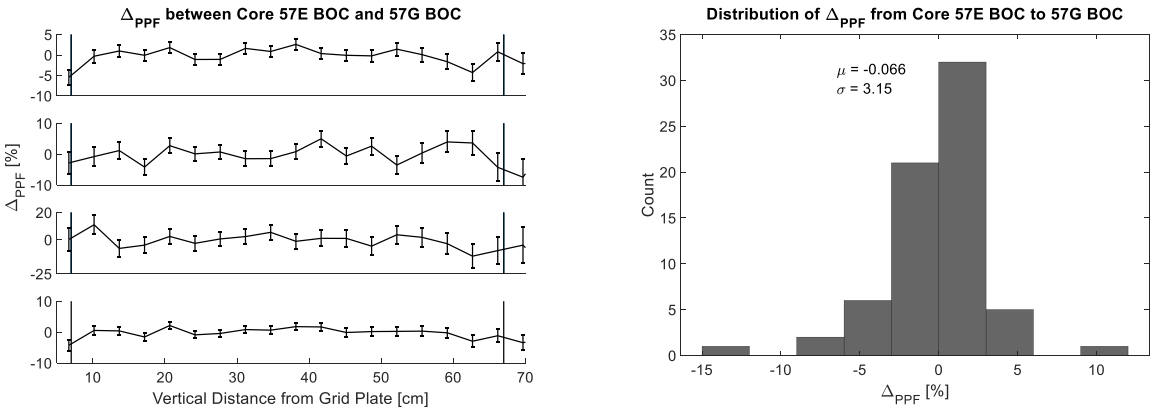

Figure 9: Change in PPFs following 4 months, 3 days of typical reactor operations. The active region of the core is indicated by the vertical lines.

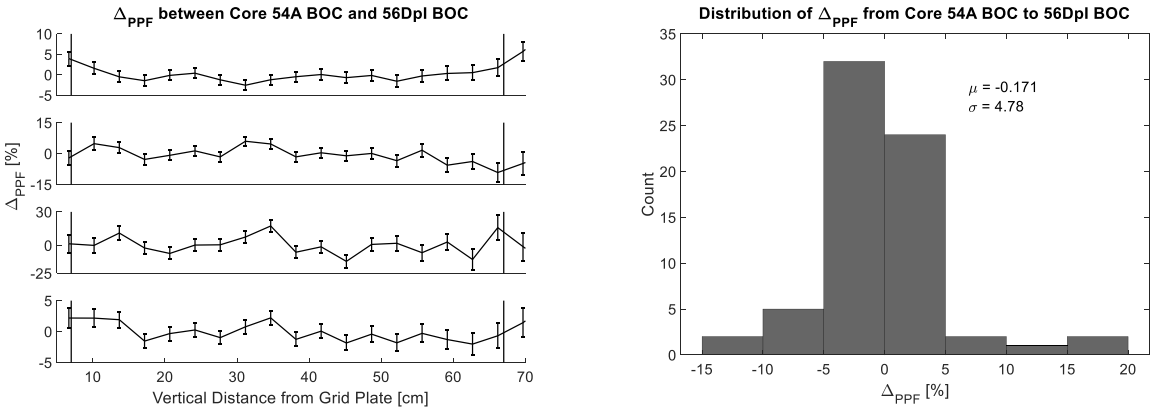

Figure 10: Change in PPFs following 2 years, 17 days of typical reactor operations. The active region of the core is indicated by the vertical lines.

The data presented in Figure 5 through Figure 9 may be used for a direct comparison to the experimental results presented in Section 4.2. The conclusions that can be drawn from this comparison – with an emphasis on the role of uncertainties present in the experimental determination of the neutron flux – are discussed in the following section.

5 Conclusions

The uncertainties reported for the total, thermal, and fast energy groups are dominated by the uncertainty associated with the sample placement in the irradiation site, and the reactor power level [59]. If these sources of uncertainty could be eliminated, the total uncertainty reported for these neutron flux values may be reduced from ~ 5.5 % to ~ 1.5 %, and would be dominated by the measurement uncertainty. As has previously been reported, a complete knowledge of the instrumentation used to measure the reactor power in MNR may result in a reduction of the power level uncertainty from 3.7 % to 3 % [1]. In this case, the combined uncertainty would be reduced

to approximately 4.5 %. In general, the uncertainty associated with the reactor power level cannot be reduced beyond this, as this would significantly disrupt normal reactor operations. The sample placement uncertainty could be reduced by constructing a modified wire holder that locks into a fixed position within the sample holders in MNR, rather than being allowed to sit in any configuration. As the construction and implementation of this may significantly disrupt typical reactor operations, this remains outside the scope of the current work.

While a significant reduction in the experimental neutron flux uncertainty may allow the effects of fuel burnup to be determined through purely experimental methods, the computational results presented in Section 4.3, indicate that the effects of fuel management operations and burnup do not significantly affect the neutron flux uncertainty calculations however, it may not be possible to discount the effects of burnup when studying the reactor kinetics, or in making local measurements of the fuel composition. The conclusions drawn from the present work should be applied only to local neutron flux measurements or other activation procedures occurring in the core.

Hence activation procedures can be performed in MNR Site 8C without any further data processing to account for burnup effects. Although some efforts may be made to reduce the total neutron flux uncertainty in activation experiments, it is sufficient to quantify the uncertainty according to [59], and general burnup effects need not be considered further.

6 Acknowledgements

Grateful acknowledgement is made towards all the operations staff and management team of MNR for their help during experimentation. Thanks also to Alice Pidruczny of the MACCNAA for her help in training on the data acquisition systems, and to the McMaster Health Physics team for their help in coordinating experimental efforts. Special thanks to Ross Harper for designing and constructing the five-wire holders, which are essential to the continued success of this project. The authors thank Dr. Simon E. Day for providing the schematic of the MNR reference core configuration used in Figure and the control room data discussed in Section 2.1. The authors thank Mohammed Alqahtani for sharing some OSCAR-4 simulation results, and his insightful discussions about burnup in MNR.

This work was funded by the Natural Sciences and Engineering Research Council of Canada (NSERC) and University Network of Excellence in Nuclear Engineering (UNENE).

7 References

[1] "The Paris Agreement," *Governement of Canada*, 2016. [Online]. Available: https://www.canada.ca/en/environment-climate-change/services/climate-change/paris-agreement.html. [Accessed: 13-Oct-2020].

[2] International Atomic Energy Agency, "Climate Change and Nuclear Energy 2020," Vienna, 2020.

[3] IEA, "Global Energy Review: CO2 Emissions in 2020," *IEA*, 2021. [Online]. Available: https://www.iea.org/articles/global-energy-review-co2-emissions-in-2020. [Accessed: 12-Jul-2021].

[4] "Nuclear Power in the World Today," *World Nuclear Association*, 2020. [Online]. Available: https://www.world-nuclear.org/information-library/current-and-future-generation/nuclear-power-in-the-world-today.aspx. [Accessed: 13-Oct-2020].

[5] "Research Reactors," *World Nuclear Association*, 2020. [Online]. Available: https://www.world-nuclear.org/information-library/non-power-nuclear-applications/radioisotopes-research/research-reactors.aspx. [Accessed: 10-Oct-2020].

[6] International Atomic Energy Agency, "Research Reactors: Purpose and Future," Vienna, 2016.

[7] International Atomic Energy Agency, "History, development and future of TRIGA research reactors IAEA TRS 482," Vienna, 2016.

[8] D. Chiesa *et al.*, "Measurement and simulation of the neutron flux distribution in the TRIGA Mark II reactor core," *Ann. Nucl. Energy*, vol. 85, pp. 925–936, 2015.

[9] B. M. Makgopa, M. Belal, and W. J. Strydom, "Neutronic Characterization of the SAFARI-1 Material Testing Reactor," in *Proceedings of the 4th International Topical Meeting on High Temperature Reactor Technology*, 2008, pp. 1–7.

[10] N. Jawerth and E. Mattar, "Exploring Research Reactors and Their Use," *International*

Atomic Energy Agency, 2020. [Online]. Available: https://www.iaea.org/newscenter/news/exploring-research-reactors-and-their-use. [Accessed: 13-Oct-2020].

[11] A. Borio *et al.*, "TRIGA reactor absolute neutron flux measurement using activated isotopes," *Prog. Nucl. Energy*, vol. 70, pp. 249–255, 2014.

[12] M. Alqahtani and A. B. Alajo, "Characterization of prompt neutron spectrum of the Missouri University of Science and Technology Reactor," *Nucl. Eng. Des.*, vol. 320, pp. 57–64, 2017.

[13] V. Radulovic, Z. Stancar, L. Snoj, and A. Trkov, "Validation of absolute axial neutron fl ux distribution calculations with MCNP with 197 Au (n , γ) 198 Au reaction rate distribution measurements at the JSI TRIGA Mark II reactor," *Appl. Radiat. Isot.*, vol. 84, pp. 57–65, 2014.

[14] A. C. Fernandes, J. P. Santos, J. G. Marques, A. Kling, A. R. Ramos, and N. P. Barradas, "Validation of the Monte Carlo model supporting core conversion of the Portuguese Research Reactor (RPI) for neutron fluence rate determinations," *Ann. Nucl. Energy*, vol. 37, no. 9, pp. 1139–1145, 2010.

[15] L. Snoj, A. Trkov, R. Jacimovic, P. Rogan, G. Zerovnik, and M. Ravnik, "Analysis of neutron flux distribution for the validation of computational methods for the optimization of research reactor utilization," *Appl. Radiat. Isot.*, vol. 69, pp. 136–141, 2011.

[16] B. Richardson, C. H. Castano, J. King, A. Alajo, and S. Usman, "Modeling and validation of approach to criticality and axial flux profile experiments at the Missouri S & T Reactor (MSTR)," *Nucl. Eng. Des.*, vol. 245, pp. 55–61, 2012.

[17] D. Chiesa *et al.*, "Fuel burnup analysis of the TRIGA Mark II reactor at the University of Pavia," *Ann. Nucl. Energy*, vol. 96, pp. 270–276, 2016.

[18] K. H. Beckurts and K. Wirtz, *Neutron Physics*. Berlin: Springer-Verlag, 1964.

[19] J. Lamarsh and A. Baratta, *Introduction to Nuclear Engineering*, Third. Upper Saddle River: Prentice-Hall, 2001.

[20] J. K. Shultis and R. E. Faw, *FUNDAMENTALS OF NUCLEAR SCIENCE AND ENGINEERING*. Manhattan: Marcel Dekker, 2002.

[21] J. J. Duderstadt and L. J. Hamilton, *Nuclear Reactor Analysis*. Ann Arbor: John Wiley & Sons, Inc., 1976.

[22] "Evaluated Nuclear Data File (ENDF)." [Online]. Available: https://www-nds.iaea.org/exfor/endf.htm.

[23] F. Salaun, "Assessment and optimization of the Canadian SCWR reactivity control systems through reactor physics and thermal-hydraulics coupling," McMaster University, 2017.

[24] B. J. Ade, "SCALE / TRITON Primer : A Primer for Light Water Reactor Lattice Physics Calculations," 2011.

[25] X-5 Monte Carlo Team, "MCNP — A General Monte Carlo N-Particle Transport Code, Version 5 Volume I: Overview and Theory," Los Alamos, 2003.

[26] I. Lux and L. Koblinger, *Particle Transport Methods : Neutron and Photon Calculations Authors*. Boca Raton: CRC Press, 1991.

[27] P. Reuss, *Neutron Physics*. Paris: EDP Sciences, 2008.

[28] F. Brown, "Monte Carlo Techniques for Nuclear Systems – Theory Lectures." Los Alamos, 2016.

[29] D. B. Pelowitz *et al.*, "MCNP6 User's Manual," Los Alamos, 2013.

[30] L. Hamidatou, H. Slamene, T. Akhal, and B. Zouranen, "Concepts, Instrumentation and Techniques of Neutron Activation Analysis," in *Imaging and Radioanalytical Techniques in Interdisciplinary Research*, F. Kharfi, Ed. Rijeka: IntechOpen, 2013.

[31] B. E. Watt, "Energy spectrum of neutrons from thermal fission of U235," *Phys. Rev.*, vol. 87, no. 6, pp. 1037–1041, 1952.

[32] "Neutron Fluence Measurements," *Iaea*, vol. TRS-107, 1970.

[33] K. C. Hines, "Energy and Lethargy Distribution of Neutrons Slowing Down in Graphite," Sydney, 1959.

[34] S. Bell, “Beginner’s Guide to Uncertainty of Measurement,” Teddington, 1999.

[35] International Bureau of Weights and Measures, “Evaluation of measurement data — Guide to the expression of uncertainty in measurement,” Sèvres, 2008.

[36] J. R. Taylor, “An Introduction to Error Analysis: The Study of Uncertainties in Physical Measurements,” 2nd ed., University Science Books, 1997, pp. 93–120.

[37] Canadian Nuclear Safety Commission, “Record of Proceedings - McMaster University - Application to Renew the McMaster Nuclear Reactor Operating Licence,” 2014.

[38] McMaster Nuclear Reactor, “Nuclear Operations and Facilities 2017,” Hamilton, 2017.

[39] S. E. Day, “McMaster Nuclear Reactor Specification - IAEA CRP 1496, Innovative Methods for Research Reactors: “Benchmarking against Experimental Data of the Neutronic and Thermalhydraulic Computational Methods and Tools for Operation and Safety Analysis for Research,” Hamilton, 2011.

[40] S. E. Day, M. P. Butler, and W. J. Garland, “Calculations in Support of the Mnr Core Conversion,” Hamilton, 2002.

[41] S. E. Day, “McMaster Nuclear Reactor Benchmark Specification - IAEA CRP 1496, Innovative Methods for Research Reactors: “Benchmarking against Experimental Data of the Neutronic and Thermalhydraulic Computational Methods and Tools for Operation and Safety Analysis for,” Hamilton, 2013.

[42] M. Alqahtani, A. Buijs, and S. E. Day, “Serpent-2 and OSCAR-4 computational tools compared against McMaster nuclear reactor improved operational data history for U-235 fuel inventory tracking , local power tracking and validation of multiplication factor,” *Ann. Nucl. Energy*, vol. 145, p. 107590, 2020.

[43] A. Klett, “Handbook of Particle Detection and Imaging,” C. Grupen and I. Buvat, Eds. Berlin: Springer, 2012, pp. 759–790.

[44] L. Snoj, M. Ravnik, A. Trkov, and G. Zerovnik, “On the self-shielding factors in neutron activation analysis,” *Nucl. Instruments Methods Phys. Res. Sect. A Accel. Spectrometers, Detect. Assoc. Equip.*, vol. 610, pp. 553–565, 2009.

[45] "NuDat 2.7." [Online]. Available: http://www.nndc.bnl.gov/nudat2/.

[46] M. Berglund and M. E. Wieser, "Isotopic compositions of the elements 2009 (IUPAC Technical Report)*," *Pure Appl. Chem.*, vol. 83, no. 2, pp. 397–410, 2011.

[47] J. Meija *et al.*, "Atomic weights of the elements 2013 (IUPAC Technical Report)," *Pure Appl. Chem.*, vol. 88, no. 3, pp. 265–291, 2016.

[48] *Genie ™ 2000 Spectroscopy Software*. 2000.

[49] D. Chandler, G. I. Maldonado, L. D. Proctor, and R. T. Primm, "Nuclear Transmutations in HFIR's Beryllium Reflector and Their Impact on Reactor Operation and Reflector Disposal," *Nucl. Technol.*, vol. 177, no. 3, pp. 395–412, 2017.

[50] M. B. Zeller, A. Celli, R. T. Jones, and G. P. McPhee, "Photo-neutron experiment performed in ZED-2," in *21st Conference of the Canadian Nuclear Society*, 2000.

[51] E. Macconnachie, D. Novog, and S. Day, "ICONE26-82412 Axial Flux Wire Measurements atthe McMaster Nuclear Reactor," 2018, pp. 1–8.

[52] G. E. Knoll, *Radiation Detection and Measurement Third Edition*, 3rd ed. Ann Arbor: John Wiley & Sons, Inc., 2000.

[53] Alfa Aesar, "Certificate of analysis." Thermo Fisher Scientific, 2018.

[54] National Institute of Standards and Technology, "Thermophysical Properties of Fluid Systems," 2018. [Online]. Available: https://webbook.nist.gov/chemistry/fluid/. [Accessed: 03-May-2019].

[55] Cole-Parmer, "Digi-Sense Prec. Ind. PRT, 0.25" x 12" , -60~160C, Bare Wire." [Online]. Available: https://www.coleparmer.com/i/digi-sense-prec-ind-prt-0-25-x-12-60-160c-bare-wire/9045200. [Accessed: 06-May-2019].

[56] Badger Meter, "Model SSL Venturi Classic Flow Meter." [Online]. Available: https://www.badgermeter.com/business-lines/flow-instrumentation/venturi-ssl/. [Accessed: 06-May-2019].

[57] B. T. Rearden and M. A. Jessee, "SCALE Code System," Oak Ridge National Laboratory, Oak Ridge, 2017.

[58] "SCALE User's Group." [Online]. Available: https://groups.google.com/forum/#!forum/scale-users-group.

[59] E. MacConnachie, D. Novog, and S. Day, "Quantification of system uncertainties in activation experiments at nuclear research reactors," *Ann. Nucl. Energy*, vol. 134, pp. 432–440, 2019.

[60] D. R. Helsel and R. M. Hirsch, "Statistical Methods in Water Resources," 2002, pp. 337–340.

[61] V. Suman and P. K. Sarkar, "Nuclear Instruments and Methods in Physics Research A Neutron spectrum unfolding using genetic algorithm in a Monte Carlo simulation," *Nucl. Inst. Methods Phys. Res. A*, vol. 737, pp. 76–86, 2014.

[62] M. Matzke, "9 UNFOLDING PROCEDURES," *Radiat. Prot. Dosimetry*, vol. 107, pp. 155–174, 2003.

[63] S. R. Malkawi and N. Ahmad, "Solution of the neutron spectrum adjustment problem in a typical MTR type research reactor," *Ann. Nucl. Energy*, vol. 28, pp. 17–22, 2001.

[64] F. Molina, P. Aguilera, J. Romero-barrientos, H. F. Arellano, J. Agramunt, and J. Medel, "Energy distribution of the neutron fl ux measurements at the Chilean Reactor RECH-1 using multi-foil neutron activation and the Expectation Maximization unfolding algorithm," *Appl. Radiat. Isot.*, vol. 129, no. August, pp. 28–34, 2017.

[65] J. A. Kennedy, "A COMPARISON OF MNR IRRADIATION EXPERIMENTS WITH SIMULATION," McMaster Univeristy, 2000.

[66] D. Chiesa, E. Previtali, and M. Sisti, "Bayesian statistics applied to neutron activation data for reactor flux spectrum analysis," *Ann. Nucl. Energy*, vol. 70, pp. 157–168, 2014.

[67] A. Leder, "Unfolding neutron spectrum with Markov Chain Monte Carlo at MIT research Reactor with He-3 Neutral Current Detectors," *Jounal Instrum.*, vol. 13, 2018.

[68] D. Chiesa *et al.*, "Measurement of the neutron flux at spallation sources using multi-foil activation," *Nucl. Instruments Methods Phys. Res. Sect. A Accel. Spectrometers, Detect. Assoc. Equip.*, vol. 902, pp. 14–24, 2018.

[69] E. L. Macconnachie and D. R. Novog, “Measurement , simulation and uncertainty quantification of the neutron flux at the McMaster Nuclear Reactor,” *Ann. Nucl. Energy*, vol. 151, 2021.

[70] B. J. Smith, “boa : An R Package for MCMC Output Convergence,” *J. Stat. Softw.*, vol. 21, no. 11, 2007.

[71] R. J. B. Goudie, R. M. Turner, and D. De Angelis, “MultiBUGS : A Parallel Implementation of the BUGS Modelling Framework for Faster Bayesian Inference,” *arXiv*, 2018.

[72] D. J. Spiegelhalter, N. G. Best, and B. P. Carlin, “Bayesian measures of model complexity and fit,” *J. R. Stat. Soc. Ser. B*, pp. 583–639, 2002.

[73] J. Wang, Z. Guo, X. Chen, and Y. Zhou, “Neutron spectrum unfolding based on generalized regression neural networks for neutron fluence and neutron ambient dose equivalent estimations,” *Appl. Radiat. Isot.*, vol. 154, no. August, p. 108856, 2019.

[74] International Atomic Energy Agency, “Compendium of Neutron Spectra and Detector Responses for Radiation Protection Purposes IAEA TRS 403,” Vienna, 2001.

6 Paper III

6.1 Publication Details

E. L. Macconnachie and D. R. Novog, "Application of Bayesian Methods to Neutron Spectrum Measurements," Submitted for consideration to the *Annals of Nuclear Energy*, 2021.

The experiments described here were designed, planned, and conducted by the first author (E. MacConnachie), with on-going support from the MNR reactor manager (Rob Pasuta), and the MNR operations staff. Data collection, processing, and analysis was performed entirely by the first author. The MCNP model of MNR was developed by Dr. Simon Day in 2001, and updated by the first author as needed for this analysis. All computational data referenced in this paper was generated and processed by the first author. Dr. David Novog provided guidance on the development of this research. This paper was written entirely by the first author, with support in editing and revisions from Dr. David Novog.

Special thanks to Alice Pidruczny of MACCNAA for granting the first author on-going access to her lab space, and the entire McMaster Health Physics team for their support during this experimental campaign – particularly at a time when COVID-19 had significantly impacted typical operations within the nuclear research department.

6.2 Preface

While the first two articles presented in this thesis made a careful examination of various effects on broad-energy-group flux measurements, an accurate knowledge of the fine structure of the neutron flux energy spectrum may be required for certain UQ procedures, validation studies, or medical isotope activation procedures. To fully represent the nuclear data uncertainties and their covariances, and to prevent mathematical ambiguities from contributing to the final uncertainty, computational Bayesian methods were applied in this publication.

The MultiBUGS software was used to construct the Bayesian model and took the following data as inputs: activation measurements of 15 different (n, x) reactions (whose uncertainties are calculated according to the methodology presented in the first article of this sandwich thesis), and the corresponding activation cross sections for each reaction. This analysis was repeated with each of the 1000 sets of perturbed nuclear data available in the SCALE-6.2.2 software package, such that the nuclear data covariance information was preserved *ab initio*. A parameterized model was adopted based on the physical characterization of the flux spectrum in a LWR system. In this way,

relatively few parameters define the flux spectrum and the results can therefore be quickly and easily integrated into reactor operations or isotope production planning. This parameterization is also advantageous as it requires relatively few activation measurements, which can generally be recovered from a single irradiation.

The thermal, the epithermal, and the fast flux spectra were defined by the following forms, respectively: a Maxwellian distribution, a modified 1/E spectrum, and the fission spectrum proposed by Grundl & Usner. The (uniformly distributed) prior was centered on the results recovered from an MCNP simulation of MNR, and was broad enough to generate a spread in flux values of approximately ± 200 %; this represents a greater uncertainty than would be accepted from a simulation result.

The results presented in this paper have demonstrated the validity of Bayesian-based methods for recovering the neutron flux energy spectrum when all significant sources of uncertainty (i.e those presented in Chapters 4 and 5, and nuclear data uncertainties) are included in the analysis. Although these methods may offer improved activation estimates for some (n, x) reactions, a comparison of the experimental results and the Bayesian outputs shows that (n, γ) reactions with a significant number of unresolved resonances may be poorly predicted by this computational technique. Additionally, an investigation of the output uncertainties from the Bayesian analysis shows that the output flux uncertainties increase across the epithermal energy range. Each of these phenomena appear to be attributed to the parameterized model used to describe the flux in this region – a modified 1/E spectrum. A more sophisticated model may be required to adequately capture the effects of either the delayed neutron spectrum or the unresolved resonance region.

The application of Bayesian methods in this paper has raised to possibility of applying other machine learning techniques to the spectrum unfolding problem. Following the submission of this article for consideration, some additional (preliminary) results using a Monte Carlo-based genetic algorithm were generated, based on the methodology described by Suman & Sarkar [61]. The following figure shows both these results and the flux spectrum generated by an MCNP simulation.

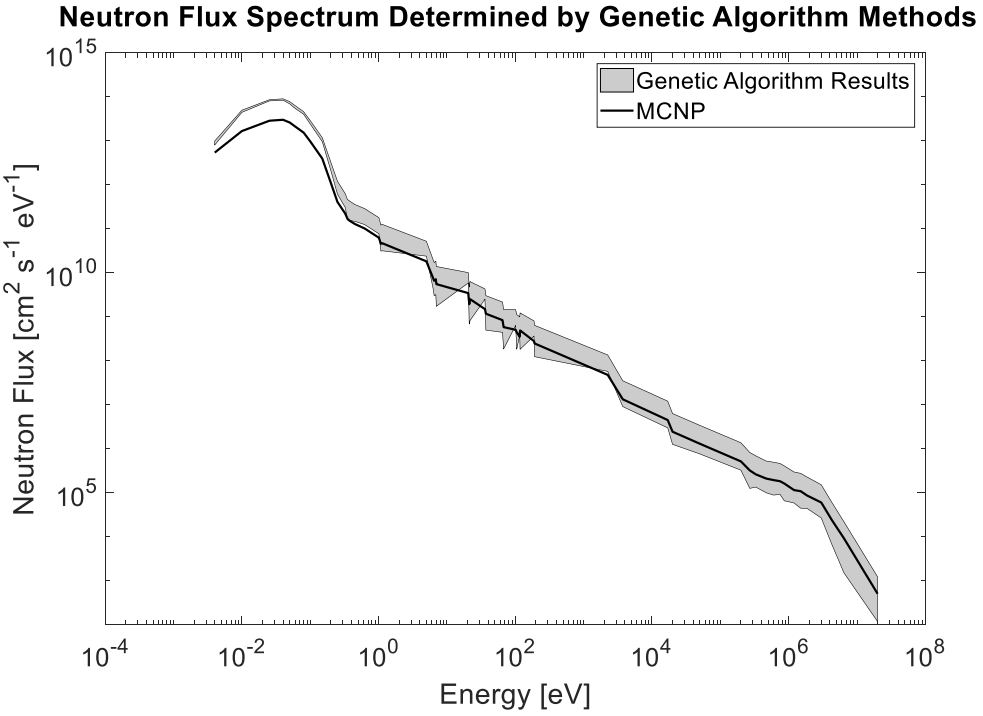

Figure 21: Preliminary neutron flux spectrum results from the Monte Carlo-based genetic algorithm methods.

As seen in the figure above, there is generally good agreement between the genetic algorithm and the MCNP results, and the uncertainties in general agree well with those discussed in the following paper. These results demonstrate the validity of applying genetic algorithms to the spectrum unfolding problem. While the results are promising, further research is warranted to fully explore machine learning applications for flux spectrum unfolding. For example, a variety of fitness functions, selection criteria, and initializing conditions must be considered. The development of a robust Monte-Carlo-based genetic algorithm (and the application of other machine learning methods where possible) may be undertaken as an extension to the current work.

Application of Bayesian Methods to Neutron Spectrum Measurements

Key Words

McMaster Nuclear Reactor

Neutron activation analysis

Nuclear data uncertainty

Uncertainty Quantification

Bayesian Methods

Markov Chain Monte Carlo

Nomenclature

BUGS	Bayesian inference Using Gibbs Sampling
DIC	Deviance Information Criteria
HPGe	High Purity Germanium
LEU	Low-enriched Uranium
MCMC	Markov Chain Monte Carlo
MCNP	Monte-Carlo N-Particle
MNR	McMaster Nuclear Reactor
MTR	Materials Testing Reactor
UQ	Uncertainty Quantification
R	Activation rate [atoms s^{-1}]
A	Activity [s^{-1}]

T	Time constant
N	Number of precursor atoms
P(data)	Evidence distribution
P(data|θ)	Likelihood distribution
P(θ)	Prior distribution
P(θ|data)	Posterior distribution
$\phi(E)$	Flux per unit energy [cm^{-2} s^{-1} eV^{-1}]
Φ	Energy-integrated flux [cm^{-2} s^{-1}]
$\sigma_{n,x}(E)$	Energy dependent cross section for reaction (n,x) [cm^2]
σ_{eff}	Effective cross section [cm^2]
$Q_{x,g}$	Perturbation factor for reaction x in energy group g [~]

1 Introduction

Accurate knowledge of the neutron flux energy spectrum in a reactor may provide key information for uncertainty quantification (UQ) procedures, code validation studies, operational decision making (such as fuelling), and a basis for optimizing activation procedures that may be used for isotope production. While it may not be feasible to make local, high-fidelity measurements of the spectrum in power reactors, irradiation experiments may be readily performed in research reactors. In addition to its energy spectrum in an irradiation site, a complete characterization of the combined flux uncertainties may provide insight into the limiting factors in operational and experimental decision making. For example, previous work at the McMaster Nuclear Reactor (MNR) has indicated that the uncertainty in the sample placement during irradiations is a significant contributor to the combined uncertainty in activation procedures, and may motivate further work to improve procedures for the production of medical isotopes [59]. The purpose of this research is to perform measurements of the neutron energy spectrum in MNR and develop a parametric approximation of the neutron spectrum (along with its uncertainties) for use in operational decision making and isotope production planning.

The neutron flux energy spectrum is typically measured by using multi-element activation data that act as inputs to a spectrum unfolding code such as SAND-II, STAY-SL, or MAXED [62]. Measurements of the neutron flux energy spectrum have been made in several different research reactors, including MNR, for the purposes of assessing the performance of a computational model [63]–[65]. However, due to the mathematical structure of many unfolding codes and the nature of covariances in nuclear data, it may not be possible to fully propagate the uncertainties present in these flux determinations [62]. Computational Bayesian methods using the Markov-Chain Monte-Carlo (MCMC) technique offer a solution to the spectrum unfolding problem where all sources of uncertainty can be systematically accounted for. Such methods have been applied for code validation studies [66] and for neutron background characterization [67] in research reactors. While a preliminary study of the effects of nuclear data uncertainties in the determination of the neutron flux energy spectrum has been carried out at the ISIS spallation source, similar studies have neither been conducted in research reactors, nor applied to broader efforts to quantify all uncertainties when making measurements of the neutron flux. Additionally, the work performed at the ISIS spallation source makes use of several different nuclear data libraries to characterize the impact of nuclear data uncertainties, rather than an application of the covariance information contained in a single library [68]. Although applying several sets of nuclear data may be used to estimate the expected spread in results, this technique cannot fully evaluate the performance of any individual nuclear data library. An investigation of the nuclear data uncertainties as tabulated by cross section covariance libraries is therefore required to understand the coherent impacts of the nuclear data uncertainties. This work aims to conduct a comprehensive study of the neutron flux energy spectrum in research reactors, with an emphasis on the inclusion of nuclear data uncertainties in the determination of measured neutron flux values using a Bayesian approach.

1.1 McMaster Nuclear Reactor

MNR is a light-water cooled and moderated, open-pool Materials Testing Reactor (MTR) located on the McMaster University campus in Ontario, Canada that currently operates at 3 MW_{th}. In addition to supporting several interdisciplinary research groups and various specialized isotope production projects, MNR is the leading supplier of ^{125}I for use its use in the treatment of prostate cancer, as well as other radiopharmaceuticals [38]. Improved accuracy in determinations of the

neutron flux spectrum and its associated uncertainties may allow researchers to optimize their experimental procedures and may improve isotopes production quality assurance.

The core of MNR is defined by a 9 x 6 grid configuration, and typically houses 34 fuel assemblies, 6 graphite reflector assemblies, 12 vacant sites, a Be reflector site, a central irradiation facility (CIF), and 6 control rod assemblies. An overhead view of a generic MNR core configuration is shown in Figure. Each MTR-type low-enriched uranium (LEU) fuel assembly consists of 16 curved plates containing uranium particles dispersed in an aluminium matrix surrounded by 2 "dummy" plates of pure aluminium [59]. Five gang-operated Ag-In-Cd shim-safety rods for coarse reactivity control and shutdown procedures are located in sites 6B, 6E, 4B, 4E, and 2C. Additionally, a stainless-steel regulating rod is housed in site 2E for automatic fine reactivity control. These control rods are driven into the core from above with motors and an electromagnetic clutch, but will fall into the core under the action of gravity in the event of a loss of electrical power, or as a result of a reactor trip signal [39].

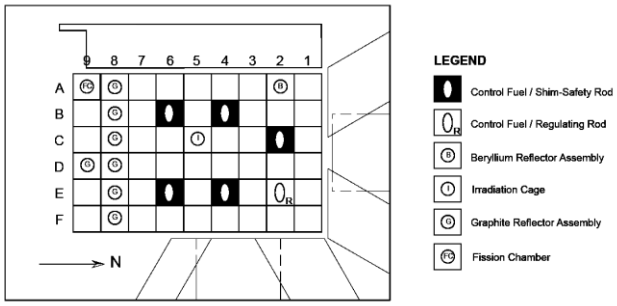

Figure 1: Overhead view of a reference core configuration in MNR. Activation procedures are typically performed in either the graphite reflector assemblies (rows 8 and 9) or the central irradiation facility in site 5C. The solid and dashed lines in the lower right-hand corner of the diagram indicate the 6 radial beam tubes that flank the core [59]**.**

Fuel management operations are performed based on burnup values determined from the results of regular activation procedures performed by operations staff. CuMn wires are irradiated at the axial centerline of each assembly to estimate the power distribution in the core. This distribution is assumed to remain constant over the cycle (i.e. between either refuelling or fuel shuffling events) of the core. For typical full-power operations, MNR is refuelled approximately twice per year, and fuel shuffling operations occur approximately every two months [39].

2 Experimental Methodology

This work involves the simultaneous irradiation of different isotopes in MNR site 8C to generate activation data for MCMC analysis to determine the neutron flux energy spectrum and its uncertainty. The activation rate measurements and nuclear data are separate inputs for this analysis; the activation uncertainties can be determined based on previous work conducted in MNR, which includes the effects of the sample placement, the reactor power, the control rod movement, and the ^{135}Xe content in the core [59]. Based on an experimental campaign performed in MNR over several different core configurations, the effects of fuel burnup and depletion during a typical cycle on these activation measurements can be neglected during data processing [69]. The activation measurement uncertainty was found to be approximately 7%, and is dominated by the uncertainties in the sample positioning and the reactor power. The treatment of these measurements and their uncertainties in the MCMC model is discussed in Section 3.

2.1 Irradiation and Data Collection

The neutron activation technique involves creating radioisotopes with a measurable activity by exposing a material to a neutron field such that they will transmute via a (n, x) reaction and become unstable. By measuring the activity of these decaying daughter isotopes, the activation rate in the sample during the irradiation procedure can be determined by the following equation [59]:

$$\boldsymbol{R = AT = N \int_0^\infty \sigma_{n,x}(E)\phi(E)dE} \quad \mathbf{1}$$

In Equation 1, A is the measured net activity of the sample, T is a time constant to account for the evolution of activity during irradiation and decay times, and N is the number of precursor atoms in the sample. Materials whose activation products decay by γ-ray emission are selected, and the γ-ray activity is then measured using a p-type, coaxial, high purity germanium (HPGe) detector, whose detection and geometrical efficiencies have been previously quantified [59]. Both the count times and the sample-to-detector distance may be adjusted so that the counting statistical uncertainties are less than 1%.

The experimental procedure used to collect the data presented in this work involves the simultaneous irradiation of several different thin wires (approximately 1 mm in diameter) housed in custom-built sample holders that can accommodate up to five wires per irradiation site. These

wires are approximately 70 cm in length, and span the entire length of the core and provide flux mapping along the entire axis of the irradiation site. Both the axial averaged flux spectrum and local effects can be determined from these irradiations. Once the reactor has been brought to the specified power, operations staff insert the sample holder into the irradiation site. To allow for safe handling, the irradiation time is typically 15 minutes, followed by a decay period of 5 days, before the activation data is collected. Each wire is cut into 21 segments, and the activation rate is measured for each segment. In this way, the spatial profile of the neutron flux along the active core region can be determined.

To generate sufficient activation data for the determination of the neutron spectrum with MCMC methods, several different isotopes and reactions must be studied. Table 7 lists the reactions being studied in this work, along with some information about their decay properties. The energies of the most prominent γ-rays are reported [45], and in the case of the (n, p) and (n, 2n) activation reactions, the threshold energy is reported [22]. To optimize the counting procedure and to avoid interference between different γ-ray emission peaks, each material was counted separately.

Table 7: List of reactions being studied, with some of their decay properties, and notes about each material.

Reaction	Half-life	E_γ [keV]	Threshold Energy [MeV]	Notes
^{50}Cr (n, γ)	27.7 d	320	-	NiCr Wire (Ni:Cr = 0.8:0.2 by weight), Ø = 1 mm
^{58}Ni (n, p)	70.86 d	810	0.8	
^{60}Ni (n, p)	1925.28 d	1173, 1332	2	
^{112}Sn (n, γ)	115.09 d	391	-	Sn Wire, Ø = 1 mm
^{116}Sn (n, γ)	13.76 d	158	-	
^{124}Sn (n, γ)	9.64 d	1067	-	
^{90}Zr (n, 2n)	3.26 d	909	12	Zr (4.5% Hf) Wire, Ø = 1 mm
^{94}Zr (n, γ)	64.03 d	756	-	
^{96}Zr (n, γ)	16.75 h	743	-	
^{174}Hf (n, γ)	70 d	343	-	
^{178}Hf (n, γ)	25.05 d	453	-	
^{180}Hf (n, γ)	42.39 d	482	-	
^{46}Ti (n, p)	83.79 d	889	1.6	Ti Wire, Ø = 1 mm
^{47}Ti (n, p)	3.35 d	159	0.1	
^{48}Ti (n, p)	43.67 h	1037	3.2	

3 Neutron Spectrum Determination

There are several methods that can be used to determine the neutron flux spectrum from the results of multi-element activation experiments. Traditional spectrum unfolding codes, and the challenges in carrying out uncertainty quantification procedures with these algorithms, are discussed in Section 3.1. Computational Bayesian methods are introduced in Section 3.2, and the specifics of model development and the treatment of nuclear data in the present application are discussed in Sections 3.2.2 and 3.2.3, respectively.

3.1 Spectrum Unfolding Codes

Traditional spectrum unfolding codes (such as SAND-II, STAY'SL, and MAXED) sub-divide the neutron flux spectrum into discrete energy groups, such that Equation 1 can be written as a set of algebraic equations, and solved using various deconvolution or iterative procedures [62]:

$$\begin{pmatrix} R_1 \\ \vdots \\ R_n \end{pmatrix} = \begin{bmatrix} \sigma_{1,1} & \cdots & \sigma_{1,n} \\ \vdots & \ddots & \vdots \\ \sigma_{m,1} & \cdots & \sigma_{m,n} \end{bmatrix} \begin{pmatrix} \phi_1 \\ \vdots \\ \phi_n \end{pmatrix} \qquad \mathbf{2}$$

$$\boldsymbol{R = \sigma \Phi}$$

In Equation 2, the neutron energy spectrum is divided into "n" energy groups, and is determined with "m" measurements. While these codes may be able to incorporate both measurement and nuclear data uncertainties as inputs in their determination of the neutron flux spectrum, several challenges may complicate uncertainty quantification.

For codes that perform a matrix inversion to determine the neutron flux spectrum, if the system is underdetermined (m < n), a unique solution to Equation 2 may not exist. Even in the case of an overdetermined system (m > n), the matrices used to define the normal equations to solve Equation 2 have been found to be ill-conditioned in practice due to the magnitude of the nuclear data matrices involved [62]. As with the underdetermined case, multiple solutions to the spectrum unfolding problem may therefore exist. As a result, there may be a strong dependence of the results on the spectrum used to initialize the algorithm in these unfolding codes. In practice this dependence on the initial spectrum cannot be fully quantified, and this additional sources of bias in the flux results may limit a comprehensive investigation of the uncertainties in the problem [66].

To recover the neutron flux spectrum and its uncertainties, MCMC methods based on Bayesian inference techniques are applied in this work. A discussion of the foundations of MCMC analysis, the development of the Bayesian statistical models, and the treatment of nuclear data in the present application is discussed in the following sections.

3.2 Bayesian Methods

The following sections introduce Bayesian methods and their application to this research. First, a summary of Bayes' Theorem is provided, along with a discussion of the MCMC technique. Section 3.2.2 and Section 3.2.3 present the general model development (with an emphasis on prior selection) and specific treatment of nuclear data in this application, respectively.

3.2.1 Theoretical Formulation

Bayes' Theorem describes the probability of an event, based on prior knowledge of conditions that relate to that event, and can be expressed by the following equation [66]:

$$\boldsymbol{P(\theta|data)} = \frac{\boldsymbol{P(data|\theta)}}{\boldsymbol{P(data)}}\boldsymbol{P(\theta)} \quad \textbf{3}$$

Each term in Equation 3 is defined as follows:

- P(θ|data) is the posterior distribution that describes θ, given some measured data and *a priori* information. In Bayesian analyses, this is the quantity to be determined.
- P(data|θ) is the likelihood function that describes the relationship between the data and θ. This function can be used to generate theoretical data sets given a fixed value of θ. In the present application, the likelihood function is defined by Equation 1.
- P(data) is the probability of measuring a data set, independent of θ. This term captures the uncertainties that are present in the measurement procedures and the data processing steps.
- P(θ) is the prior distribution, which describes the knowledge of the scope of θ before any measurements are made. A discussion concerning the prior selection for the current application can be found in Section 3.2.2.

The aim of this research is to estimate the posterior distribution of the neutron flux spectrum given a set of multi-element activation data, and the associated activation cross section libraries.

Computational methods based on the MCMC technique will be applied to determine the neutron flux energy spectrum in MNR. The MCMC technique involves approximating the posterior

distribution with an ergodic Markov chain, such that samples of the quantities of interest – i.e. the mean or standard deviation of the parameters under investigation – can be drawn from the chain. There are several algorithms that can be applied to construct an appropriate Markov chain for analysis however, Bayesian inference Using Gibbs Sampling (BUGS) software will be used to determine the joint posterior distribution due to its availability and efficiency. Gibbs sampling determines the next state in the Markov chain by sampling from the full conditional probability distribution of θ.

The results from a Bayesian analysis using MCMC methods must be tested for convergence before conclusions can be drawn from the posterior distribution. An open-source analysis package written in R (R.boa) was developed to interface with BUGS so that convergence testing and descriptive statistics of the Markov chain could be automatically calculated [70]. Four commonly used convergence metrics can be applied to the data in the R.boa package: the Brooks, Gelman, & Rubin, the Geweke, and the Heidelberger & Welch tests. Each of these tests were applied during model development to determine the appropriate parameters (i.e. the chain length, burn-in, and thinning) required to achieve convergence. A detailed discussion of the model development, and results from these convergence tests, can be found in the following sections.

3.2.2 Model Development

A statistical model to determine the neutron flux energy spectrum was developed and implemented using MultiBUGS, a program which applies Gibbs sampling to perform MCMC simulations for Bayesian analysis. This software was chosen for its parallelization capabilities, which significantly reduced the run-times required to achieve convergence when compared to other similar programs for Bayesian analysis [71].

The likelihood (given by Equation 1) is defined in MultiBUGS as:

$$\boldsymbol{K_i \sim dnorm}\left(\sum_j \boldsymbol{\sigma_{i,j}\phi_j}, \boldsymbol{\delta K_i}\right) \quad \textbf{4}$$

Here, the ~ symbol indicates that the quantity on the left-hand side is treated as a stochastic draw from the distribution defined on the right-hand side of the equation [66]. In this case, a normal distribution ($dnorm(\mu, \sigma)$) is used. The observed reaction rates $K_i = R_i/N_i$ are sampled from a normal distribution with a mean defined by the multi-group cross sections and unknown neutron

flux spectrum, and a width defined by the experimental uncertainties δK_i. The treatment of the multi-group cross sections is discussed in detail in the following section.

A parametric prior, which is defined in Equation 5, was adopted for the neutron flux spectrum with the spectrum parameters based on the outputs from a full core MCNP simulation. By adopting a parameterized flux spectrum with relatively few free parameters, the number of degrees of freedom are reduced, and a single (or small number of) irradiation can be used to generate the necessary activation data. This is contrasted with an approach which treats each discrete energy group as an unknown flux which generates a large number of unknowns and may require many irradiations to generate sufficient data to resolve each group. The parameterized approach, with fewer activations can be performed over a relatively short period of reactor operation which may reduce contributions that depend on the reactor power or control rod movement. Finally, a parameterized flux spectrum provides a quick method for operations staff to generate a flux spectrum for their own experimental needs – for example, in radioisotope production planning.

This parameterized prior for this work is defined by i) a Maxwellian distribution for thermal neutrons, ii) a modified $1/E$ spectrum in the epithermal energy region, and iii) a modified fission spectrum for fast neutrons [18], [32]. Although the Watt spectrum is typically adopted to describe the fast neutron flux, an investigation of the MCNP results found that the formalism of Grundl & Usner better described the fast spectrum in MNR [31], [32]. The flux spectrum used in this work is:

$$\boldsymbol{\phi(E)} = \begin{cases} \boldsymbol{\phi_{thermal}} = \dfrac{\boldsymbol{A}}{\boldsymbol{(kT)^2}}\boldsymbol{E e^{-\frac{E}{kT}}} \\ \boldsymbol{\phi_{epithermal}} = \dfrac{\boldsymbol{B}}{\boldsymbol{E^{1+\alpha}}} \\ \boldsymbol{\phi_{fast}} = \boldsymbol{F\sqrt{E}e^{-HE}} \end{cases} \quad \mathbf{5}$$

The parameters defining the amplitude (A, B, and F) and the shape (kT, α, and H) of the neutron flux are to be recovered from this Bayesian analysis. The priors for each parameter were sampled from uniform distributions centered on the parameters recovered from the MCNP results. These prior distributions were defined such that the spread in the sampled values approximately ± 200%, and centered on MCNP reference values. This is a significantly greater uncertainty than would be accepted from an MCNP simulation result and therefore represents an appropriate domain for this analysis (i.e. this provides a bounded, non-informative prior for this work). It was found that additional broadening of the prior distributions (within physically acceptable bounds) did not

change the final results (but increased computation time significantly), indicating that the model is generally insensitive to the choice of prior.

As the posterior distributions were found to be normal, the deviance information criterion (DIC) may be used to assess various forms of the prior. The sensitivity of the prior to constraints that may be placed on the parameters defined in Equation 5 (i.e. by fixing the shape parameters at their theoretical values, kT = 0.0253, α = 1 etc.) was also investigated. The DIC was recorded from a series of MCMC simulations where every combination of the shape parameters (kT, α, and H) being either fixed or free was considered. The model with the lowest DIC is taken to be the most appropriate, and will be adopted for the purposes of this research [72].

This investigation revealed that the MCMC posterior was equally sensitive to the inclusion of any shape parameters (i.e. no particular spectrum parameter dominates the posterior), and a fully parameterized prior was found to have the lowest DIC, and will therefore be adopted in this analysis.

Following prior selection and model definition, the Brooks, Gelman, & Rubin diagnostic was used to determine if several independent chains in a MCMC simulation have converged to the same result, which may indicate that the model is insensitive to the initial values of the Markov Chain. This is done by comparing the variance within each chain to the variance across all the chains – if the chains converge to a common solution, the ratio $R = \frac{\sigma_{within}}{\sigma_{between}}$ will approach one [70]. Three sets of initial values were used to start the MCMC simulation (two user-generated and one randomly generated by the MultiBUGS program), and it was determined that all chains had converged to a common posterior distribution after approximately 5,000 iterations. This, along with the general insensitivity of the results to the prior selection, indicates that the model is robust.

3.2.3 Treatment of Nuclear Data

Nuclear data uncertainties are provided in the SCALE-6.2.2 software package in the form of 1000 perturbed libraries. Although the covariance matrices are available, the MultiBUGS software is limited to sampling from univariate distributions and hence the covariance information would be lost. As an alternative, this work utilizes each of the 1000 nuclear data sets as separate inputs to the MultiBUGS model, therefore allowing the execution to make use of the code's parallel

computational capability while preserving the covariance information via the SCALE supplied 1000 sets of nuclear data.

These perturbed libraries in SCALE are generated by applying perturbation factors to the reference set of nuclear data (based on the ENDF/B-VII.1 library). The perturbation factors are defined by the following equation [57]:

$$\boldsymbol{Q_{x,g} = 1 + \frac{\Delta\sigma_{x,g}}{\sigma_{x,g}}} \quad \textbf{6}$$

In Equation 6, the subscript x refers to a nuclear interaction and the subscript g indicates the energy group, of interest. Applying these factors to the reference data generates new sets of infinitely-dilute nuclear data. The PALEALE module of SCALE was used to generate 1000 sets of perturbed nuclear data for each reaction listed in Table 7 [58]. The model treats the activation cross sections as fixed values within a single run, and independent MultiBUGS simulations are performed with each of the 1000 different sets of nuclear data. By treating the nuclear data in this way, the covariance information is preserved *ab initio.*

4 Results

Irradiation experiments were carried out in MNR Site 8C to generate the activation data that act as inputs to the MultiBUGS models. The activation data and their uncertainties were processed according to the methodology developed in previous studies of irradiation procedures in MNR [59], [69]. It was found that the flux results from the analysis of these irradiations agreed within uncertainty in the majority of the 56 energy groups.

By applying each set of perturbed nuclear data to the MultiBUGS model, 1000 flux spectrum results are generated and the mean and standard deviation can be determined over the population. In what follows, the results and figures from the data collected during July, 2020 will be presented as a representative data, and the general results will be discussed. Owing to the large amount of information (21 wire segments x 56 energy groups x 1000 nuclear data libraries) contained in the MCMC output, the results will be presented either as axially-averaged values or as a representative sample of data.

4.1 Reaction Rate Comparisons

To assess the performance of the MCMC model, the (n,x) reaction rates can be used as a figure of merit. Figure 2 shows the axially-averaged (n,x) reaction rates for each reaction being studied (see Table 7) as determined from the MCMC output, the experimental data, and an MCNP simulation in MNR Site 8C.

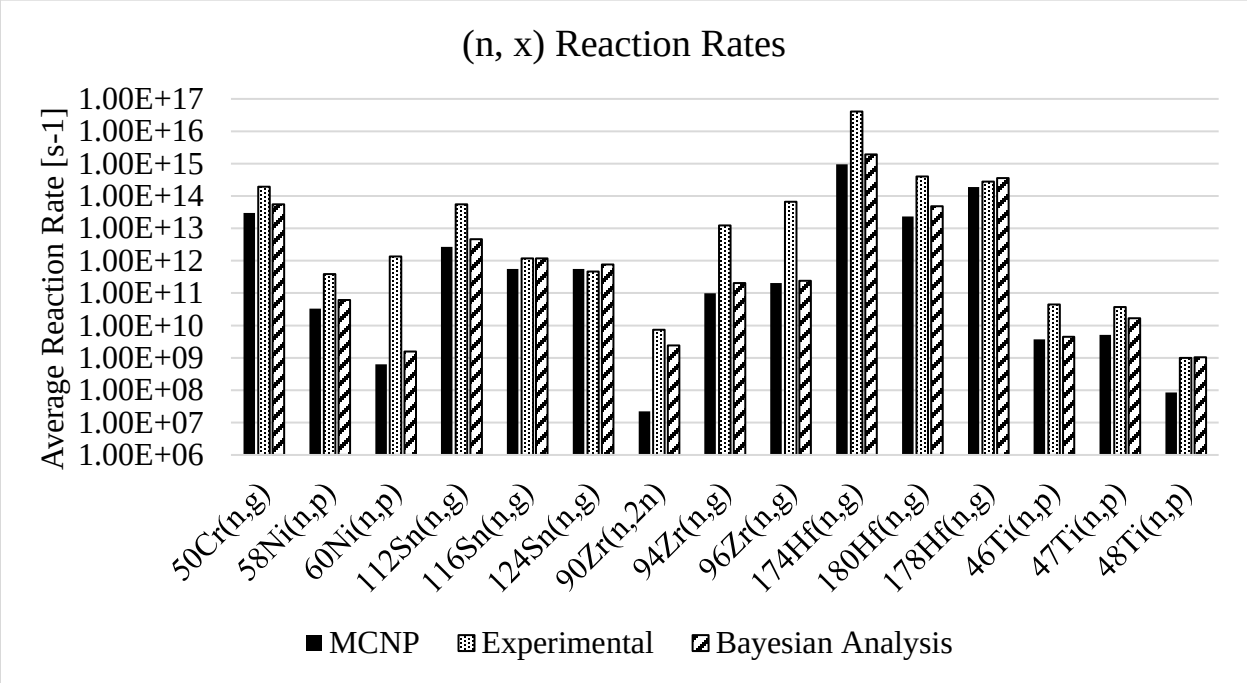

Figure 2: Comparison between the (n,x) reaction rates as determined experimentally, via MCMC Bayesian inference, and from an MCNP simulation in. Uncertainties are not shown as they are insignificant compared to the scale of the figure.

Figure 2 shows that the MCMC results predict the reaction rates for threshold reactions (i.e. the (n,2n) and the (n,p) reactions) more accurately than the MCNP results. This indicates that the neutron flux spectrum above approximately 0.1 MeV is generally well represented by the MCMC results. By contrast, there is a less consistent trend in the differences between the experimental and computationally-determined (n, γ) reaction rates. In general, the MCNP results tend to underpredict the experimental (n, γ) reaction rates, while the MCMC results show varying levels of improvement. For reactions dominated by a single broad resonance peak between ~ 5 eV and ~ 10 keV (i.e. the ^{50}Cr, ^{116}Sn, ^{124}Sn, and ^{178}Hf (n, γ) reactions), the Bayesian results show an improvement compared to the MCNP model however, for (n, x) reactions dominated by either overlapping resonance peaks or the unresolved resonance region, the MCMC results underpredict

the experimentally determined reaction rates and the improvement as compared to MCNP is less noticeable.

This suggest that, while the thermal and the fast neutron fluxes may be appropriately described by the MCMC results, the modified 1/E spectrum adopted in this work may not be sufficient to capture the effects of the unresolved resonance region, the delayed neutron spectrum, or the effects of multiple low-lying capture resonances. A more sophisticated definition of the epithermal neutron flux may be needed to improve the results for these reactions. However, since many of the materials commonly used in irradiation procedures (e.g. ^{197}Au, ^{176}Lu, ^{115}In) are dominated by a single broad resonance, MCMC methods may show considerable improvement in their activation predictions.

4.2 Neutron Flux Energy Spectrum

Figure shows the axially-averaged, mean values of the neutron flux spectrum results from MCNP and from the MCMC model. Uncertainties have been omitted from this figure, and are discussed separately in Section 4.3.

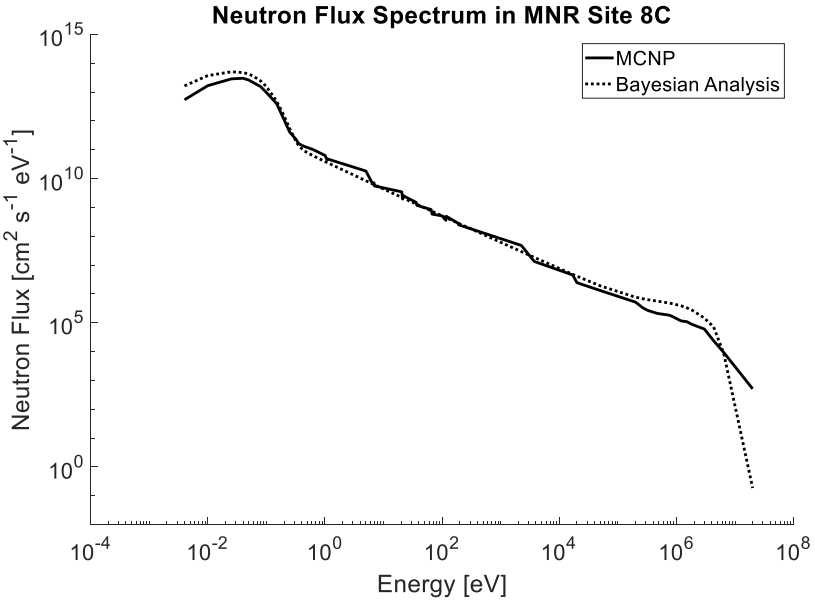

Figure 3: Axially-average neutron flux spectrum results. Uncertainties are not shown here, for visual clarity.

As can be seen from Figure 3 there is generally good agreement between the MCNP results and the MCMC outputs across most of the energy spectrum, with significant differences appearing above 10^4 eV (i.e. in the upper epithermal and fast flux energy regions), and below 0.01 eV.

The thermal and the epithermal neutron flux spectra estimated by MCMC methods are defined by shape parameters having typical values of kT = 0.0267 ± 0.00143, and α = -0.0985 ± 0.00016 (based on wire segments within the bounds of the active core region) and α = 0.18 ± 0.001822 (based on wire segments extending above and below the active core region). The values of kT recovered from the MCMC results agree with the expected peak of a Maxwellian distribution dictated by the moderator and coolant temperature in the core (i.e. this is above the theoretical value of kT = 0.0253 eV).

4.3 Uncertainty Analysis

Figure shows the relative uncertainties from the Bayesian analysis, computed using data over the entire core length. These results are indicative of the uncertainties obtained at all axial locations.

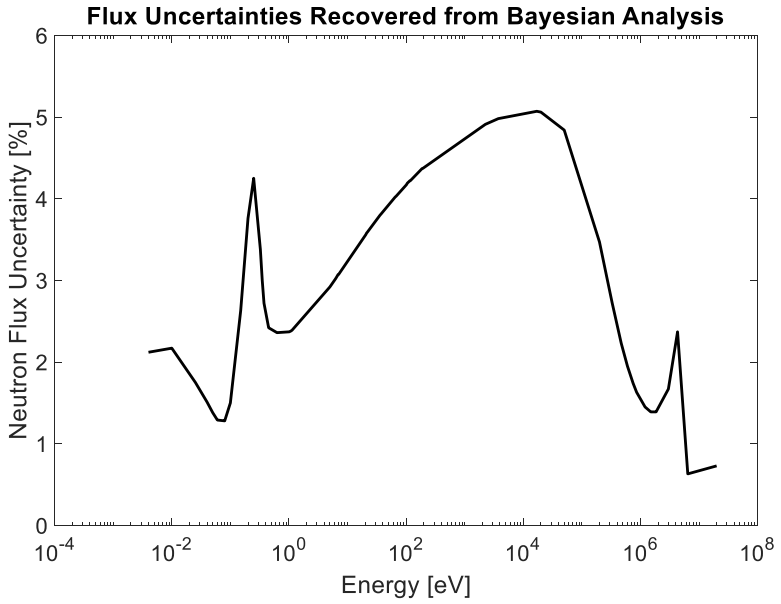

Figure 4: Trends in the MCMC neutron flux spectrum uncertainties. Axially-averaged values are presented, for ease in data visualization. The trends remain consistent along the length of the wire.

Figure shows that the flux uncertainties recovered from the MCMC results range from approximately 1 % to 5 %, which is generally consistent with previous assessments of broad-group flux uncertainties in MNR, and provides new information about the spectrum specific uncertainties which have not been previously studied [59], [69].

The small spike in uncertainty at E = 0.025 eV may be due to the significant contribution of kT at the peak of the thermal neutron flux spectrum; as reported in Section 4.2, this shape parameter has

an uncertainty of approximately 5%, and therefore may directly lead to a higher uncertainty at this energy range.

As described in Section 4.1, an investigation of the recovered reaction rates suggest that the thermal neutron flux spectrum is generally well described by the MCMC results – this is corroborated by the relatively small MCMC output uncertainties below approximately 1 eV (excepting at 0.025 eV, as described above). However, in the epithermal energy region (where the spectrum definition may not be sufficiently sophisticated), the uncertainty determined by the MCMC method increases with increasing energy. This may indicate that the parameterized epithermal model (rather than either the measurements or nuclear data inputs) is contributing significantly to the output uncertainties. It may be possible to improve the epithermal behaviour by subdividing this region further; two epithermal energy groups may be considered, where the high energy region models both the unresolved resonances and delayed neutron spectrum, and a modified 1/E spectrum is adopted at lower energies.

5 Conclusions

This work has demonstrated that by combining prior information (recovered from MCNP results) with new activations measurements, Bayesian methods may be used to generate improved estimates of the in-core neutron flux spectrum. The experimentally determined (n, x) reaction rates were to the Bayesian posterior distributions, and a set of MCNP simulation results; the outputs from the Bayesian framework showed considerable improvement compared to the MCNP predictions for threshold reactions and for those reactions that are dominated by a broad low-lying resonance. For other reactions, both the MCNP and the MCMC results generally under-predict the measured reaction rates. Although the MCMC results showed some improvement, the modified 1/E spectrum adopted in this analysis may not be sufficient to represent the unresolved resonance region, and further work is required to refine the model definition in this energy region.

The flux spectrum results indicate generally good qualitative agreement between the MCNP and MCMC results below approximately 10^4 eV, and both the thermal and the epithermal neutron fluxes parameters are physically consistent with the moderation and thermalization processes within the irradiation site. Although there are deviations between the MCNP and MCMC results above 10^4 eV, a comparison of the recovered reaction rates (discussed in Section 4.2) indicates

that the fast flux spectrum as determined by MCMC methods provides a better estimate of experimentally determined (n, x) activation data. The recovered MCMC flux spectrum uncertainty increases with increasing energy over the intermediate portion of the spectrum – which further points to an underlying issue in the parameterization of the epithermal spectrum, and is consistent with a comparison of the estimates (n, x) reaction rates. As the 1/E spectrum is derived based on a set of simplifying assumptions (whose validity is difficult to assess under real reactor conditions), it may be necessary to derive a more sophisticated form of the epithermal neutron flux that accounts for both moderation and absorption more completely. Given the improvement in the activation results using the Bayesian approach, the parameterized flux spectrum can be used by operations staff to better predict radiopharmaceutical activations, and hence improve quality control during production.

An investigation of the MCMC outputs revelated that, in energy regions where the parameterized model is thought to be well-suited (the thermal and the fast energy regions), the magnitude of output uncertainties is generally consistent with the uncertainties in the measurements. While there are some non-monotonic spikes in the estimated MCMC uncertainties, this may be attributed to the spectrum parameters that dominate at those energies (i.e. kT at the peak of the thermal neutron flux spectrum). In general, applying multiple sets of perturbed nuclear data to a MCMC-based Bayesian model may generate improved estimates of the neutron flux spectrum, (n, x) reaction rates, and a quantitative measure of their respective output uncertainties.

Taken together, the comparison of the (n, x) reaction rates, the flux spectrum results, and the trends in output uncertainties indicate that a modified 1/E spectrum in the epithermal energy region may be prohibitively simple; the evidence suggests that describing the neutron flux in this way may not account for the unresolved resonance region, the delayed neutron spectrum, or the effects of multiple capture resonances in the target materials. This work may be continued by investigating other epithermal neutron spectrum definitions present in the literature, and by deriving a more complete form of this flux from first principles.

6 Acknowledgements

Grateful acknowledgement is made towards all the operations staff and management team of MNR for their help during experimentation. Thanks also to Alice Pidruczny of the MACCNAA for her

help in training on the data acquisition systems, and to the McMaster Health Physics team for their help in coordinating experimental efforts. Special thanks to Ross Harper for designing and constructing the five-wire holders, which are essential to the continued success of this project. The authors thank Dr. Simon E. Day for providing the schematic of the MNR reference core configuration used in Figure.

This work was funded by the Natural Sciences and Engineering Research Council of Canada (NSERC) and University Network of Excellence in Nuclear Engineering (UNENE).

7 References

[1] "The Paris Agreement," *Governement of Canada*, 2016. [Online]. Available: https://www.canada.ca/en/environment-climate-change/services/climate-change/paris-agreement.html. [Accessed: 13-Oct-2020].

[2] International Atomic Energy Agency, "Climate Change and Nuclear Energy 2020," Vienna, 2020.

[3] IEA, "Global Energy Review: CO2 Emissions in 2020," *IEA*, 2021. [Online]. Available: https://www.iea.org/articles/global-energy-review-co2-emissions-in-2020. [Accessed: 12-Jul-2021].

[4] "Nuclear Power in the World Today," *World Nuclear Association*, 2020. [Online]. Available: https://www.world-nuclear.org/information-library/current-and-future-generation/nuclear-power-in-the-world-today.aspx. [Accessed: 13-Oct-2020].

[5] "Research Reactors," *World Nuclear Association*, 2020. [Online]. Available: https://www.world-nuclear.org/information-library/non-power-nuclear-applications/radioisotopes-research/research-reactors.aspx. [Accessed: 10-Oct-2020].

[6] International Atomic Energy Agency, "Research Reactors: Purpose and Future," Vienna, 2016.

[7] International Atomic Energy Agency, "History, development and future of TRIGA research reactors IAEA TRS 482," Vienna, 2016.

[8] D. Chiesa *et al.*, "Measurement and simulation of the neutron flux distribution in the TRIGA

Mark II reactor core," *Ann. Nucl. Energy*, vol. 85, pp. 925–936, 2015.

[9] B. M. Makgopa, M. Belal, and W. J. Strydom, "Neutronic Characterization of the SAFARI-1 Material Testing Reactor," in *Proceedings of the 4th International Topical Meeting on High Temperature Reactor Technology*, 2008, pp. 1–7.

[10] N. Jawerth and E. Mattar, "Exploring Research Reactors and Their Use," *International Atomic Energy Agency*, 2020. [Online]. Available: https://www.iaea.org/newscenter/news/exploring-research-reactors-and-their-use. [Accessed: 13-Oct-2020].

[11] A. Borio *et al.*, "TRIGA reactor absolute neutron flux measurement using activated isotopes," *Prog. Nucl. Energy*, vol. 70, pp. 249–255, 2014.

[12] M. Alqahtani and A. B. Alajo, "Characterization of prompt neutron spectrum of the Missouri University of Science and Technology Reactor," *Nucl. Eng. Des.*, vol. 320, pp. 57–64, 2017.

[13] V. Radulovic, Z. Stancar, L. Snoj, and A. Trkov, "Validation of absolute axial neutron fl ux distribution calculations with MCNP with 197 Au (n , γ) 198 Au reaction rate distribution measurements at the JSI TRIGA Mark II reactor," *Appl. Radiat. Isot.*, vol. 84, pp. 57–65, 2014.

[14] A. C. Fernandes, J. P. Santos, J. G. Marques, A. Kling, A. R. Ramos, and N. P. Barradas, "Validation of the Monte Carlo model supporting core conversion of the Portuguese Research Reactor (RPI) for neutron fluence rate determinations," *Ann. Nucl. Energy*, vol. 37, no. 9, pp. 1139–1145, 2010.

[15] L. Snoj, A. Trkov, R. Jacimovic, P. Rogan, G. Zerovnik, and M. Ravnik, "Analysis of neutron flux distribution for the validation of computational methods for the optimization of research reactor utilization," *Appl. Radiat. Isot.*, vol. 69, pp. 136–141, 2011.

[16] B. Richardson, C. H. Castano, J. King, A. Alajo, and S. Usman, "Modeling and validation of approach to criticality and axial flux profile experiments at the Missouri S & T Reactor (MSTR)," *Nucl. Eng. Des.*, vol. 245, pp. 55–61, 2012.

[17] D. Chiesa *et al.*, "Fuel burnup analysis of the TRIGA Mark II reactor at the University of

Pavia," *Ann. Nucl. Energy*, vol. 96, pp. 270–276, 2016.

[18] K. H. Beckurts and K. Wirtz, *Neutron Physics*. Berlin: Springer-Verlag, 1964.

[19] J. Lamarsh and A. Baratta, *Introduction to Nuclear Engineering*, Third. Upper Saddle River: Prentice-Hall, 2001.

[20] J. K. Shultis and R. E. Faw, *FUNDAMENTALS OF NUCLEAR SCIENCE AND ENGINEERING*. Manhattan: Marcel Dekker, 2002.

[21] J. J. Duderstadt and L. J. Hamilton, *Nuclear Reactor Analysis*. Ann Arbor: John Wiley & Sons, Inc., 1976.

[22] "Evaluated Nuclear Data File (ENDF)." [Online]. Available: https://www-nds.iaea.org/exfor/endf.htm.

[23] F. Salaun, "Assessment and optimization of the Canadian SCWR reactivity control systems through reactor physics and thermal-hydraulics coupling," McMaster University, 2017.

[24] B. J. Ade, "SCALE / TRITON Primer : A Primer for Light Water Reactor Lattice Physics Calculations," 2011.

[25] X-5 Monte Carlo Team, "MCNP — A General Monte Carlo N-Particle Transport Code, Version 5 Volume I: Overview and Theory," Los Alamos, 2003.

[26] I. Lux and L. Koblinger, *Particle Transport Methods : Neutron and Photon Calculations Authors*. Boca Raton: CRC Press, 1991.

[27] P. Reuss, *Neutron Physics*. Paris: EDP Sciences, 2008.

[28] F. Brown, "Monte Carlo Techniques for Nuclear Systems – Theory Lectures." Los Alamos, 2016.

[29] D. B. Pelowitz *et al.*, "MCNP6 User's Manual," Los Alamos, 2013.

[30] L. Hamidatou, H. Slamene, T. Akhal, and B. Zouranen, "Concepts, Instrumentation and Techniques of Neutron Activation Analysis," in *Imaging and Radioanalytical Techniques in Interdisciplinary Research*, F. Kharfi, Ed. Rijeka: IntechOpen, 2013.

[31] B. E. Watt, "Energy spectrum of neutrons from thermal fission of U235," *Phys. Rev.*, vol.

87, no. 6, pp. 1037–1041, 1952.

[32] "Neutron Fluence Measurements," *Iaea*, vol. TRS-107, 1970.

[33] K. C. Hines, "Energy and Lethargy Distribution of Neutrons Slowing Down in Graphite," Sydney, 1959.

[34] S. Bell, "Beginner's Guide to Uncertainty of Measurement," Teddington, 1999.

[35] International Bureau of Weights and Measures, "Evaluation of measurement data — Guide to the expression of uncertainty in measurement," Sèvres, 2008.

[36] J. R. Taylor, "An Introduction to Error Analysis: The Study of Uncertainties in Physical Measurements," 2nd ed., University Science Books, 1997, pp. 93–120.

[37] Canadian Nuclear Safety Commission, "Record of Proceedings - McMaster University - Application to Renew the McMaster Nuclear Reactor Operating Licence," 2014.

[38] McMaster Nuclear Reactor, "Nuclear Operations and Facilities 2017," Hamilton, 2017.

[39] S. E. Day, "McMaster Nuclear Reactor Specification - IAEA CRP 1496, Innovative Methods for Research Reactors: "Benchmarking against Experimental Data of the Neutronic and Thermalhydraulic Computational Methods and Tools for Operation and Safety Analysis for Research," Hamilton, 2011.

[40] S. E. Day, M. P. Butler, and W. J. Garland, "Calculations in Support of the Mnr Core Conversion," Hamilton, 2002.

[41] S. E. Day, "McMaster Nuclear Reactor Benchmark Specification - IAEA CRP 1496, Innovative Methods for Research Reactors: "Benchmarking against Experimental Data of the Neutronic and Thermalhydraulic Computational Methods and Tools for Operation and Safety Analysis for," Hamilton, 2013.

[42] M. Alqahtani, A. Buijs, and S. E. Day, "Serpent-2 and OSCAR-4 computational tools compared against McMaster nuclear reactor improved operational data history for U-235 fuel inventory tracking , local power tracking and validation of multiplication factor," *Ann. Nucl. Energy*, vol. 145, p. 107590, 2020.

[43] A. Klett, "Handbook of Particle Detection and Imaging," C. Grupen and I. Buvat, Eds.

Berlin: Springer, 2012, pp. 759–790.

[44] L. Snoj, M. Ravnik, A. Trkov, and G. Zerovnik, “On the self-shielding factors in neutron activation analysis,” *Nucl. Instruments Methods Phys. Res. Sect. A Accel. Spectrometers, Detect. Assoc. Equip.*, vol. 610, pp. 553–565, 2009.

[45] “NuDat 2.7.” [Online]. Available: http://www.nndc.bnl.gov/nudat2/.

[46] M. Berglund and M. E. Wieser, “Isotopic compositions of the elements 2009 (IUPAC Technical Report)*,” *Pure Appl. Chem.*, vol. 83, no. 2, pp. 397–410, 2011.

[47] J. Meija *et al.*, “Atomic weights of the elements 2013 (IUPAC Technical Report),” *Pure Appl. Chem.*, vol. 88, no. 3, pp. 265–291, 2016.

[48] *Genie ™ 2000 Spectroscopy Software*. 2000.

[49] D. Chandler, G. I. Maldonado, L. D. Proctor, and R. T. Primm, “Nuclear Transmutations in HFIR’s Beryllium Reflector and Their Impact on Reactor Operation and Reflector Disposal,” *Nucl. Technol.*, vol. 177, no. 3, pp. 395–412, 2017.

[50] M. B. Zeller, A. Celli, R. T. Jones, and G. P. McPhee, “Photo-neutron experiment performed in ZED-2,” in *21st Conference of the Canadian Nuclear Society*, 2000.

[51] E. Macconnachie, D. Novog, and S. Day, “ICONE26-82412 Axial Flux Wire Measurements atthe McMaster Nuclear Reactor,” 2018, pp. 1–8.

[52] G. E. Knoll, *Radiation Detection and Measurement Third Edition*, 3rd ed. Ann Arbor: John Wiley & Sons, Inc., 2000.

[53] Alfa Aesar, “Certificate of analysis.” Thermo Fisher Scientific, 2018.

[54] National Institute of Standards and Technology, “Thermophysical Properties of Fluid Systems,” 2018. [Online]. Available: https://webbook.nist.gov/chemistry/fluid/. [Accessed: 03-May-2019].

[55] Cole-Parmer, “Digi-Sense Prec. Ind. PRT, 0.25" x 12" , -60~160C, Bare Wire.” [Online]. Available: https://www.coleparmer.com/i/digi-sense-prec-ind-prt-0-25-x-12-60-160c-bare-wire/9045200. [Accessed: 06-May-2019].

[56] Badger Meter, "Model SSL Venturi Classic Flow Meter." [Online]. Available: https://www.badgermeter.com/business-lines/flow-instrumentation/venturi-ssl/. [Accessed: 06-May-2019].

[57] B. T. Rearden and M. A. Jessee, "SCALE Code System," Oak Ridge National Laboratory, Oak Ridge, 2017.

[58] "SCALE User's Group." [Online]. Available: https://groups.google.com/forum/#!forum/scale-users-group.

[59] E. MacConnachie, D. Novog, and S. Day, "Quantification of system uncertainties in activation experiments at nuclear research reactors," *Ann. Nucl. Energy*, vol. 134, pp. 432–440, 2019.

[60] D. R. Helsel and R. M. Hirsch, "Statistical Methods in Water Resources," 2002, pp. 337–340.

[61] V. Suman and P. K. Sarkar, "Nuclear Instruments and Methods in Physics Research A Neutron spectrum unfolding using genetic algorithm in a Monte Carlo simulation," *Nucl. Inst. Methods Phys. Res. A*, vol. 737, pp. 76–86, 2014.

[62] M. Matzke, "9 UNFOLDING PROCEDURES," *Radiat. Prot. Dosimetry*, vol. 107, pp. 155–174, 2003.

[63] S. R. Malkawi and N. Ahmad, "Solution of the neutron spectrum adjustment problem in a typical MTR type research reactor," *Ann. Nucl. Energy*, vol. 28, pp. 17–22, 2001.

[64] F. Molina, P. Aguilera, J. Romero-barrientos, H. F. Arellano, J. Agramunt, and J. Medel, "Energy distribution of the neutron fl ux measurements at the Chilean Reactor RECH-1 using multi-foil neutron activation and the Expectation Maximization unfolding algorithm," *Appl. Radiat. Isot.*, vol. 129, no. August, pp. 28–34, 2017.

[65] J. A. Kennedy, "A COMPARISON OF MNR IRRADIATION EXPERIMENTS WITH SIMULATION," McMaster Univeristy, 2000.

[66] D. Chiesa, E. Previtali, and M. Sisti, "Bayesian statistics applied to neutron activation data for reactor flux spectrum analysis," *Ann. Nucl. Energy*, vol. 70, pp. 157–168, 2014.

[67] A. Leder, “Unfolding neutron spectrum with Markov Chain Monte Carlo at MIT research Reactor with He-3 Neutral Current Detectors,” *Jounal Instrum.*, vol. 13, 2018.

[68] D. Chiesa *et al.*, “Measurement of the neutron flux at spallation sources using multi-foil activation,” *Nucl. Instruments Methods Phys. Res. Sect. A Accel. Spectrometers, Detect. Assoc. Equip.*, vol. 902, pp. 14–24, 2018.

[69] E. L. Macconnachie and D. R. Novog, “Measurement , simulation and uncertainty quantification of the neutron flux at the McMaster Nuclear Reactor,” *Ann. Nucl. Energy*, vol. 151, 2021.

[70] B. J. Smith, “boa : An R Package for MCMC Output Convergence,” *J. Stat. Softw.*, vol. 21, no. 11, 2007.

[71] R. J. B. Goudie, R. M. Turner, and D. De Angelis, “MultiBUGS : A Parallel Implementation of the BUGS Modelling Framework for Faster Bayesian Inference,” *arXiv*, 2018.

[72] D. J. Spiegelhalter, N. G. Best, and B. P. Carlin, “Bayesian measures of model complexity and fit,” *J. R. Stat. Soc. Ser. B*, pp. 583–639, 2002.

[73] J. Wang, Z. Guo, X. Chen, and Y. Zhou, “Neutron spectrum unfolding based on generalized regression neural networks for neutron fluence and neutron ambient dose equivalent estimations,” *Appl. Radiat. Isot.*, vol. 154, no. August, p. 108856, 2019.

[74] International Atomic Energy Agency, “Compendium of Neutron Spectra and Detector Responses for Radiation Protection Purposes IAEA TRS 403,” Vienna, 2001.

7 Conclusions and Future Work

7.1 Summary of Findings

Nuclear research reactors provide a unique opportunity to perform high-fidelity experiments that may contribute both to the advancement of reactor physics and to operational decision making, in the nuclear industry. Of particular interest to the community is the in-core neutron flux; this quantity provides information about all neutron-induced reactions in the core, and can therefore be used to understand the fission power, fuel burnup, and yield of medical isotopes being produced in the facility. Uncertainties related to experimental determination of the neutron flux have previously been limited to both measurement and instrumentation uncertainties. However, the possibility that other reactor conditions may contribute significantly to the final flux uncertainty has been raised, but not yet fully studied [8], [11], [13], [15].

This thesis quantified significant sources of uncertainty in measurements of the neutron flux due to reactor parameters and develops a methodology for propagating these values such that high-fidelity flux results may be used directly in code validation studies, UQ procedures, or operational decision making. The results presented in this thesis are a combination of several experimental campaigns in MNR and full-core MCNP simulation results. Although this thesis develops a novel body of work based on results recovered in MNR Site 8C, these procedures may be applied in other sites in MNR, or in other facilities, where precise flux measurements are required.

Chapter 4 presented a method for quantifying and propagating the contributions of the following reactor parameters to the total neutron flux uncertainty: the sample position, the reactor power determination, the presence of ^{135}Xe, control rod movement, and general nuclear data uncertainties. These effects were quantified through a series of irradiation experiments and Monte Carlo simulations in MNR Site 8C. It was determined that the neutron flux uncertainty is dominated by the effects of sample positioning and by the reactor power determination; these parameters were found to contribute relative uncertainties of 3.49 % and 3.25 %, respectively. It is recommended that these sources of uncertainty be quantified before activation data or flux measurements are used as inputs to further analyses such as code validation studies, UQ procedures, or unfolding methods.

The effects of fuel management operations and burnup on flux measurements were investigated in Chapter 5 to determine if an additional source of uncertainty is required to account for measurements taken under different core configurations. The results from a 4-month long

experimental campaign were combined with an analysis of 5 pairs of historical core configurations in MNR. The experimental procedure applied the cadmium difference method and the use of threshold activation such that the neutron flux in the thermal, the epithermal, and the fast energy groups could be recovered. While it was determined that no statistically significant trends were present in the experimental data over this period of time, it has been noted that the magnitude of the flux uncertainties propagated according to Chapter 4 may obscure the fine details of these effects. Although a significant reduction in the neutron flux uncertainty may be required to understand these effects through purely experimental means, these results are corroborated by an investigation of the differences between MCNP results for each historical core pair. In general, it is sufficient to combine uncertainties according to the work presented in Chapter 4; the effects of burnup and fuel management need not be considered further for irradiations performed in MNR Site 8C.

The work presented in Chapter 4 and Chapter 5 applied nuclear data homogenization procedures to convert an activation measurement to a neutron flux value either in a particular energy group, or over the entire energy spectrum, as appropriate. Chapter 6 utilized Markov-Chain Monte-Carlo (MCMC) methods within a Bayesian framework to recover the flux spectrum in a 56-group structure such that the nuclear data uncertainties and their covariances were accounted for without additional data processing. The 1000 sets of perturbed nuclear data available through SCALE were each individually applied to the Bayesian model, generating a distribution of flux values in each energy group. A comparison of the (n, x) reaction rates generated with three methods: from the MCNP model, that were measured, and those that were determined from the MCMC model revealed that – although the Bayesian model makes improved predictions for both the thermal and the fast flux spectra – the modified 1/E parametrization of the epithermal spectrum may not be sufficient to capture the effects of unresolved resonances above ~ 10 keV. This is supported by an analysis of the MCMC output flux uncertainties; in the epithermal region, the flux uncertainties increase with increasing energy, suggesting that the model (rather than input uncertainties) is dominating the output uncertainty.

7.2 Discussion of Future Work

The work presented in this thesis provides novel methodologies and results regarding in-core neutron flux measurements. Some recommendations to overcome limitations of the original

methodologies or to extend this research to include new techniques are presented and discussed here.

7.2.1 Reactor Facilities

The uncertainties associated with the sample positioning and the reactor power should be studied further so that their contributions to the overall flux uncertainty may be minimized. The means to achieve this may significantly disrupt regular reactor operations, and therefore remained outside the scope of this thesis however, a collaboration between MNR operators and reactor physicists is recommended so that future irradiation procedures may be further optimized.

The positional uncertainty is due to the nature of the irradiation equipment being used; to facilitate the insertion and removal of wire holders from the core, the wire holders sit freely in the irradiation site, and their diameter is much smaller than the sample holders which house them. To eliminate this source of uncertainty, the design of either the wire holder or the sample holder must be modified to ensure the sample sits in a precise location in the irradiation site, and that its placement is repeatable. Some possible solutions to this problem are briefly presented here.

- The diameter of the wire holder's end-caps may be increased to ensure a tighter tolerance between the wire holder and the sample holder. The increase in the dimensions of the end-caps would be limited by the ability of MNR operators to insert and remove the wire holders from the sample holder. While this would not eliminate the positional source of uncertainty, it may be significantly reduced from the reported value of 3.49% [59].
- A designated sample holder and wire holder may be fitted with a set of hooks and pins, respectively, so that the wire holder rests in a precise location during each irradiation procedure. As this may limit the use of that sample holder, it may be necessary to procure an additional sample holder for use when high-fidelity irradiation procedures are required.

These modifications to a sample holder or wire holder should reduce the positional uncertainty in the case of a single-wire irradiation. If the custom-built 5-wire holder is used, a mechanism to "lock" the wire holder in a fixed direction would result in the positional effects manifesting as a bias in the results, rather than an uncertainty value.

An estimate of the reactor power uncertainty was estimated by applying the instrumentation uncertainties of commercially available flow meters and thermocouples; in order to precisely

determine the reactor power uncertainty, the specifications of the instruments used in MNR must be known. No detailed calibration information is available power related measurements in MNR, and a project to recover this information, and if necessary, replace certain instruments in MNR is recommended such that this quantity can be precisely known. Replacing either the flow meter or the thermocouples should be planned in advance to coincide with regularly scheduled shut-down maintenance in MNR.

7.2.2 Extended Experimental Campaigns

The study of the effects of fuel management operations on flux measurements presented in Chapter 5 combined a 4-month experimental campaign with historical MNR core data. An extended experimental campaign – carried out over a period of years and in different core sites – may eliminate the need to rely on historical computational data and may also be used to support on-going core-follow calculations in MNR.

Prior to carrying out a campaign of this nature, the uncertainties described in Chapter 4 must be quantified in each irradiation site being used (i.e. each site in rows 8 and 9 of MNR). If precise activation measurements are not required, these irradiations may also be conducted in fuel sites, and may be used to support the efforts of MNR operators in their determination of fuel burnup. Regular irradiation procedures (i.e. at monthly or twice-monthly intervals) should be performed over a period of several years to capture the effects of several fuel shuffling and refuelling operations; this may be used to further understand the nature of fuel burnup on irradiation procedures in MNR.

7.2.3 Spectrum Unfolding with Machine Learning

The application of MCMC Bayesian methods in this thesis (presented in Chapter 6) has demonstrated that machine learning techniques may be used in place of traditional unfolding codes to recover the in-core neutron flux from a set of activation measurements. This work could be extended by investigating the application of other machine learning techniques to this problem.

Various types of neural networks have been identified as appropriate methods to solve the unfolding problem in general however, their ability to recover the fine structure of the neutron energy spectrum may be limited by the availability of validated training data [73]. The reference spectra and detector response information published in a 2001 IAEA compendium is not cast in a

standard energy group structure, and is generally limited to ex-core reactor power data [74]. While the former may be overcome by making use of the ANGELO-LAMBDA code, it may be necessary to generate a new set of activation data for training neural networks such that they can recover the in-core neutron flux in research reactors. A prolonged experimental campaign to recover activation measurements of other (n, x) reactions (i.e. in addition to those presented in Chapter 6) may be required before neural networks can be applied to solve the spectrum unfolding problem. While it may be possible to generate the required training data in MNR, a collaboration with other research reactor facilities would ensure that the training data set is sufficiently varied that the neural network can output reliable results.

In the absence of a sufficiently large validated training data set, it may be possible to combine Monte Carlo methods with genetic algorithms to recover the neutron flux spectrum, using only the measured activation data as inputs [61]. While a framework to apply this method has been presented in Chapter 6 as an extension to the MCMC methods, a more detailed investigation is required to understand the limitations of and the uncertainties generated by this method.

7.3 Conclusion

This thesis has presented an investigation of significant sources of uncertainty in measurements of the neutron flux in research reactors; a novel methodology for quantifying and propagating these uncertainties has been developed. Additionally, a framework for extending this work (in either extended experimental campaigns or in the application of machine learning techniques) has been suggested. These results can be applied to the synthesis of medical isotopes, radiation safety and code validation studies, and reactor operational decision making in any research reactor that faithfully applies the methods described in the main body of this thesis.

Works Cited

[1] "The Paris Agreement," *Governement of Canada*, 2016. [Online]. Available: https://www.canada.ca/en/environment-climate-change/services/climate-change/paris-agreement.html. [Accessed: 13-Oct-2020].

[2] International Atomic Energy Agency, "Climate Change and Nuclear Energy 2020," Vienna, 2020.

[3] IEA, "Global Energy Review: CO2 Emissions in 2020," *IEA*, 2021. [Online]. Available: https://www.iea.org/articles/global-energy-review-co2-emissions-in-2020. [Accessed: 12-Jul-2021].

[4] "Nuclear Power in the World Today," *World Nuclear Association*, 2020. [Online]. Available: https://www.world-nuclear.org/information-library/current-and-future-generation/nuclear-power-in-the-world-today.aspx. [Accessed: 13-Oct-2020].

[5] "Research Reactors," *World Nuclear Association*, 2020. [Online]. Available: https://www.world-nuclear.org/information-library/non-power-nuclear-applications/radioisotopes-research/research-reactors.aspx. [Accessed: 10-Oct-2020].

[6] International Atomic Energy Agency, "Research Reactors: Purpose and Future," Vienna, 2016.

[7] International Atomic Energy Agency, "History, development and future of TRIGA research reactors IAEA TRS 482," Vienna, 2016.

[8] D. Chiesa *et al.*, "Measurement and simulation of the neutron flux distribution in the TRIGA Mark II reactor core," *Ann. Nucl. Energy*, vol. 85, pp. 925–936, 2015.

[9] B. M. Makgopa, M. Belal, and W. J. Strydom, "Neutronic Characterization of the SAFARI-1 Material Testing Reactor," in *Proceedings of the 4th International Topical Meeting on High Temperature Reactor Technology*, 2008, pp. 1–7.

[10] N. Jawerth and E. Mattar, "Exploring Research Reactors and Their Use," *International Atomic Energy Agency*, 2020. [Online]. Available:

https://www.iaea.org/newscenter/news/exploring-research-reactors-and-their-use. [Accessed: 13-Oct-2020].

[11] A. Borio *et al.*, "TRIGA reactor absolute neutron flux measurement using activated isotopes," *Prog. Nucl. Energy*, vol. 70, pp. 249–255, 2014.

[12] M. Alqahtani and A. B. Alajo, "Characterization of prompt neutron spectrum of the Missouri University of Science and Technology Reactor," *Nucl. Eng. Des.*, vol. 320, pp. 57–64, 2017.

[13] V. Radulovic, Z. Stancar, L. Snoj, and A. Trkov, "Validation of absolute axial neutron fl ux distribution calculations with MCNP with 197 Au (n , γ) 198 Au reaction rate distribution measurements at the JSI TRIGA Mark II reactor," *Appl. Radiat. Isot.*, vol. 84, pp. 57–65, 2014.

[14] A. C. Fernandes, J. P. Santos, J. G. Marques, A. Kling, A. R. Ramos, and N. P. Barradas, "Validation of the Monte Carlo model supporting core conversion of the Portuguese Research Reactor (RPI) for neutron fluence rate determinations," *Ann. Nucl. Energy*, vol. 37, no. 9, pp. 1139–1145, 2010.

[15] L. Snoj, A. Trkov, R. Jacimovic, P. Rogan, G. Zerovnik, and M. Ravnik, "Analysis of neutron flux distribution for the validation of computational methods for the optimization of research reactor utilization," *Appl. Radiat. Isot.*, vol. 69, pp. 136–141, 2011.

[16] B. Richardson, C. H. Castano, J. King, A. Alajo, and S. Usman, "Modeling and validation of approach to criticality and axial flux profile experiments at the Missouri S & T Reactor (MSTR)," *Nucl. Eng. Des.*, vol. 245, pp. 55–61, 2012.

[17] D. Chiesa *et al.*, "Fuel burnup analysis of the TRIGA Mark II reactor at the University of Pavia," *Ann. Nucl. Energy*, vol. 96, pp. 270–276, 2016.

[18] K. H. Beckurts and K. Wirtz, *Neutron Physics*. Berlin: Springer-Verlag, 1964.

[19] J. Lamarsh and A. Baratta, *Introduction to Nuclear Engineering*, Third. Upper Saddle River: Prentice-Hall, 2001.

[20] J. K. Shultis and R. E. Faw, *FUNDAMENTALS OF NUCLEAR SCIENCE AND*

ENGINEERING. Manhattan: Marcel Dekker, 2002.

[21] J. J. Duderstadt and L. J. Hamilton, *Nuclear Reactor Analysis*. Ann Arbor: John Wiley & Sons, Inc., 1976.

[22] "Evaluated Nuclear Data File (ENDF)." [Online]. Available: https://www-nds.iaea.org/exfor/endf.htm.

[23] F. Salaun, "Assessment and optimization of the Canadian SCWR reactivity control systems through reactor physics and thermal-hydraulics coupling," McMaster University, 2017.

[24] B. J. Ade, "SCALE / TRITON Primer : A Primer for Light Water Reactor Lattice Physics Calculations," 2011.

[25] X-5 Monte Carlo Team, "MCNP — A General Monte Carlo N-Particle Transport Code, Version 5 Volume I: Overview and Theory," Los Alamos, 2003.

[26] I. Lux and L. Koblinger, *Particle Transport Methods : Neutron and Photon Calculations Authors*. Boca Raton: CRC Press, 1991.

[27] P. Reuss, *Neutron Physics*. Paris: EDP Sciences, 2008.

[28] F. Brown, "Monte Carlo Techniques for Nuclear Systems – Theory Lectures." Los Alamos, 2016.

[29] D. B. Pelowitz *et al.*, "MCNP6 User's Manual," Los Alamos, 2013.

[30] L. Hamidatou, H. Slamene, T. Akhal, and B. Zouranen, "Concepts, Instrumentation and Techniques of Neutron Activation Analysis," in *Imaging and Radioanalytical Techniques in Interdisciplinary Research*, F. Kharfi, Ed. Rijeka: IntechOpen, 2013.

[31] B. E. Watt, "Energy spectrum of neutrons from thermal fission of U235," *Phys. Rev.*, vol. 87, no. 6, pp. 1037–1041, 1952.

[32] "Neutron Fluence Measurements," *Iaea*, vol. TRS-107, 1970.

[33] K. C. Hines, "Energy and Lethargy Distribution of Neutrons Slowing Down in Graphite," Sydney, 1959.

[34] S. Bell, "Beginner's Guide to Uncertainty of Measurement," Teddington, 1999.

[35] International Bureau of Weights and Measures, “Evaluation of measurement data — Guide to the expression of uncertainty in measurement,” Sèvres, 2008.

[36] J. R. Taylor, “An Introduction to Error Analysis: The Study of Uncertainties in Physical Measurements,” 2nd ed., University Science Books, 1997, pp. 93–120.

[37] Canadian Nuclear Safety Commission, “Record of Proceedings - McMaster University - Application to Renew the McMaster Nuclear Reactor Operating Licence,” 2014.

[38] McMaster Nuclear Reactor, “Nuclear Operations and Facilities 2017,” Hamilton, 2017.

[39] S. E. Day, “McMaster Nuclear Reactor Specification - IAEA CRP 1496, Innovative Methods for Research Reactors: “Benchmarking against Experimental Data of the Neutronic and Thermalhydraulic Computational Methods and Tools for Operation and Safety Analysis for Research,” Hamilton, 2011.

[40] S. E. Day, M. P. Butler, and W. J. Garland, “Calculations in Support of the Mnr Core Conversion,” Hamilton, 2002.

[41] S. E. Day, “McMaster Nuclear Reactor Benchmark Specification - IAEA CRP 1496, Innovative Methods for Research Reactors: “Benchmarking against Experimental Data of the Neutronic and Thermalhydraulic Computational Methods and Tools for Operation and Safety Analysis for,” Hamilton, 2013.

[42] M. Alqahtani, A. Buijs, and S. E. Day, “Serpent-2 and OSCAR-4 computational tools compared against McMaster nuclear reactor improved operational data history for U-235 fuel inventory tracking , local power tracking and validation of multiplication factor,” *Ann. Nucl. Energy*, vol. 145, p. 107590, 2020.

[43] A. Klett, “Handbook of Particle Detection and Imaging,” C. Grupen and I. Buvat, Eds. Berlin: Springer, 2012, pp. 759–790.

[44] L. Snoj, M. Ravnik, A. Trkov, and G. Zerovnik, “On the self-shielding factors in neutron activation analysis,” *Nucl. Instruments Methods Phys. Res. Sect. A Accel. Spectrometers, Detect. Assoc. Equip.*, vol. 610, pp. 553–565, 2009.

[45] “NuDat 2.7.” [Online]. Available: http://www.nndc.bnl.gov/nudat2/.

[46] M. Berglund and M. E. Wieser, “Isotopic compositions of the elements 2009 (IUPAC Technical Report)*,” *Pure Appl. Chem.*, vol. 83, no. 2, pp. 397–410, 2011.

[47] J. Meija *et al.*, “Atomic weights of the elements 2013 (IUPAC Technical Report),” *Pure Appl. Chem.*, vol. 88, no. 3, pp. 265–291, 2016.

[48] *Genie ™ 2000 Spectroscopy Software*. 2000.

[49] D. Chandler, G. I. Maldonado, L. D. Proctor, and R. T. Primm, “Nuclear Transmutations in HFIR’s Beryllium Reflector and Their Impact on Reactor Operation and Reflector Disposal,” *Nucl. Technol.*, vol. 177, no. 3, pp. 395–412, 2017.

[50] M. B. Zeller, A. Celli, R. T. Jones, and G. P. McPhee, “Photo-neutron experiment performed in ZED-2,” in *21st Conference of the Canadian Nuclear Society*, 2000.

[51] E. Macconnachie, D. Novog, and S. Day, “ICONE26-82412 Axial Flux Wire Measurements atthe McMaster Nuclear Reactor,” 2018, pp. 1–8.

[52] G. E. Knoll, *Radiation Detection and Measurement Third Edition*, 3rd ed. Ann Arbor: John Wiley & Sons, Inc., 2000.

[53] Alfa Aesar, “Certificate of analysis.” Thermo Fisher Scientific, 2018.

[54] National Institute of Standards and Technology, “Thermophysical Properties of Fluid Systems,” 2018. [Online]. Available: https://webbook.nist.gov/chemistry/fluid/. [Accessed: 03-May-2019].

[55] Cole-Parmer, “Digi-Sense Prec. Ind. PRT, 0.25" x 12" , -60~160C, Bare Wire.” [Online]. Available: https://www.coleparmer.com/i/digi-sense-prec-ind-prt-0-25-x-12-60-160c-bare-wire/9045200. [Accessed: 06-May-2019].

[56] Badger Meter, “Model SSL Venturi Classic Flow Meter.” [Online]. Available: https://www.badgermeter.com/business-lines/flow-instrumentation/venturi-ssl/. [Accessed: 06-May-2019].

[57] B. T. Rearden and M. A. Jessee, “SCALE Code System,” Oak Ridge National Laboratory, Oak Ridge, 2017.

[58] “SCALE User’s Group.” [Online]. Available:

https://groups.google.com/forum/#!forum/scale-users-group.

[59] E. MacConnachie, D. Novog, and S. Day, "Quantification of system uncertainties in activation experiments at nuclear research reactors," *Ann. Nucl. Energy*, vol. 134, pp. 432–440, 2019.

[60] D. R. Helsel and R. M. Hirsch, "Statistical Methods in Water Resources," 2002, pp. 337–340.

[61] V. Suman and P. K. Sarkar, "Nuclear Instruments and Methods in Physics Research A Neutron spectrum unfolding using genetic algorithm in a Monte Carlo simulation," *Nucl. Inst. Methods Phys. Res. A*, vol. 737, pp. 76–86, 2014.

[62] M. Matzke, "9 UNFOLDING PROCEDURES," *Radiat. Prot. Dosimetry*, vol. 107, pp. 155–174, 2003.

[63] S. R. Malkawi and N. Ahmad, "Solution of the neutron spectrum adjustment problem in a typical MTR type research reactor," *Ann. Nucl. Energy*, vol. 28, pp. 17–22, 2001.

[64] F. Molina, P. Aguilera, J. Romero-barrientos, H. F. Arellano, J. Agramunt, and J. Medel, "Energy distribution of the neutron fl ux measurements at the Chilean Reactor RECH-1 using multi-foil neutron activation and the Expectation Maximization unfolding algorithm," *Appl. Radiat. Isot.*, vol. 129, no. August, pp. 28–34, 2017.

[65] J. A. Kennedy, "A COMPARISON OF MNR IRRADIATION EXPERIMENTS WITH SIMULATION," McMaster Univeristy, 2000.

[66] D. Chiesa, E. Previtali, and M. Sisti, "Bayesian statistics applied to neutron activation data for reactor flux spectrum analysis," *Ann. Nucl. Energy*, vol. 70, pp. 157–168, 2014.

[67] A. Leder, "Unfolding neutron spectrum with Markov Chain Monte Carlo at MIT research Reactor with He-3 Neutral Current Detectors," *Jounal Instrum.*, vol. 13, 2018.

[68] D. Chiesa *et al.*, "Measurement of the neutron flux at spallation sources using multi-foil activation," *Nucl. Instruments Methods Phys. Res. Sect. A Accel. Spectrometers, Detect. Assoc. Equip.*, vol. 902, pp. 14–24, 2018.

[69] E. L. Macconnachie and D. R. Novog, "Measurement , simulation and uncertainty

quantification of the neutron flux at the McMaster Nuclear Reactor," *Ann. Nucl. Energy*, vol. 151, 2021.

[70] B. J. Smith, "boa : An R Package for MCMC Output Convergence," *J. Stat. Softw.*, vol. 21, no. 11, 2007.

[71] R. J. B. Goudie, R. M. Turner, and D. De Angelis, "MultiBUGS : A Parallel Implementation of the BUGS Modelling Framework for Faster Bayesian Inference," *arXiv*, 2018.

[72] D. J. Spiegelhalter, N. G. Best, and B. P. Carlin, "Bayesian measures of model complexity and fit," *J. R. Stat. Soc. Ser. B*, pp. 583–639, 2002.

[73] J. Wang, Z. Guo, X. Chen, and Y. Zhou, "Neutron spectrum unfolding based on generalized regression neural networks for neutron fluence and neutron ambient dose equivalent estimations," *Appl. Radiat. Isot.*, vol. 154, no. August, p. 108856, 2019.

[74] International Atomic Energy Agency, "Compendium of Neutron Spectra and Detector Responses for Radiation Protection Purposes IAEA TRS 403," Vienna, 2001.

Appendix A: Standard Operation Procedure for Neutron Flux Measurements via Neutron Activation in MNR

This appendix contains a SOP for preparing, performing, and processing neutron flux measurements via neutron activation in MNR. Although a general description of this methodology has been presented in Chapter 3, this section is intended to provide a detailed, step-by-step description of the experimental procedure, including (but not limited to): required lab equipment, useful online resources, scheduling guidelines, and addressing common procedural pitfalls.

This appendix will be structured as a series of descriptive paragraphs outlining the important steps of the procedure and highlighting some useful tips for the continued success of these experiments; an itemized, sequential list of steps that other experimentalists may follow will be provided at the end of each section.

Standard Operating Procedure

There are three distinct phases of a flux measurement procedure in MNR: the scheduling and the sample irradiation, the post-irradiation sample handling, and the data collection and processing steps. Prior to carrying out any of these steps however, there are certain equipment and safety requirements that must be fulfilled; first, the laboratory resources and infrastructure that are necessary to conduct (and recover data from) repeated flux measurements in MNR are described. Then, detailed descriptions of the experimental procedure itself are provided, which may be referenced as the SOP for future neutron flux measurements.

Requirements for Neutron Activation Experiments

Certain safety requirements must be satisfied and certain laboratory equipment must be in place before it is possible to repeatedly carry out neutron flux measurements via NAA in MNR. These requirements and some useful resources will be discussed here; while meeting these standards are critical to the continued success of neutron flux measurements, this is not presented as part of the

SOP as these criteria must be met before experimentation, and the specifics may vary depending on the lab space available to the experimenter.

Safety Requirements

A permit for the possession, use, and disposal of radioactive material must be granted by the McMaster Health Physics Advisory Committee prior to flux measurements being carried out in MNR – this permit must be updated as necessary to include **every** radionuclide being studied. Dose estimates for each radionuclide must be provided when applying for this permit; while these estimates can be generated using MCNP, the following websites may also be consulted:

- https://www.wise-uranium.org/rnac.html
- http://www.radprocalculator.com/Gamma.aspx

In general, the permit holder will be required to post the permit in each approved space, must perform regular radiation surveying, must store radioactive material in a locked container, and must work with exclusively sealed sources that are disposed of in clearly identified containers. As such, the following equipment is required for the radiation safety requirements of this work:

- A pancake-type detector for radiation surveying, procured from McMaster Health Physics.
- A lock-box for radionuclide storage. For low-activity samples, it is generally not required that this be lead-lined. An appropriately-sized container may be acquired from McMaster-Carr (https://www.mcmaster.com/).
- Radiation disposal containers. Lead-lined waste containers may be provided by McMaster Health Physics, but other vessels shielded by lead blocks may also be used.

Laboratory Requirements

In order to perform regular gamma-ray spectroscopy, both and HPGe and its accompanying hardware/software, and the resources required to maintain it, must be fully integrated into the lab space where data collection takes places.

Prior to use, an HPGe must be cooled with LN2 – additionally, its energy efficiency curve must be studied to fully understand the data being collected. Geometrical effects must also be quantified – this can be realized with MCNP simulations based on the sample/detector configuration.

If this work is being done in collaboration with the MACCNAA, it may not be necessary for the experimenter to perform either the cooling or the calibration; for this thesis however, all detector maintenance was regularly carried out by the author. The lab space must therefore be equipped with the following equipment to realize this detector maintenance:

- Infrastructure to cool the HPGe – this includes a cryogenic storage dewar to store the LN2, appropriate tubing to connect the detector to the dewar, and a source of compressed air to circulate the LN2 through the detector. The LN2 itself can be collected from the liquid nitrogen delivery station at the North end of the Nuclear Research Building. The gas cylinder training available through McMaster is required for this portion of work.
- Standardized radiation sources for the efficiency calibration of the HPGe. The spectra generated by these sources should span as wide an energy range as possible; the following radionuclides were used to generate the efficiency curve in this work: ^{22}Na, ^{54}Mn, ^{57}Co, ^{60}Co, ^{65}Zn, ^{109}Cd, and ^{152}Eu – covering an energy range of 90 keV to 1408 keV – these sources may also be used for the regular energy calibration of the HPGe that must be performed.

Planning and Performing an Activation Procedure in MNR

The following steps provide instructions for planning, preparing, and conducting an irradiation experiment in MNR. Before these steps are carried out, an activation estimate should be generated (using any of the resources provided above) so that irradiation and decay times can be adjusted accordingly. It is also **strongly suggested** that the experimenter becomes familiar with the physical practicalities of working with the different materials being studied – for instance, Sn is soft and requires delicate handling, while Zr is springy and may need to be forced into a straight shape in the wire holder. Additionally, these steps must also be planned/scheduled to accommodate the preparation and data collection that follows – as radioactive material is involved, the timing of each of these phases must be considered.

The following resources are required to plan and perform an activation procedure in MNR:

- Flux wires. Many useful isotopes in wire form for neutron flux measurements can be purchased from Alfa Aesar (https://www.alfa.com/en/pure-elements/).

- Wire-cutters for precisely cutting the flux wires to size. These should be used **only** for working with the flux wires to avoid dulling them unnecessarily. Appropriate wire cutters can be purchased from McMaster-Carr (https://www.mcmaster.com/wire-cutters/).
- Plastic shipping tubes for wire storage before and after activation. The tubes used in this work were purchased from McMaster-Carr and cut to a length of approximately 90 cm (https://www.mcmaster.com/cut-to-length-shipping-tubes/).

1. Prepare the flux wire for transport to MNR.
    a. Cut a length of wire approximately 80 to 85 cm in length (this will be cut down to the size of the wire holder once in MNR).
    b. Mark the wire at intervals of 3.5 cm with a permanent marker (if more data points are required, adjust this interval accordingly).
    c. Mark **one end** of the wire with a permanent marker (of a different colour than in b.) to denote the bottom of the wire.
    d. If a multi-wire irradiation is being performed, repeated a. through c. for each wire, making additional markings in step c. to indicate the different wires being used.
    e. Carefully place the wire(s) in the plastic shipping tube and make note of the irradiation date with a masking tape label on the tube.

2. Set up for the procedure in MNR – *nota bene* this step should be performed **at least** one day before the activation takes place. In this work, this step was typically performed on a Friday in anticipation of a Monday-morning activation.
    a. Remove the flux wires from the shipping tube and insert them into the wire holder, taking care not to physically damage the wire (especially if a softer metal is being used). Metal tongs in MNR can be used to push the wire through the holder.
    b. Using the designated wire-cutters, cut the flux wire to size – leave **at least** a centimeter of extra wire on both ends of the holder to physically secure the wire in the holder. Ensure that the markings made in Step 1 b. are flush with the bottom of the wire holder.

c. Using the extra length of wire from b., physically fasten the wire to the holder by folding the wire over the end caps at the top and bottom of the holder. The top of the wire holder can be further denoted by creating a distinct loop of wire.
d. Fill out an irradiation request form. The following information is required:
    i. Material, physical form, and approximate mass (i.e. Sn, thin wire, ~8 g).
    ii. Irradiation date, sample position, length of irradiation and reactor power (i.e. August 24 2020, Site 8C, for 15 minutes, at 500 kW).
    iii. Special loading instructions. This may vary depending on the experimental requirements however, for this work these instructions were: "bring the reactor to power, then load the wire holder directly into the sample holder".

3. Return to MNR on the specified day to oversee the irradiation procedure. Record the following information at regular intervals (i.e. at 5-minute intervals, as in this work):
    a. Date and time.
    b. Shim rod and regulating rod positions, as a percentage withdrawn from the core.
    c. ΔT across the core [^{o} F].
    d. Q through the core [USGPM].
    e. Reactor power [kW].

Preparing Activated Samples for Data Collection

The following steps provide instruction for recovering the irradiated flux wires from MNR and preparing them for data collection. In this work, the author was generously granted access to the MACCNAA lab to facilitate working with radioactive material.

1. Fill out a Radioactive Material Acquisition Approval Form to provide a record of radioisotopes being transferred from MNR to the permit being used in these experiments. This can be done several days in advance of the actual material transfer from MNR. The following information is required:
    a. List of every radionuclide and their activity.
    b. Radiation possession limit for the receiving permit.
    c. Receiving permit number, permit holder, and permit holder signature.
    d. Date of transfer.

e. Health physics approval (i.e. signature).
f. Experimenter contact information.

2. Collect the irradiated flux wires from MNR.
    a. Work with MNR operators to remove the wires from the wire holder and insert them into the plastic shipping tube for further transport. The experimenter **must** wear latex gloves and use metal tongs throughout to avoid physical contact with the wires.
    b. Survey the radiation field at the surface and at a distance of 1 meter using the gamma guns available in MNR. Use this information to fill out the remaining portion of the irradiation request form.

3. Transport the wires either directly to MACCNAA for preparation **or if there is** a delay before Step 4, the radioactive samples must be stored in the lab lock-box, with the total activity of the stored material clearly indicated.

4. Bring the wires to MACCNAA and prepare them for data collection. Here, 21 data points per flux wire were generated, and these instructions reflect that – if either more or less data points are adopted in the future, that number can be directly substituted in what follows.
    a. Using a permanent marker, label 21 polyethylene vials to accommodate the wire segments after they have been cut. In this work, the bottom of the wire was taken as segment 1, and the top as segment 21. If multiple wires are being prepared, create additional labels to distinguish them during data collection (i.e. through colour-coding, or identifying the wires as “A”, “B”, “C”, etc.).
    b. With the designated wire-cutters in the dominant hand and metal tongs in the non-dominant hand, **carefully** hold and cut each segment along the lines indicated in Section 0 Step 1b. Use the tongs to place each segment in the appropriately marked vial.
    c. Carefully use the tongs to sequentially remove each segment from its vial, measure its mass using a high-precision scale, and return the segment to the vial. Record this

mass on a Counting Record form in the "weight" column – at this stage, the sample ID (i.e. 1 at the bottom, 21 at the top) can also be entered on the form.

d. Seal each vial with the locking end-caps available in the MACCNAA lab.
e. If multiple wires are being prepared, repeat a. through d. for each wire.

5. Return the wires to the lab where data collection is taking place. **If there is** a delay before data collection, the radioactive samples must be stored in the lock-box, with the total activity of the stored material clearly indicated.

Data Collection and Processing

The following steps outline the data collection procedure; in this work, the Genie 2000 software was used in conjunction with a HPGe detector system to collect and save data. Other software packages may be used to the same effect however, this appendix makes specific reference to the Genie 2000 software and some useful information contained in its manual. As discussed, the HPGe **must** be cooled, and both the energy and geometrical effects must be quantified before data collection can occur. These instructions **do not** include general descriptions of how to power on and setup the detector/software system – instructions on how to do so can be found in the Genie 2000 Operations Manual, Chapter 2 [48].

1. Perform an energy calibration immediately before starting data collection. This must be done **every time** the system is restarted/powered on. In this work, ^{22}Na (511 keV and 1274.537 keV) and ^{54}Mn (834.848 keV) were regularly used for energy calibration. Instructions to perform the energy calibration can be found in the Genie 2000 Operations Manual, Chapter 3 (Energy Only Calibration) section on page 64 [48].

2. Adjust the data acquisition time (i.e. the **live time**) to achieve the desired counting statistics. A correction factor to account for the difference between the live time and the real time may be included during data processing however, in this work, the isotopes being studied had sufficiently long half-lives that this effect was insignificant. Instructions can be found in the Genie 2000 Operations Manual, Chapter 3 (Acquire Setup) section on page 47.

3. Place the sample (i.e. the vial containing a single wire segment) at the desired distance from the detector. In this work, a 3D-printed component was used to ensure each wire was always at the same distance (and in the same configuration) from the detector.

4. Start the data acquisition. Record the following information on the Counting Record form:
    a. Counting time [s].
    b. Start-of-count time.
    c. Sample ID for bookkeeping purposes (in this work, the following convention was adopted: monthDay_wire_segmentNumber e.g. july27_tin_005).

5. Save the spectrum data using the IEC 1455 (.IEC) format. These files can be readily converted to .txt documents for processing with additional scripts in MATLAB, Python, etc. In this work, the sample ID adopted in Step 4c. was also used to save data – an example file name is therefore: july27_tin_005.IEC and july27_tin_005.txt.

6. Repeat Step 3 through Step 5 for all the segments in a single wire.

7. If **multiple different** wires are being counted, repeat Step 2 through Step 6 for each wire.

8. Perform at 1000 s data acquisition to collect a background spectrum.

9. After all the required data has been collected, power down the HPGe and software system. Dispose of all sealed vials in the appropriately labelled containers.

10. Processing the raw .txt files involves passing said files through a series of MATLAB scripts. A main driver script takes as inputs the information contained on the counting record form, and an identification tag to recover the material properties required for analysis (see Table 1) from a separate Excel file (.xlsx). The γ-ray peaks are identified, fit, and the peak-area and count-rates (i.e. activity) are calculated; these values can then be used to recover the (n, x) reaction rate in the sample. The scripts are written in such a way

that nuclear data may also be passed as an input parameter such that neutron flux is also calculated.